FISSIONABILITY AND CHARGE DISPERSION STUDIES OF THORIUM BY PROTONS OF ENERGY TO 90 MeV

by

© Chien CHUNG

A thesis submitted to the
Faculty of Graduate Studies and Research
in partial fulfillment of the
requirements for the degree of
Doctor of Philosophy

Department of Chemistry
McGill University
Montreal, PQ
Canada

January 1980

ABSTRACT

Ph.D. Chien Chung Chemistry

Fissionability and Charge Dispersion Studies
of Thorium by Protons of Energy to 90 MeV

Production cross sections have been determined for the reactions of (p,pXn) with X = 1, 4-6 and (p,3pXn) with X = 5-7 on a ^{232}Th target at proton energies to 90 MeV. These measured excitation functions, together with ten others compiled from the literature, are compared to calculations using the theoretical framework of the Pre-equilibrium / Exciton Model of nuclear reactions with a newly developed fission option. The fit of the theory to the experimental data is excellent, lending confidence to the treatment of the competition between fission and particle evaporation.

Based on the same treatment of fission, calculations have been extended to obtain detailed information of the fission process such as the number of pre- and post-fission neutrons, and the most probable charge Z_p in fission from each of several different charge distribution postulates. The experimental values of Z_p in the ^{232}Th(p,Fission) reaction, compiled from the literature, fit very well by correlating the Minimum Potential Energy (MPE) hypothesis (or to a lesser extent the Equal Charge Displacement (ECD) rule) to asymmetric fission, and the Unchanged Charge Distribution (UCD)

postulate to symmetric fission. The division of asymmetric/symmetric fissions by a simple $(Z^2/A)_{A/S}$ value proposed in this work is also found to account for a wide range of measured mass yield curves in fission.

Résumé

Ph.D. Chien Chung Chimie

Etudes de fissibilité et de dispersion de charge du thorium par des protons d'énergie jusqu'à 90 MeV

Les sections efficaces de production des réactions (p,pXn) avec X = 1,4,5,6 et (p,3pXn) avec X = 5,6,7 sur le ^{232}Th ont été mesurées pour des protons incidents d'énergie jusqu'à 90 MeV. Les fonctions d'excitation mesurées, et dix autres fonctions déjà publiées, ont été comparées aux résultats de calculs utilisant le modèle "Pré-équilibre / Exciton" des réactions nucléaires avec une option nouvelle pour la fission. L'accord excellent entre les résultats théoriques et expérimentaux prête son appui au traitement de la compétition entre l'évaporation des particules et la fission.

En utilisant le même traitement de fission, les calculs ont été développés pour avoir des renseignements détaillés sur le processus de la fission: le nombre de neutrons pré- et post-fission et la charge la plus probable Z_p de fission, en partant d'un choix de postulats de distribution de charge. Les valeurs expérimentales de Z_p pour ^{232}Th(p,fission), obtenues de sources publiées, s'accordent très bien avec un modèle fondé, pour la fission asymétrique, sur l'hypothèse d'énergie potentielle minimum (ou moins bien sur la règle de déplacement égal de charge), et pour la fission symétrique,

sur le postulat de distribution inchangée de charge. La division des fissions en asymétrique ou symétrique par le simple critère de $(Z^2/A)_{A/S}$, proposée dans ce travail, arrive à expliquer une grande gamme de courbes de rendement de masse mesurées en fission.

ACKNOWLEDGEMENTS

I wish to express my sincere appreciation and thanks to Professor James J. Hogan for his continual interest, encouragement, enthusiasm, and for the suggestion regarding the investigative areas covered by this dissertation.

Special thanks are due to Professor Leo Yaffe for his interest in this investigation and offering details of the experimental data of his research group.

Sincere thanks are due to Professor Mirko Diksic, Montreal Neurological Institute, for his interest and advice, especially during Professor Hogan's sabbatical leave.

I would also like to thank Professor Ettore Gadioli, Istituto di Scienze Fisiche in Italy, for his indispensable guidance and discussions, and for offering the original computer code of the Pre-equilibrium / Exciton Model calculation.

Very helpful discussions with all colleagues in Radiochemistry groups, in particular Kerry Burns, during the preparation of this work are greatly appreciated. Thanks are also extended to Michael Attas who translated the ABSTRACT.

I would like to record my gratitude to Professor J.K.P. Lee and the cyclotron's operating crew for the permission to use the McGill Synchrocyclotron.

I acknowledge with thanks the benefits accrued from the

departmental laboratory demonstrating appointment while preparing and completing the requirements for my postgraduate degree at the Department of Chemistry. Financial assistance during this period through the following sources is also gratefully acknowledged:

T. Sterry Hunt Award (1975-76);

Max Binz Bursary (1976);

Coll McFee Memorial Scholarship (1976-77);

Graduate Faculty Summer Research Fellowships (1977-79);

Richard T. Mohan Memorial Scholarship (1977-1979);

Research grants from NRC, Ottawa (1976-79).

This work has been completed while residing in Montreal, CANADA, and special gratitude is reserved for Teddy Hogan and Renée Charron for effectively dealing with difficulties of personal situations such as cultural barrier and visa problems during this stay, thereby helping to eliminate hindrance to the progress of this work.

This work would not have been possible without the patience and understanding of my wife, Ching Ling, and constant encouragement from my parents, Mr. and Mrs. H.P. Chung.

To my parents and my wife

TABLE OF CONTENTS

	page
ABSTRACT	i
RESUME	iii
ACKNOWLEDGEMENTS	v
TABLE OF CONTENTS	vii
LIST OF TABLES	xii
LIST OF FIGURES	xiv
I. INTRODUCTION	1-15
A. Previous Work	2
A1. Experimental approach to fission competition	2
A2. Theoretical approach to fission competition	4
A3. Nuclear charge dispersion in fission	6
B. Present Work	9
B1. Fission competition and nuclear charge dispersion	10
B2. Experiment and calculation	14
II. EXPERIMENTAL PROCEDURES, DATA TREATMENT, AND RESULTS	16-51
A. Irradiation	16

page

A1. Target arrangement 16

A2. Proton beam monitoring 18

B. Post Irradiation Chemistry 20

B1. Radiochemical separations 20

B2. Carrier standardization 23

B3. Counting the samples 25

C. Radioactive Detection Systems 25

C1. Lithium drifted germanium, Ge(Li), detectors 25

C2. Thallium activated sodium iodide, NaI(Tl), detector 28

C3. Calibration of the detection systems 29

D. Data Treatment 30

D1. Cross section calculation 31

D2. Contamination 35

D3. Error analysis 37

E. Experimental Results 38

E1. Monitoring cross sections of ^{143}Ce 38

E2. Excitation functions of the $^{232}Th(p,pXn)Th$ reactions 41

E3. Excitation functions of the $^{232}Th(p,3pXn)Ra$ reactions 46

E4. General trend of measured excitation functions 48

page

III. THEORETICAL PREDICTION OF THE ^{232}Th(p,X) REACTIONS 52-68

A. The Spallation Data 52

B. Prediction of the ^{232}Th(p,X) Reactions 53

B1. The total fission cross sections 54

B2. The cross sections of the ^{232}Th(p,Xn)Pa reactions 56

B3. The cross sections of the ^{232}Th(p,pXn)Th reactions 59

B4. The cross sections of the ^{232}Th(p,2pXn)Ac reactions 62

B5. The cross sections of the ^{232}Th(p,3pXn)Ra reactions 65

C. Summary of the Predictions 67

IV. FISSIONABILITY AND FISSION CROSS SECTIONS 69-95

A. Fission Probability 69

A1. The fission barrier 71

A2. Fission probability as a function of Z^2/A 72

A3. Fission probability as a function of E^*... 79

B. Fission Information 83

B1. The average fission information 84

B2. The fissioning spectra 88

C. Summary of the Pre-fission Calculation 93

page

V. CALCULATION OF POST-FISSION NEUTRONS 96-126

A. Fission Process 96

B. Calculation of Properties of the Primary Fragments 100

B1. Mass difference at fission, ΔM 101

B2. Total kinetic energies for the primary fragments, E_k 105

B3. Internal excitation energy of the primary fragments, $E^*_{L,H}$ 107

B4. Prompt gamma ray energy, E_γ 108

B5. Neutron binding energy, B_n 110

B6. Kinetic energy of the prompt neutrons, KE_n 112

C. Calculation of the Numbers of Prompt Neutrons 112

C1. The numbers of prompt neutrons in the ^{232}Th(p,Fission) reaction 114

C2. The numbers of post-fission neutrons in the ^{232}Th(p,Fission) reaction 118

D. Summary of the Post-fission Neutron Calculation 125

VI. CALCULATION OF NUCLEAR CHARGE DISPERSION IN FISSION 127-166

A. The Postulates 127

A1. The most stable charge, Z_A 130

A2. The average $\bar{D}$ value 133

page

B. Experimental Z_p Data 134

B1. Experimental Z_p data in the (n_{th},F) reactions 135

B2. Experimental Z_p data in the $^{232}Th(p,Fission)$ reaction 136

C. Fit to the Experimental Z_p Data in the (n_{th},F) Reactions 141

D. Fit to the Experimental Z_p Data in the $^{232}Th(p,Fission)$ Reaction 145

D1. Fit by uniform Z_p(postulate) 147

D2. Fit by E^*_F-dependent Z_p 150

D3. Fit by combined Z_p dependent upon (Z_F,A_F) 155

D4. The combined Z_p(MPE/UCD) 160

E. Summary of the Fit 164

VII. CORRELATION OF THE ASYMMETRIC/SYMMETRIC FISSIONS TO THE IDENTITY OF THE FISSIONING NUCLEUS 167-183

A. Decomposition of Mass Yield Curves 168

B. The Asymmetric/Symmetric Split 174

C. Charge Distribution and Asymmetric/Symmetric Fissions 182

VIII. SUMMARY AND CONTRIBUTION TO KNOWLEDGE 184-186

APPENDIX - THE SI UNITS 187

REFERENCES 188

LIST OF TABLES

page

Table 01 Nuclear properties of products observed in this work 32

Table 02 Monitoring cross sections used in this work 34

Table 03 The systematic and random errors in this work 39

Table 04 Experimental reaction cross sections 42

Table 05 Calculated and experimental reaction thresholds of interest 50

Table 06 Calculated result of the average information of the ^{232}Th(p,Fission) reaction 85

Table 07 Theoretical calculation of the fissioning nuclides and cross sections of the ^{232}Th(p,Fission) reaction 89

Table 08 Calculated numbers of fission-related neutrons in the ^{232}Th(p,Fission) reaction .. 124

Table 09 Experimental Z_p data of the ^{233,235}U, ^{239}Pu(n_{th},F) reactions, after (Wa62) 137

Table 10 Experimental Z_p data of the ^{232}Th(p,Fission) reaction 142

Table 11 Quantitative comparison between calculation and experiment of Z_p in the ^{233,235}U, ^{239}Pu(n_{th},F) reactions 144

page

Table 12 Qualitative comparison of uniform Z_p to the experimental data in the $^{232}Th(p,Fission)$ reaction 148

Table 13 Qualitative comparison of the E^*_F-dependent Z_p to the experimental data in the $^{232}Th(p,Fission)$ reaction 153

Table 14 Qualitative comparison of the combined Z_p to the experimental data in the $^{232}Th(p,Fission)$ reaction 158

Table 15 Quantitative comparison of all calculated Z_p to the experimental data in the $^{232}Th(p,Fission)$ reaction 159

Table 16 Quantitative comparison between the combined Z_p(MPE/UCD) and Z_p(experiment) of the $^{232}Th(p,Fission)$ reaction 163

Table 17 Data used for asymmetric/symmetric split in this work 175

LIST OF FIGURES

page

Figure 01 (a) Target assembly, (b) Target position .. 17

Figure 02 McGill Synchrocyclotron internal beam energy vs. target radius, after Moore (Mo75) 19

Figure 03 Block diagrams of detection system: (a) 40 cm^3 Ge(Li), (b) 30 cm^3 Ge(Li), (c) 3" x 3" NaI(Tl) 27

Figure 04 Excitation function of the $^{232}Th(p,Fission)^{143}Ce_{cum}$ reaction 40

Figure 05 Excitation functions of the $^{232}Th(p,pXn)Th$ reaction 43

Figure 06 Excitation functions of the $^{232}Th(p,3pXn)Ra$ reaction 47

Figure 07 Comparison between experiments and calculation on total fission cross sections of the $^{232}Th(p,Fission)$ reaction 55

Figure 08 Comparison between experiments and calculation in the $^{232}Th(p,Xn)Pa$ reactions 57

Figure 09 Comparison between experiments and calculation in the $^{232}Th(p,pXn)Th$ reactions 60

Figure 10 Comparison between experiments and calculation in the $^{232}Th(p,2pXn)Ac$ reactions 64

page

Figure 11 Comparison between experiments and calculation in the ^{232}Th(p,3pXn)Ra reactions 66

Figure 12 The ratio of $\Gamma_{\text{charged particle}}/\Gamma_n$ 70

Figure 13 The fission barriers 73

Figure 14 Calculated fissility as a function of Z^2/A at E^* = 100 MeV 75

Figure 15 Calculated fissionability as a function of A_F at (a) E^* = 30 MeV, (b) E^* = 60 MeV, (c) E^* = 90 MeV, (d) reproduced from (Va58) 77

Figure 16 Calculated fissility as a function of E^* at (a) thorium, (b) protactinium 81

Figure 17 Spectra of the excitation energy associated with the fissioning nuclides in the ^{232}Th(p,Fission) reaction 91

Figure 18 Calculated ΔM and E_k in the present work .. 104

Figure 19 Prompt neutron distribution as a function of primary fragment mass 115

Figure 20 Post-fission neutron distribution as a function of heavy fragment mass 119

Figure 21 Fragmental mass yield curves for the ^{232}Th(p,Fission) reactions with protons to 53 MeV, after (Cr69) 121

Figure 22 Calculated numbers of fission-related neutrons in the ^{232}Th(p,Fission) reaction 124

page

Figure 23 Values of (a) Z_A and (b) $\bar{D}$ used in this work 132

Figure 24 Calculated and experimental Z_p in the $^{232}Th(p,Fission)$ reaction 161

Figure 25 Decomposition of the mass yield curves of the $^{232}Th(p,Fission)$ reaction into asymmetric and symmetric fissions 171

Figure 26 Symmetric fission in experimental mass distribution of the (p,Fission) reactions (a) $^{232}Th(p,Fission)$ reactions, (b) U(p,Fission) reaction 172

Figure 27 The asymmetric and symmetric fissions of the fissioning nuclides, $80 \leqslant Z_F \leqslant 105$ 177

I

INTRODUCTION

The first artificially induced nuclear reaction was accomplished 60 years ago in 1919 by Rutherford and co-workers (Rul9); the first nuclear fission was recognized 40 years ago in 1939 by Hahn and Strassman (Ha39) and Meitner and Frisch (Me39). One would expect with the vast amount of experimental information since then that exactly what happens in a nucleus during the process of reaction and fission would by now be well known. However, owing to the lack of detailed knowledge of the dissipation of energy in the nucleus and the formidable number of degree of freedom, a simplified description of reaction/fission process is still required nowadays.

The simplification is provided by models and postulates, introducing some parameters to reproduce the general experimental results. The parameters must be limited to allow a clear picture of the physical processes involved in the description of models and postulates, and must be derivable from the basic laws. Existing experimental information provides a critical test for postulates and models as well as the impetus for new proposals. Step by step, a picture is continuously improving, coming closer to the truth.

In this work, the general intention is to examine the experimental data of nuclear reaction and fission cross sections by calculations based on the current model of nuclear reaction with a newly developed fission option, then expand the calculation to post-fission properties such as nuclear

charge dispersion and compare the predictions, based upon different charge distribution postulates, to the experimental data. A new proposal is also made to split the asymmetric and symmetric fission in this investigation.

A. Previous Work

In general, when an energetic projectile x and target nucleus A come very close together after overcoming their Coulomb repulsion, a rearrangement of nucleons of this system in terms of deexcitation may occur; this may result in a "nuclear reaction". A nuclear reaction is designated by the symbols A(x,y)B, where y and B are the outgoing particles and reaction product, respectively. If the y involves only a few nucleons or particles, the nuclear reaction is historically referred to as a "spallation reaction" and B may be called the spallation product. On the other hand, a nucleus may also undergo the "fission" process, splitting into at least two comparable parts, whenever it is excited with sufficient energy to overcome the fission barrier. Thus, fission may compete with other deexcitation modes in a nuclear reaction initiated by an energetic projectile.

A1. Experimental approach to fission competition

Competition between fission and spallation reactions has been a major topic of considerable interest to nuclear

scientists since the discovery of fission. Numerous experimental approaches to this problem have been mostly concentrated on comparison of total fission cross sections to spallation reaction cross sections. Such experimental studies could derive an average value of the fissility, defined as the fractional probability that the excited nucleus goes to fission, as functions of both the identity of the fissioning nucleus and its excitation energy. Unfortunately, except at very low excitation energies, the problem was further complicated by fast deexcitation process leading to various fissioning nuclei associated with widely distributed excitation energies.

The first experimental study of the fissility was done by Tewes (Te55) and was followed by many fission studies for a quarter century in an effort to gain insight into the fission competition in the deexcitation process. None of these studies found clear evidence for an excitation energy dependence of the average fissility and the simplification was made that it is generally dependent only upon the value of Z^2/A of the average fissioning nucleus. The pioneer works of Vandenbosch and Huizenga (Va58) summarized the general pattern of the variation of the average fissility with Z^2/A that remains today as the most extensive guidance for excitation energy greater than 25 MeV.

However, the sharply increasing fission cross sections in target mass region lighter than radium, having lower Z^2/A

value and projectile energy up to hundreds of MeV, first extensively investigated by Fairhall (Fa56), made the energy dependence of fissility appear likely at least for the low Z^2/A nuclides (although it is not absolutely necessary owing to the long deexcitation chain).

Whether the dependence of fissility is on the excitation energy or the Z^2/A value, or both, has been a point of debate for many years. Part of the reason for the controversy is that no complete set of experimental data were available to allow a detailed examination of the problem.

A2. Theoretical approach to fission competition

Dostrovsky, Frankel, and Rabinowitz (Do58) were among the first to calculate the fission competition. They used the Bohr-Wheeler formulation of fission width (Bo39) in conjunction with a Monte Carlo type evaporation calculation to compare the total fission cross sections with experimental results on the ^{238}U(p,Fission) reaction with protons to 460 MeV. The detailed predictions should be treated with reservation despite the good fit to the experimental data, since the charge, mass, and excitation energy of residual nuclei, or implicitly the spallation reaction cross sections, in the cascade calculation were parameters.

The opposite approach, evaluating the spallation residues rather than the fission cross sections for the Th,U(p,Spallation) reactions with 340 MeV protons by using the late version

of the Monte Carlo calculation (Me58), was performed by Lindner and Turkevich (Li60). They attempted to extract information about energy dependence of the fissility which best fit the experimental data. Unfortunately the unreliability of the early day intranuclear cascade calculation prevented a definitive answer to whether the fission-evaporation competition is energy dependent.

Hahn et al. (Ha72) calculated the $^{231}Pa,^{232}Th$(p, Spallation) reaction cross sections with protons to 63 MeV, using the Compound-nucleus Model with fission on one hand and the Intranuclear Cascade Model combined with a Monte Carlo calculation, including fission competition in the compound-nuclear deexcitation phase, on the other. Based on the assumption that the fissility is only dependent upon the identity of the fissioning nucleus, they concluded that neither model was successful in interpreting all experimental data.

Suk, Crawford, and Moore (Su74) measured and calculated the ^{232}Th(p,6n) and (p,7n) reaction cross sections with protons to 100 MeV. They used a refined Jackson Model (Ja56) with fission competition as a normalization factor. They found an energy independent fissility that gave good fit to the experimental data. However, their conclusion should be treated with reservation since in their calculation the nuclear temperature and the excitation energy associated with the excited nucleus along the deexcitation chain were

parameters, in addition to the assumption that charged particle emission was negligible.

More recently, Delagrange, Fleury, and Alexander (De78) calculated both spallation and fission reaction cross sections of the U(α,X) reaction with alpha energies to 40 MeV, utilizing the Pre-equilibrium, geometry-dependent Hybrid Model coupled with evaporation, developed by Blann (Bl75). Though the approach is far more realistic than those in earlier works, they concluded that fits of spallation results under fission competition required as many as 5 to 13 times the changes on the parameters from those in non-fission fit. This conclusion, however, should not be interpreted as the failure of the well established Pre-equilibrium de-excitation process, but rather as a failure of their fission-evaporation competition.

In all, the unsuccessful theoretical approaches of previous investigations are due to the uncertainty of either the formulation of the fissility, or the treatment of fission in the reaction model, or even the reaction model itself.

A3. Nuclear charge dispersion in fission

Although no theory exists which suitably explains the nuclear charge distribution in fission, various hypotheses have been made. Three of these are presently in general use: (1) the Equal Charge Displacement (ECD) rule, first introduced by Glendenin, Coryell and Edwards (Gl49), assumes that

the most probable charge Z_p for light and heavy fragments A' in fission are equally distant from the corresponding $Z_A(A')$, the most stable charge for the isobar A'; (2) the Minimum Potential Energy (MPE) hypothesis, first proposed by Present (Pr47) and outlined by Way and Wigner (Wa48), suggests that an equilibrium be attained between the primary fragments at scission and that the sum of the nuclear potential energy be minimized; and (3) the Unchanged Charge Distribution (UCD) postulate, first suggested by Goeckermann and Perlman (Go48,49), assumes that the Z_p for both primary fragments maintains the neutron to proton ratio of the fissioning nucleus.

Despite the controversy of these different aspects, in general, it may be stated that the ECD rule agrees well with low energy fission data, the MPE hypothesis correlates low / medium energy fission data, and the UCD postulate gives satisfactory predictions among high energy fission data. This distinction, however, is not made without a great deal of uncertainty and conflicting reports have been made. For instance, if one studies the fit to experimental Z_p data and measured fractional chain yields in the $^{232}Th(p,Fission)$ reaction with protons to 90 MeV, the following conflicting reports are found to have been made by previous investigators.

Pate (Pa58) calculated the most probable charge required to fit the experimental Z_p data in the fission product mass region 130-135 with protons to 87 MeV; he found that the

charge dispersion in this mass region proceeded predominantly via the ECD rule rather than via the UCD postulate. Based upon each postulate, Freid, Anderson, and Choppin (Fr68) calculated the fractional chain yield for ten fission products for 11 MeV proton fission; the best fit was obtained by the ECD rule. However, Tofe (To69) used a more sophisticated mass equation to recalculate their results and found that the best fit was credited to the MPE hypothesis, although that calculated by the ECD rule was almost as satisfactory. Benjamin et al. (Be69) also calculated the most probable charge in fission product mass region 130-138 with protons to 85 MeV; they found that neither the ECD rule nor the UCD postulate could fit the experimental data. McGee, Rao, and Yaffe (Mc71) evaluated the Z_p for product mass region 90-98 with protons to 85 MeV; they found that the experimental Z_p data were lying closer to those based on the UCD postulate than to those based on the ECD rule. More recently, Eaker and Choppin (Ea76) calculated the fractional chain yield of many fission products for 15.6 MeV protons using the three different postulates; they concluded that the MPE hypothesis gave the best fit to the experimental data.

It is obvious from the example of the $^{232}Th(p,Fission)$ reaction discussed above that none of the postulates have successfully become a general rule to explain the charge dispersion problem at incident proton with energies to 90 MeV. The multiplicity of charge distribution concepts and

inconsistent results in previous investigations are due to: (1) no reaction model can successfully predict the competition between fission and spallation simultaneously, thus reliable information about fission, such as the identity of the fissioning nuclide, its excitation energy, and the specific fission probability, could not be obtained; (2) no thorough understanding of the post-fission properties such as the excitation energy division between primary fragments is available; and (3) the predictions, in particular the MPE hypothesis, are very sensitive to the mass equation used. A sophisticated formula may yield a completely different prediction from those using simplified formulas.

Again the first step toward the clarification of charge distribution in fission is using an appropriate reaction model with fission option. It must be recognized that even using a proper reaction model with fission option, a correct treatment of post-fission properties, and a sophisticated mass equation may not necessarily guarantee that any single postulate will satisfy all the experimental results, especially in reactions where multi-chance fission is possible.

B. Present Work

Among several reaction models developed in recent years, the Pre-equilibrium / Exciton Model derived by Gadioli and Milazzo-Colli (Ga73) has proved to be highly successful; in

particular, experimental results of more than 100 spallation reactions induced by protons to 100 MeV in the spallation residues mass region 38-201 were well explained by this model in (Ho77), (Ho77A), (Ga77), (Ga77A), (Fe79A), and (Bu80). This reaction model, however, is not necessarily conclusive without extending the prediction to heavy mass region with mass numbers A > 220 where fission plays an important role.

B1. Fission competition and nuclear charge dispersion

During the preparation of this work Gadioli provided his latest version of the calculation, based on the Pre-equilibrium / Exciton Model for nuclear reaction with a newly developed fission option, to the present author. This calculation, originating from the theoretical fit to the experimental fissility in zero energy pion-induced fissions in (Ga78), is outlined as a two-stage deexcitation process with fission option in the latter.

Fission has been assumed by (Ga78) to appear only at the second stage of the calculation, the evaporation stage. This is because the fission is highly unlikely to occur in the first stage, the pre-equilibrium stage, where a collective motion involving only a few nucleons occurs. The various events occurring in the second stage are estimated by means of a Monte Carlo procedure similar to the one introduced by Dostrovsky et al. (Do59). The excited nucleus in the

evaporation chain is given the option of fission by computing a fission width, Γ_f, which has been taken as a function of both Z and A, and the excitation energy of the nucleus. The emission of charged particles, protons, and alphas is not ignored in the calculation.

According to Gadioli, Gadioli-Erba, and Hogan (Ga77), the expressions used for neutron, proton, and alpha widths are the ones in (Do59) divided by the square of the average excitation energy, $\overline{U}^2$, in order to take into account the pre-exponential energy dependent factor of level density expression, which was neglected in original Dostrovsky formulas:

$$\Gamma_i = \frac{\mu_i r_{oi}^2 A_i^{2/3} (2s_i + 1)}{\overline{U}_i^2 \, 2\pi\hbar^2 \, a_i \rho(E)} \cdot \left[\frac{3}{4a_i} (x_i^2 - 2x_i + 2) + \beta(x_i - 1) - (E - B_i - C_i - \Delta_i) \right] \cdot e^{x_i} \qquad (01)$$

where μ_i = reduced mass of the reaction system,

r_{oi} = radius parameter, from (Ga77),

s_i = spin of the emitted particle i,

$x_i = 2 \cdot [a_i \cdot (E - B_i - C_i - \Delta_i)]^{\frac{1}{2}}$,

$a_i = A_i/8$, 1/MeV,

B_i = binding energy of emitted particle i, from (Wa71),

$\beta = \frac{2.12\, A_i^{-2/3} - 0.050}{0.76 + 2.2\, A_i^{-1/3}}$ for neutron, = 0 otherwise,

C_i = Coulomb barrier for the emission of particle i,

Δ_i = pairing energy of the residual nucleus A_i after the emission of particle i, from (Ne62),

$\rho(E)$ = level density of A_i at excitation energy E.

The same modification, introduced by (Ga78), is also applied to the energy dependent fission width formula from (Va73):

$$\Gamma_f = \frac{[2\sqrt{a_f(E-B_f-\Delta_s)} - 1] \cdot \exp[2\sqrt{a_f(E-B_f-\Delta_s)}]}{[\bar{U}_s^2 \cdot 4\pi a_f \cdot \rho(E)]} \qquad (02)$$

where $\bar{U}_s$ = average excitation energy at saddle point,

$\rho(E)$ = level density of the fissioning nucleus at excitation energy E,

B_f = fission barrier, from (Ga78),

Δ_s = pairing energy modified at the saddle point by -0.5 MeV from (Ne62), as discussed in (Ga78),

a_f = level density parameter of the nucleus when deformed to the saddle configuration, 1/MeV.

Several points in this fission added program should be specifically noticed:

(1) The fission barrier, B_f, is defined only by its height, the barrier is treated as single peaked; no account is taken of its detailed structure. Fission is assumed to take place above the barrier with unity transmission coefficient and below the barrier with zero transmission. The overall calculation based on this treatment of B_f is not severely affected by this assumption except in the case of low excitation energy.

(2) No account is taken of angular momentum effects in the

calculation of widths Γ_i and Γ_f. As mentioned in (Ga77), it is difficult to define spin distribution at the beginning of the calculation where the excitation energy is shared only among a few excitons. It is more difficult to establish such a distribution after the nucleus has completed the pre-equilibrium cascade later. Although angular momentum may be expected to play an important role in reactions induced by high energy alpha particles and heavy ions, it is less likely that its effects seriously alter the result of proton induced reactions.

(3) Ratio of a_f/a_n is treated as the only freely variable parameter in the calculation. Although experimental values of the neutron level density parameter a_n are well established (La61), little information is available for a_f.

In charge dispersion studies, a modified version of the provided program code is made and used in this work to evaluate the detailed fission information such as the identity of the fissioning nuclide, its excitation energy, and the specific fission probability. The calculation is then extended to evaluate the numbers of post-fission neutrons; this is indispensable for the calculation of Z_p. By using the Droplet Model mass equation, the most recent mass formula derived by Myers (My77), the Z_p based on the ECD, MPE, and UCD postulates may be evaluated.

B2. Experiment and calculation

In this work thorium was chosen as the target nuclide for the investigation of proton induced reaction and fission. This system was taken because: (1) thorium represents a midway choice between the highly fissionable transuranium nuclei for which (p,Spallation) reaction has very low cross sections compared to that of fission, and the lighter nuclei with $Z < 90$ where fission plays only a minor role owing to the high fission barrier; and (2) the experimental data of the most probable charge Z_p in the ^{232}Th(p,Fission) reaction are very abundant, mainly investigated by Yaffe and co-workers in (Pa58A), (Fo66), (Be69), (Mc71), (Di78), and (Di79); it provides a critical test of the present treatment of the pre- and post-fission properties.

There are three main problems to measuring ^{232}Th(p, Spallation) excitation functions. First, spallation reaction cross sections are relatively small in comparison with fission cross sections at proton energies above 20 MeV; secondly, radiochemical separations on spallation products are necesssary owing to the heavy interference from fission products; and lastly, contamination of the spallation products from either the decay of other spallation products or natural daughters of ^{232}Th is frequently encountered. Hence, measurements of spallation excitation functions in previous studies with incident proton energies up to 100 MeV were confined to (p,Xn) studies with X = 1, 3, 5-7 and (p,2pXn) studies with

X = 3-7 in (Te52), (Te55), (Me56), (Le61), (Le62), (Br62), (Ga62), (Ga63), and (Su74). Some sporadic measurements on (p,pXn) with X = 1, 4-6 have also been made in the same energy range mentioned above by (Le61,62).

It is the goal of this work to measure more spallation excitation functions, namely, (p,pXn) with X = 1, 4-6 and (p,3pXn) with X = 5-7 with incident proton energies between 13 and 90 MeV, to show how these measurements, together with other spallation excitation functions and total fission cross sections reported previously can be well explained by the Pre-equilibrium / Exciton Model with the newly developed fission option. Later on, the calculation is extended to the evaluation of Z_p on the basis of each charge distribution postulate in fission, to show that the reported experimental data of Z_p can be fitted very well by correlating the MPE hypothesis, or to a lesser extent the ECD rule, to asymmetric fission and the UCD postulate to symmetric fission. Finally, a simple $(Z^2/A)_{A/S}$ value is proposed in this work to separate the asymmetric and symmetric fissions on the basis of the identity of the fissioning nucleus rather than the traditional excitation energy; this asymmetric/symmetric split has also found support from a wide range of observed mass distribution in fission.

II

EXPERIMENTAL PROCEDURES, DATA TREATMENT, AND RESULTS

A. Irradiation

A1. Target arrangement

The thorium metal foil was of natural thorium with a thickness of about 0.0076 cm. It was cleaned in 0.06M HNO_3 solution for several hours, washed in distilled water, ethanol, and acetone, and put in a desiccator before assembling for irradiation. The copper monitor foil had a thickness of about 0.0051 cm. The degradation in the proton bombardment energy, caused by the target/monitor thickness, was computed at each bombarding energy using the data of Williamson, Boujot and Picard (Wi66) and was found to lie within the ±2 MeV limit for proton in the internal beam energy spread of the McGill Synchrocyclotron, except in the case of the lowest bombarding energy.

To eliminate recoil losses, three copper and three thorium foils were used. Only the middle foils of copper and thorium were processed chemically, while the front and the back foils acted as catchers to compensate the recoiled particles of interest from both directions. Arrangement of the target assembly is shown in Figure 01(a).

The foils used in target assembly were trimmed on three sides prior to irradiation in order to make sure that identical surface area of both target and monitor foils were exposed to the beam. The entire target assembly was then fixed on a target holder which in turn was attached to the

Figure 01

(a) Target assembly

(b) Target position

Figure-01(a)

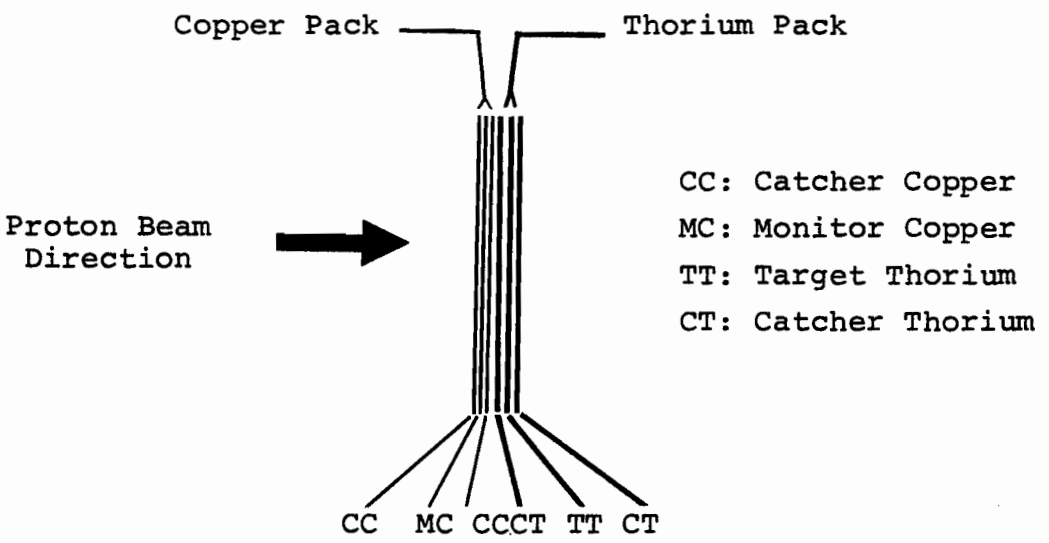

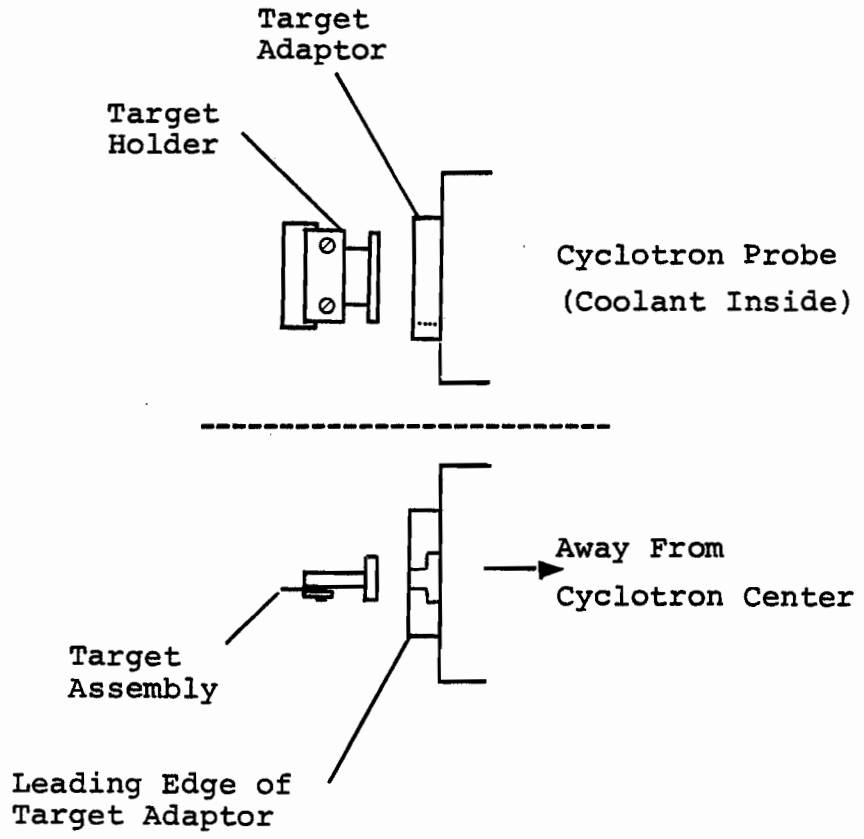

Figure-01(b)

cyclotron probe for irradiation. The monitor pack was placed upstream from the target pack, so as to measure a beam which has not been degraded in the thorium target pack and to avoid possibilities of reactions in the monitor foil induced by secondary neutrons produced from thorium. The physical arrangement is shown in Figure 01(b).

A2. Proton beam monitoring

Irradiations were performed in the internal circulating proton beam of the McGill Synchrocyclotron which was refitted and reconditioned in mid-1978.

Beam energy. Precise bombarding energy was obtained from insertion of the cyclotron probe at the appropriate radial distances according to the data obtained by Moore (Mo75) with correction for the gap from the target assembly to the leading edge of the target adaptor, and proton energy loss calculation. The relation between bombarding energy and distance from center is illustrated in Figure 02. Bombarding energies of 13, 18, 20, 30, 40, 45, 49, 51, 57, 64, 70, 75, 85, and 90 MeV were obtained in this work.

Irradiation time. The irradiation period, t_I, is not only a factor in evaluating the cross sections of reaction products of interest, but also directly related to the health hazard from induced radioactivity in target. In order to obtain a good experimental result, a long t_I is desirable,

Figure 02

McGill Synchrocyclotron internal beam energy

vs. target radius, after Moore (Mo75)

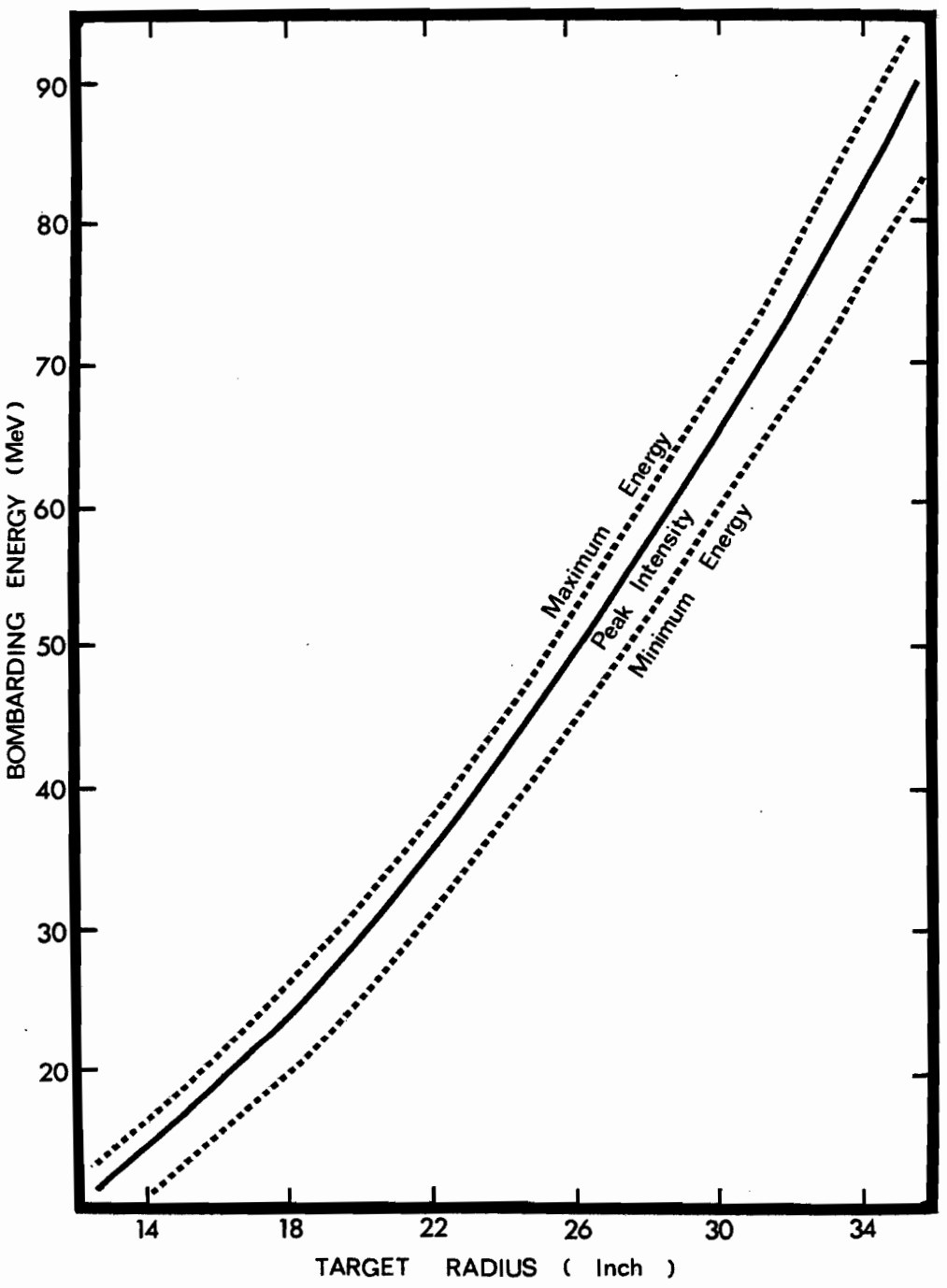
BOMBARDING ENERGY (MeV)
90
80
70
60
50
40
30
20
14
18
22
26
30
34
TARGET RADIUS (Inch)
Maximum Energy
Peak Intensity
Minimum Energy

while to keep the radiation hazard to a minimum, a short t_I is preferable. Compromise between these extremes gives irradiation times up to five minutes in this work.

Beam monitoring. The cross section of $^{65}Cu(p,pn)^{64}Cu$ reaction at various bombarding energies using the McGill Synchrocyclotron proton beam has been utilized in this Radiochemistry Laboratory to monitor the internal beam for quite a long time. The most recent measurement with bombarding energies ranging from 23.2 to 102 MeV were made by Newton et al. (Ne73). On the other hand, the fission cross section of cumulative $^{232}Th(p,Fission)^{143}Ce$ is also a convenient beam monitor for thorium target. A full investigation of this potential monitoring cross sections is implemented in this work.

B. Post Irradiation Chemistry

B1. Radiochemical separations

After irradiation, the target assembly was dismantled and the target thorium foil was weighed, then dissolved in 3 mL of hot, concentrated HCl in the presence of five drops of 20:1 HF. In this dissolving process HF served as a catalyst and although the amount needed was very small, about 0.0003 mole, its presence for rapid dissolution was essential. After dissolution was completed within one

minute, the volume was made up to 15 mL with distilled water and all the following separations were performed on aliquots from this mother solution.

Thorium purification. Spallation products of the $^{232}Th(p,pXn)Th$ reactions were determined directly from the purified thorium sample. The chemical procedure used in this work was essentially a combination of both Newton, Hyde, and Meinke (Ne49) and Prestwood (Pr58) with simplification since no transuranium elements were present in the irradiated foils. Three principal steps were employed: (a) $Th(IO_3)_4$ precipitation gave separation from the bulk of rare earths fission products; (b) $Th(C_2O_4)_2$ precipitation effected separation from zirconium; and (c) extraction of thorium from $Al(NO_3)_3 / HNO_3$ mixture solution by means of mesityl oxide gave excellent decontamination from radium, the alkali and alkaline earth metal ions. The thorium was finally precipitated as $Th(C_2O_4)_2$ and ignited to convert to ThO_2; in such form it was weighed for chemical yield and mounted for counting. Analyses can be performed in approximately three hours with a chemical yield of about 65%.

Radium separation. Spallation products of the ^{232}Th-(p,3pXn)Ra reactions are assumed both qualitatively and quantitatively to follow barium chemistry. This assumption can be proved valid by comparing results of barium chemical yield (by using a standard Ba-carrier) to radium chemical

yield (by counting the natural ^{228}Ra in secular equilibrium state with natural thorium). The barium chemistry used in this work was the combination from Meinke (Me49) and Warren (Wa58) with slight modification. Three major steps were performed: (a) Ra/Ba were separated from the bulk of thorium by way of precipitation of $Th(OH)_4$ in mother solution; (b) Ra/Ba were separated from other fission products by the specific precipitation in cold as $BaCl_2 \cdot H_2O$ by means of the HCl/ether reagent; and (c) further purifications from fission products were made by $Fe(OH)_3$ and $La(OH)_3$ scavenging procedures. Ra/Ba products were then converted into $BaCrO_4$, dried, weighed for chemical yield, and mounted for counting. In order to obtain a fully cumulative cross section of radium from its beta-unstable precursors, namely francium and radon, radium separations should not be performed until ten hours after the irradiation. Overall analyses were carried out in about three hours with a chemical yield of around 60%.

Cerium isolation. As a potential proton beam monitor for thorium target, ^{143}Ce must be isolated at least two hours after the irradiation in order to get a fully cumulative cross section from among isobars. The cerium chemistry, taken from Glendenin et al. (Gl55), was simple, fast, and effective procedure for cerium isolation. This procedure centered on the solvent extraction of Ce(IV) with methyl isobutyl ketone, later converted to $Ce(C_2O_4)_2$, ignited to

CeO_2, dried, weighed for chemical yield, and mounted for counting. Overall analyses were carried out in about one hour with a chemical yield of around 60%.

Copper purification. Radiochemical processing of copper foils, frequently used for proton beam monitoring purposes in this Radiochemistry Laboratory, is based on the procedure of Kraus and Moore (Kr53). The copper was purified in an ion exchange column and later precipitated as CuSCN, then weighed for chemical yield. The purification was not executed until a day after the irradiation in order to reduce the radioactivity in the foil. Actual analyses were performed in about five hours with a chemical yield of around 60%.

B2. Carrier standardization

For barium chemistry in conjunction with radium chemistry, a 10 mg Ba^{++}/mL standard carrier, added as $Ba(NO_3)_2$ in distilled water, was required. To standardize it, 5 mL of carrier solution was pipetted into a beaker and diluted to 100 mL by distilled water. 10 mL each of 6 M $C_2H_4O_2$ and 3 M $NH_4C_2H_3O_2$ was added. The solution was heated to boiling and then 5 mL of 1.5 M Na_2CrO_4 was added dropwise with stirring for about one minute. The $BaCrO_4$ was cooled and filtered through a sintered glass crucible, washed by distilled water and EtOH, dried at 110°C, cooled and weighed as $BaCrO_4$.

Four standardizations were performed with 0.34% uncertainty.

For the cerium chemistry, a 10 mg Ce^{+++}/mL standard carrier, added as $Ce(NO_3)_3 \cdot 6H_2O$ in distilled water, was required. To standardize it, 5 mL of cerium carrier was pipetted into a beaker and diluted to 20 mL by distilled water. The solution was warmed while adding 50 mL saturated $(NH_4)_2C_2O_4$ solution. Heating was continued until the precipitates had coagulated. It was then cooled in an ice-bath for 15 minutes and filtered as $Ce(C_2O_4)_2$, ignited in a porcelain crucible in a 900°C oven for half an hour, cooled and weighed as CeO_2. Nine standardizations were performed with 0.61% uncertainty.

For thorium and copper purifications, no standard carriers were required since the target and monitor foils themselves acted as carriers. However, in order to count correctly the radioactive ^{228}Th, ^{228}Ra, and ^{224}Ra daughters in secular equilibrium with ^{232}Th, a standardized sample of natural thorium was required. A clean, unirradiated thorium foil was dissolved and converted to ThO_2, by a chemistry similar to that in the last section less decontamination. This standard sample had exactly the same geometry as those irradiated thorium and radium samples. Therefore, reaction products such as ^{228}Th, ^{228}Ra, and ^{224}Ra in irradiated samples can be compared to the standard sample with a definite amount of corresponding radionuclides in it.

B3. Counting the samples

After each chemical separation procedure, samples except copper were mounted at the center of a pre-cut standard 3" x 2.5" cardboard, covered by two layers of 7 mg/cm^2 3M-MAGIC scotch tape. The radioactive sample was secured under this arrangement. Counting of the specific radioactivity was taken at least three times for each half-life period for three half-lives. In the case of 1.9-year ^{228}Th, measurement was extended to seven months.

For copper samples, weighed CuSCN was dissolved in a standard glass vial with 10 mL concentrated NH_4OH. After the copper dissolved completely, the vial was sealed and the liquid sample was ready for counting. The activity of the 12.8-hour ^{64}Cu is measured as the 511 keV gammas produced following the annihilation of the positrons; however, the 3.3-hour ^{61}Cu is also an annihilation gamma emitter in the copper sample. Hence, the measurement was delayed at least three days after the end of irradiation until most of the ^{61}Cu decayed away.

C. Radioactive Detection Systems

C1. Lithium drifted germanium, Ge(Li), detectors

Spallation and fission products from thorium, together with their daughters in decay chains studied in this work were determined by making use of the excellent resolving

power of lithium drifted germanium, or Ge(Li), detectors to select the characteristic gamma rays associated with these radionuclides. If the gamma ray energies from the decay of radionuclides are known, assignments of the "fingerprint" peaks in the gamma ray spectrum to a specific radionuclide can be made with a high degree of certainty. There were two Ge(Li) detectors used in this work:

40 cm^3 Ge(Li) detection system. This system consisted of a 41.7 cm^3 Ge(Li) detector (ORTEC Model 8101-0725), a multi-channel analyzer (CANBERRA Model 8100), a high voltage power supply (ORTEC Model 456), a preamplifier (ORTEC Model 120-2B), and a digital recorder (HP Model 5055A). A block diagram of the system is shown in Figure 03(a). The resolution of the system, in the gamma ray energy range pertinent to this work, was found to be 2.1% for 164 keV gamma of ^{231}Th and 0.21% for 911 keV gamma of ^{232}Th, corresponding to the Full Width at Half Maximum (FWHM) of the said peaks.

30 cm^3 Ge(Li) detection system. This system consisted of a 31.25 cm^3 Ge(Li) detector (ORTEC Model 8001-0536), a multi-channel analyzer (NUCLEAR DATA Model 2200), a high voltage power supply (Baird-Atomic), a preamplifier (ORTEC Model 120-2F), a spectroscopic amplifier (ORTEC Model 451), a cathode-ray tube (HP Model 1208B), and a digital printer (Mohawk DSS-1200). A block diagram of the system is shown in Figure 03(b). The resolution of the system, in the gamma

Figure 03

Block diagrams of detection system:

(a) 40 cm^3 Ge(Li)

(b) 30 cm^3 Ge(Li)

(c) 3" x 3" NaI(Tl)

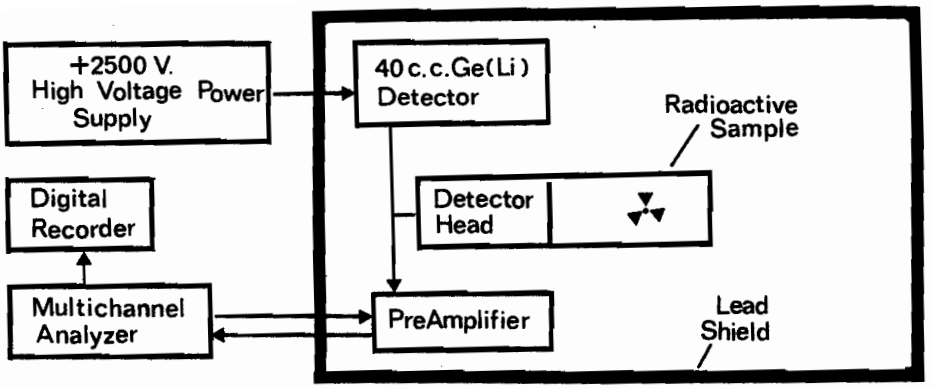

Figure – 03 (a)

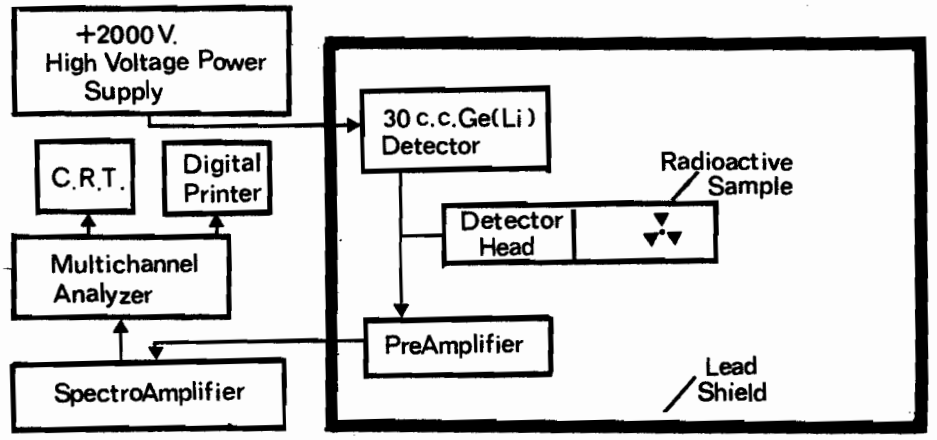

Figure – 03 (b)

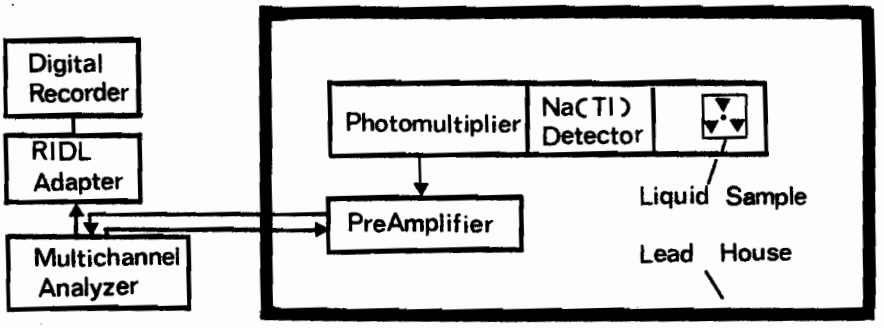

Figure – 03 (C)

ray energy pertinent to the early stage of this work, was found to be 0.95% for the 240 keV gamma of ^{228}Th corresponding to the FWHM of the said peak.

In both systems the Ge(Li) detector, the preamplifier, and the radioactive sample were placed inside a thick lead shield to minimize the radioactive interference from the environment. The interior of the lead shield was covered with copper foil and a lucite sheet to reduce gamma ray back scattering which increased the error of counting. Each measurement was recorded with the starting time of counting, the duration of counting, and the percentage of dead-time loss. This information was indispensable for later data treatment.

C2. Thallium activated sodium iodide, NaI(Tl), detector

Measurement of the liquid CuSCN sample required a scintillation detection system. This system consisted of a 3" x 3" NaI(Tl) detector (HARSHAW Type-686), a photomultiplier (RCA 6342-A), a multi-channel analyzer (NUCLEAR CHICAGO RIDL 34-12B), a preamplifier (RIDL Model 31-15), an adaptor (RIDL Model 78-1), and a digital recorder (HP Model 562A). A block diagram of the system is shown in Figure 03(c). The NaI(Tl) detector, the photomultiplier, the preamplifier, and the radioactive sample were put in a small lead cave having iron and copper layers on the interior wall to diminish the fluorescent radiations from lead.

C3. Calibration of the detection systems

The Ge(Li) detection systems must be calibrated for both energy and efficiency. Energy calibration, necessary for identification of various gamma ray peaks, may be done by counting standard radionuclides along with samples of interest.

40 cm^3 Ge(Li) detection system. This system has been calibrated in this work for both energy and absolute efficiency (over gamma ray energies between 80 keV and 1775 keV) by using standard radioactive point sources. The primary calibration is made at 149 mm source-to detector distance with 0.25" plastic absorber in place to prevent coincidence events like beta-gamma summation.

30 cm^3 Ge(Li) detection system. This system has also been calibrated for both energy and absolute efficiency over gamma ray energies between 100 keV and 2000 keV by Fowler (Fo72). The primary calibration had been made at 108 mm source-to-detector distance with a thick 0.375" plastic absorber placed right in front of the detector can.

NaI(Tl) detection system. The absolute efficiency for the annihilation gamma is determined by using a liquid ^{22}Na standard source, under geometrical condition identical to that for the ^{64}Cu samples. The use of ^{22}Na for calibration is dictated by the fact that the maximum energy of its

positrons, 545 keV, is not far away from that of ^{64}Cu, 656 keV. The contribution of high energy gammas to the 511 keV gamma by pair-production is assumed to be negligible in both the copper sample and the standard source.

D. Data Treatment

The gamma ray peak areas, which are representative of the total net counts of specific gamma rays, were determined by summing over counts registered on each spectral channel within a region of interest, followed by subtracting of the spectral background in the same region. Calculated peak areas were then used as input for computer code EXPONENT for further analyses.

The EXPONENT program code, introduced by Newton (Ne71), is a FORTRAN program which analyzes radioactive decay curve data by a linear least squares technique. The initial counting rate, calculated by the EXPONENT, is then corrected for absolute detector efficiency, gamma ray abundance, and chemical yield in order to convert it into initial disintegration rate according to the following equation:

$$D(0) = \frac{A(0)}{60 \cdot e_{ff} \cdot S \cdot Ir \cdot Y \cdot F} \qquad (03)$$

where $D(0)$ = initial disintegration rate at time zero for the radionuclide, Bq,

A(0) = initial counting rate at time zero for the radionuclide, cpm,

e_{ff} = absolute efficiency of the detection system at the specific gamma ray of the radionuclide, counts/gamma,

S = shelf ratio of e_{ff} at the actual shelf used to that at the standard shelf in the detection system,

Y = separation factor of the chemistry pertinent to the radionuclide,

F = dilution factor in the chemical separation,

Ir = gamma ray abundance, gamma/disintegration.

In this equation, $e_{ff} \cdot S$ is associated with the detector efficiency, $Y \cdot F$ is associated with the chemical yield; for radionuclides pertinent to this work, the gamma ray abundance and half-lives are given in Table 01.

D1. Cross section calculation

During irradiation, growth and decay of the reaction products induced by spallation reaction can be expressed by the following differential equation:

$$\frac{d}{dt}N(t) = -\lambda \cdot N(t) + B \cdot w \cdot N_o \cdot \sigma/(M \cdot A) \qquad (04)$$

where N(t) = number of the nucleus of the spallation product produced at time t after the initiation of the irradiation,

λ = decay constant of the spallation product, s^{-1},

B = beam intensity, number of protons/s,

w = weight of the target, g,

Table 01

Nuclear properties of products observed in this work.

Radio-nuclide	Half-life*	Characteristic gamma ray(s), keV	Gamma ray abundance (%)	Reference
^{231}Th	25.52 H	163.1 165.0	0.159	(Sc77)
^{228}Th	1.91313 Y	238.6 (^{212}Pb) 241.0 (^{224}Ra)	48.8	(El76)
^{227}Th	18.718 D	234.9 236.0	11.6	(Ma77)
^{226}Th	30.9 M	242.1	0.866	(To77)
^{228}Ra	5.75 Y	911.1 (^{228}Ac)	29.000	(El76)
^{225}Ra	14.8 D	439.7 (^{225}Ac)	21	(Ma73)
^{224}Ra	3.66 D	241.0 238.6 (^{212}Pb)	48.8	(El76)
^{223}Ra	11.434 D	154.2	5.59	(Ma77)
^{143}Ce	33.0 H	293.3	42	(Tu78)
^{64}Cu	12.82 H	511.0	38.6	(Ne73)

* Half-life is represented by M - minutes, H - hours, D - days, and Y - years.

N_o = Avogadro's number, atoms/mole,

σ = cross section of the spallation reaction, cm^2/atom,

M = atomic weight of the target, g/mole,

A = effective area for radiochemical work, cm^2.

Solving Eq. (04) at the end of the irradiation for both the monitor reaction and the $^{232}Th(p,Spallation)$ reaction, and combining with Eq. (03), the cross section of the spallation reaction can be expressed as:

$$\sigma_p = \sigma_{Cu} \frac{A_p(t_I) \cdot e_{ff_{Cu}} \cdot S_{Cu} \cdot Ir_{Cu} \cdot Y_{Cu} \cdot F_{Cu} \cdot b \cdot w_{Cu} \cdot M_{Th} \cdot (1 - e^{-\lambda_{Cu} \cdot t_I})}{A_{Cu}(t_I) \cdot e_{ff_p} \cdot S_p \cdot Ir_p \cdot Y_p \cdot F_p \cdot w_{Th} \cdot M_{Cu} \cdot (1 - e^{-\lambda_p \cdot t_I})} \qquad (05)$$

where b is the ^{65}Cu abundance in natural copper and subscripts p and Cu represent the spallation product and the copper monitor, respectively. Monitor cross sections of the ^{65}Cu-$(p,pn)^{64}Cu$ reaction used in this work are given in the second column in Table 02. On the other hand, if the cumulative fission reaction $^{232}Th(p,Fission)^{143}Ce$ is used as monitor, Eq. (05) can be further simplified by eliminating all weighing factors:

$$\sigma_p = \sigma_{Ce} \frac{A_p(t_I) \cdot e_{ff_{Ce}} \cdot S_{Ce} \cdot Ir_{Ce} \cdot Y_{Ce} \cdot F_{Ce} \cdot (1 - e^{-\lambda_{Ce} \cdot t_I})}{A_{Ce}(t_I) \cdot e_{ff_p} \cdot S_p \cdot Ir_p \cdot Y_p \cdot F_p \cdot (1 - e^{-\lambda_p \cdot t_I})} \qquad (06)$$

Table 02

Monitoring cross sections used in this work.

Incident proton energy (MeV)	Cross section of ^{64}Cu (mb)	Cross section of ^{143}Ce (mb)
13	--	5.0 ± 4.0*
18	--	19.1 ± 2.9*
20	327.4 ± 19.3**	20.8 ± 2.4
30	400.0 ± 23.6	21.2 ± 3.2
40	--	17.8 ± 2.7*
45	195.0 ± 11.6	15.2 ± 2.3
49	--	14.2 ± 2.1*
51	--	13.8 ± 2.1*
57	170.0 ± 10.0*	12.7 ± 1.9*
64	--	12.0 ± 1.8*
70	155.0 ± 9.2	10.7 ± 1.6*
75	151.1 ± 8.9	10.3 ± 1.2
85	141.3 ± 8.3	9.0 ± 1.4
90	--	8.9 ± 1.3**

* Interpolated value; ** extrapolated value.

D2. Contamination

For simple cases without any contamination, the reaction cross section can be calculated from Eq. (05) or (06) with all the given data and experimental results at the right hand side of the equal sign; however, for those cases in which there is contamination, calculation of the reaction cross section is complicated and some correction factors should be added to Eqs. (05) and (06). Contamination may come from either the decay of other reaction products or the decay of those radionuclides in secular equilibrium with natural thorium. Details of the contamination for each case are discussed below:

^{232}Th(p,p4n)^{228}Th. Contamination includes (1) natural ^{228}Th in secular equilibrium with natural thorium, (2) ^{228}Th decayed from the 22-hour ^{228}Pa, induced by the (p,5n) reaction, and (3) ^{228}Th decayed from the 6.1-hour ^{228}Ac, induced by the (p,2p3n) reaction.

^{232}Th(p,p5n)^{227}Th. Contamination arises from the 38-minute ^{227}Pa, induced by the (p,6n) reaction.

^{232}Th(p,p6n)^{226}Th. Contamination includes (1) ^{226}Th decayed from the 1.8-minute ^{226}Pa, induced by the (p,7n) reaction, and (2) ^{226}Th decayed from the 29-hour ^{226}Ac, induced by the (p,2p5n) reaction.

^{232}Th(p,3p6n)^{224}Ra. Contamination includes (1) natural

^{224}Ra, ^{228}Ra, and ^{228}Th in secular equilibrium with natural thorium, (2) ^{224}Ra decayed from reaction induced 1.9-year ^{228}Th, and (3) ^{224}Ra decayed from the 2.9-hour ^{224}Ac, induced by the (p,2p7n) reaction.

$^{232}Th(p,3p7n)^{223}Ra$. Contamination includes (1) ^{223}Ra decayed from the 18.7-day ^{227}Th, induced by the (p,p5n) reaction, and (2) ^{223}Ra decayed from the 2.2-minute ^{223}Ac, induced by the (p,2p8n) reaction.

In the cases mentioned above, the reaction cross section calculated from Eqs. (05) and (06) comprises the true cross section plus some contaminating parts which are in turn a function of the irradiation period, the time of chemical separation, half-life of the relevant radionuclide, branching ratio of the contaminating decay, cross section of the contaminating reaction, and the amount of natural thorium. A detailed derivation of the effect of contamination may be found elsewhere (St66).

For contamination from the decay of natural radionuclides, correction can be made by comparing the activities to those in the standard natural thorium sample; for contamination from the decay of other spallation reaction products except the (p,2p8n) reaction, correction can be calculated using those spallation cross sections investigated in this work, together with others in (Br62), (Ga63), and (Su74). Since no experimental cross sections of $^{232}Th(p,2p8n)^{223}Ac$ have

been measured, an estimate is required in order to evaluate its degree of contamination on the $^{232}Th(p,3p7n)^{223}Ra$ reaction. It is assumed to be 2 ± 2 mb above reaction threshold of the (p,α6n) reaction, 51 MeV; this estimation is derived from the fact that all (p,2pXn) reactions with X = 3-7 have cross sections around 2 mb in the proton energy range pertinent to this work. Since the 2.2-minute ^{223}Ac completely decays to the ^{223}Ra via a branching ratio of 1% before the initiation of the radium chemistry, a 0.02 ± 0.02 mb contamination is deducted from the cross section calculation of the (p,3p7n) case.

D3. Error analysis

In this work two kinds of errors occur: systematic errors and random errors. The systematic error is associated with imprecise knowledge of certain constants and may affect all the results in the same way once the constants have been adopted. The random error is associated with imprecisions in measurement, in particular the inherent randomness of the radioactive decay process.

The systematic errors involve reported monitor cross sections, proton beam energy spread, efficiency of the detection systems, and decay schemes including half-lives, branching ratios, and gamma ray abundance. The random errors involve gamma ray peak area determinations, shelf ratios of the detection systems, and chemical yields including weighing,

pipetting, diluting, and timing the separation. For reactions near their threshold, the random error becomes large due to the low activity with a large statistical counting uncertainty; for contaminating cases, the random error also becomes large when the correction approaches the experimental result. All kinds of errors mentioned above, together with representative magnitudes, are listed in Table 03.

The rigorous total error calculation involving the exponential relations in differential equations is tedious. It is considered sufficient for the purpose of this work to give an indicative total error by taking the square root of the sum of the squares on all cited errors. For the cross section calculation, the total error quoted in this work varied from 10% to 26%, except for the extreme cases of those near reaction threshold and those having large deductions arising from contamination.

E. Experimental Results

E1. Monitoring cross sections of ^{143}Ce

The cumulative cross sections of the $^{232}Th(p,Fission)-^{143}Ce$ reaction have been measured by Choppin and Tofe (Ch71), Holub and Yaffe (Ho73), Eaker and Choppin (Ea76), and Diksic (Di78). These measurements are supplemented by the present work with incident proton energies at 20, 30, and 75 MeV. Results of experimental data are plotted in Figure 04, where

Table 03

The systematic and random errors in this work.

Cause	Representative error
Systematic error	
Monitor cross section of ^{64}Cu	5.9%
Efficiency of the 30 cm^3 Ge(Li)	3.0%
Efficiency of the 40 cm^3 Ge(Li)	2.7%
Efficiency of the 3" x 3" NaI(Tl)	1.5%
Half-life	0.7%
Decay branching ratio	0.1%
Gamma ray abundance	3.0%
Random error	
Gamma ray peak area determination	1.0%
Shelf ratio for the Ge(Li) systems	8.0%
Weighing in chemistry	0.2%
Pipetting in chemistry	0.8%
Diluting in chemistry	1.0%
Timing at precipitation	0.7%
Timing at solvent extraction	0.9%
Standard carrier	0.6%

Figure 04

Excitation function of the
$^{232}Th(p,Fission)^{143}Ce_{cum}$ reaction

⊙ : this work

● : after (Di78)

▲ : after (Ea76)

■ : after (Ho73)

▼ : after (Ch71)

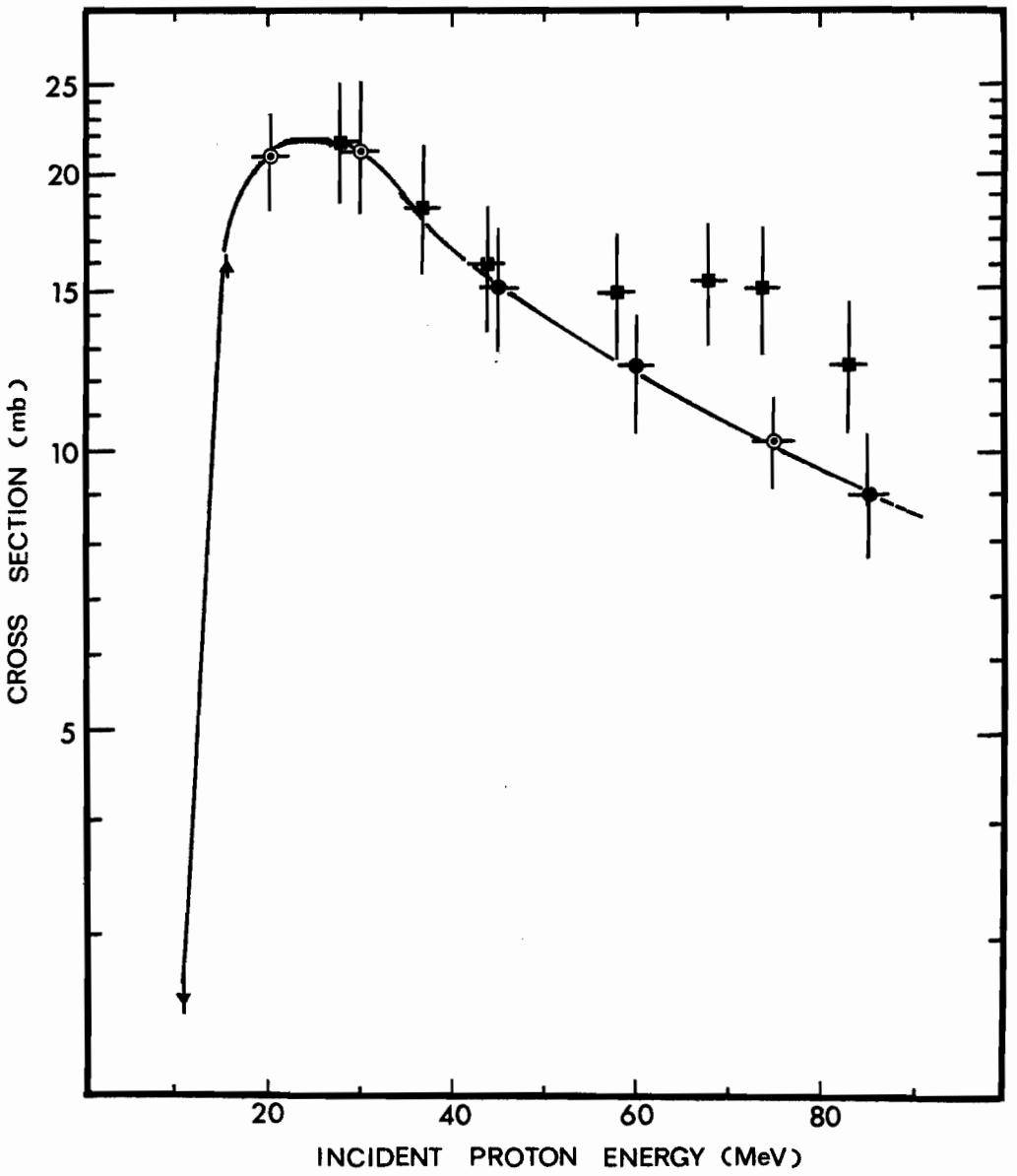
25
20
15
10
5
CROSS SECTION (mb)
20
40
60
80
INCIDENT PROTON ENERGY (MeV)

Holub's results have been modified to take account of the updated ^{64}Cu monitor cross sections.

As mentioned in the previous section, the cumulative cross section of ^{143}Ce is a potential monitor for proton induced reactions on natural thorium. The advantages of using ^{143}Ce, in comparison with using ^{64}Cu, are: (1) elimination of weighing factors (and therefore a reduction in random errors) in the cross section calculation; (2) reduction of the radiation hazard by eliminating the copper foils; (3) a less rapidly varying excitation function in the energy region ranging from 30 to 40 MeV than that of ^{64}Cu; and (4) at least five intense gamma rays suitable for identification using gamma ray spectrometry. However, uncertainty associated with the cross sections for ^{143}Ce is large, about 15% in average, relative to 5.9% in ^{64}Cu; therefore the convenience of using a cerium monitor is balanced by an increase in the systematic error for the calculation. A list of cumulative cross sections of ^{143}Ce used in this work as monitor is given in the third column in Table 02.

E2. Excitation functions of the $^{232}Th(p,pXn)Th$ reactions

Experimental results of these cross sections are listed in Table 04. Excitation functions are plotted against incident proton energy in Figure 05. The individual results are discussed below:

Table 04

Experimental reaction cross sections.

Incident proton energy (MeV)	Cross sections (mb)						
	^{231}Th	^{228}Th	^{227}Th	^{226}Th	^{225}Ra	^{224}Ra	^{223}Ra
13	2.9 ± 2.4	--[a]	--	--			
18	45.8 ± 5.6	--	--	--			
20	96.5 ± 11.2	--	--	--			
30	112.3 ± 12.3	--	--	--			
40	94.1 ± 11.9	6.6 ± 4.2	--	--	--	--	--
45	109.6 ± 13.3	36.6 ± 6.5	0.8 ± 0.5	--			
49	98.6 ± 11.2	36.8 ± 6.6	4.5 ± 1.2	--			
51	85.8 ± 16.3	35.9 ± 6.5	7.8 ± 1.3	1.6 ± 1.2	0.02 ± 0.01	--	--
57	95.6 ± 12.3	58.2 ± 10.2	23.4 ± 2.9	3.8 ± 1.0	0.05 ± 0.03	--	--
64			27.7 ± 3.0		0.19 ± 0.04	--	--
70	100.0 ± 13.5	59.6 ± 6.5	39.8 ± 6.5	21.0 ± 2.7	0.23 ± 0.05	--	0.04 ± 0.03
75	88.5 ± 10.0	63.1 ± 9.0	39.4 ± 4.6	26.9 ± 2.6	0.33 ± 0.05	0.20 ± 0.17	0.29 ± 0.08
85					0.44 ± 0.08	0.53 ± 0.25	0.48 ± 0.12
90	69.9 ± 8.0	42.8 ± 7.4	32.2 ± 3.8	24.1 ± 2.4	0.45 ± 0.08	0.62 ± 0.22	0.49 ± 0.12

[a] Below detection limit.

Figure 05

Excitation functions of the ^{232}Th(p,pXn)Th reaction

◆ : this work

◇ : after (Le61), (Le62)

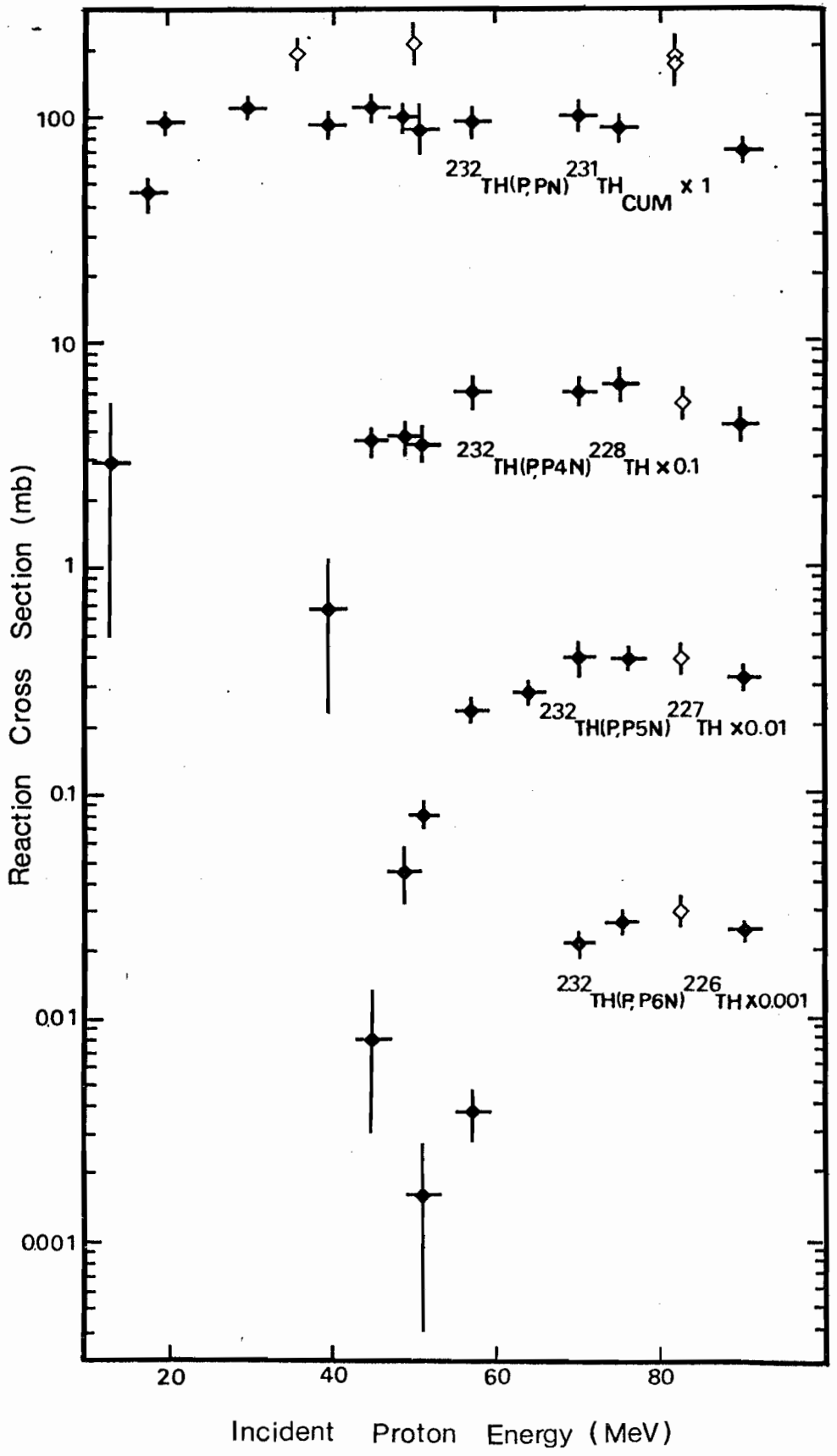
100
10
1
0.1
0.01
0.001
Reaction Cross Section (mb)
232TH(P,PN)231TH CUM x 1
232TH(P,P4N)228TH x 0.1
232TH(P,P5N)227TH x0.01
232TH(P,P6N)226TH x0.001
20
40
60
80
Incident Proton Energy (MeV)

^{231}Th. The average uncertainty of the cumulative cross sections is around 13% except for the one measured at 13 MeV, near the reaction threshold. Also shown in the figure are measurements from Lefort, Simonoff, and Tarrago (Le61,62). Disagreement between Lefort's results and those of the present work is large, a factor of two. Inaccuracy in the early work arises from insufficient information on the decay scheme existing twenty years ago. They measured ^{231}Th using the 39% 0.3 MeV betas; a modern value of these betas is 84% (Sc77). After the correction, Lefort's data agree with the present work very well.

In the thorium chemistry, no attempt has been made to separate the 7.5-minute ^{231}Ac from thorium since the actinium decays completely into ^{231}Th well before the initiation of the chemistry. However, the measured results on ^{231}Th can still be representing the independent cross section of the ^{232}Th(p,pn)^{231}Th reaction since the cross section of ^{232}Th-(p,2p)^{231}Ac is small, about 2 mb above its reaction threshold, 35 MeV. This estimation is similar to that of ^{232}Th-(p,2p8n)^{223}Ac mentioned in the last section.

^{228}Th. The reaction cross sections listed in the third column in Table 04 are those corrected from natural ^{228}Th and the two contaminating reactions, (p,5n) and (p,2p3n). Also shown in the figure is a measurement at 82 MeV from (Le61); in their work alpha particles were counted and the

result does agree well with the present work. The average uncertainty of the cross sections is about 18% except at 40 MeV measurement. At that energy the detection limit is around 2.5 mb both because of the heavy contamination from the decay of ^{228}Pa and because of approaching the reaction threshold.

^{227}Th. The reaction cross sections listed in the fourth column in Table 04 are those corrected for the contaminating reaction (p,6n). The average uncertainty of the cross sections is about 13% except those near the reaction threshold. The detection limit is dependent on the magnitude of contamination from ^{227}Pa and is calculated to be around 0.5 mb. Also shown in the figure is a single data point at 82 MeV from (Le61), which again agrees with the present work.

^{226}Th. The reaction cross sections listed in the fifth column in Table 04 are those corrected for the contaminating reactions (p,7n) and (p,2p5n). The average uncertainty of the cross sections is about 11% except those near the reaction threshold. The detection limit is dependent upon the magnitude of the contamination from the decay of ^{226}Pa and ^{226}Ac, and is calculated to be around 1 mb. Also shown in the figure is again the data point at 82 MeV from (Le61), which is slightly greater than those of the present work. The higher result reported by Lefort's group is actually the sum of the independent cross sections of (p,p6n) and those contamination cross sections from (p,7n) reaction;

otherwise, their result does agree with measurement in this work.

E3. Excitation functions of the ^{232}Th(p,3pXn)Ra reactions

Experimental cross sections of these reactions are also listed in Table 04. Excitation functions are plotted against incident proton energy in Figure 06. Individual cases are discussed below:

^{225}Ra. The cumulative cross sections of ^{225}Ra, listed in the sixth column in Table 04, have an average uncertainty of about 19% except those near the reaction threshold. Since no contamination is encountered in this case, the detection limit on cross sections is about 0.01 mb.

^{224}Ra. The cumulative cross sections of ^{224}Ra, listed in the seventh column in Table 04, are those corrected from natural ^{228,224}Ra and the two contamination reactions (p,p4n) and (p,2p7n). The average uncertainty of the cross sections is about 35% owing to the very heavy contamination from the decay of natural ^{228}Th and reaction product ^{224}Ac. The detection limit is calculated to be around 0.1 mb.

^{223}Ra. The cumulative cross sections of ^{223}Ra, listed in the eighth column in Table 04, are those corrected for the two contaminating reactions (p,p5n) and (p,2p8n). The average uncertainty of the cross sections is around 25%

Figure 06

Excitation functions of the $^{232}Th(p,3pXn)Ra$ reaction

◆ : this work

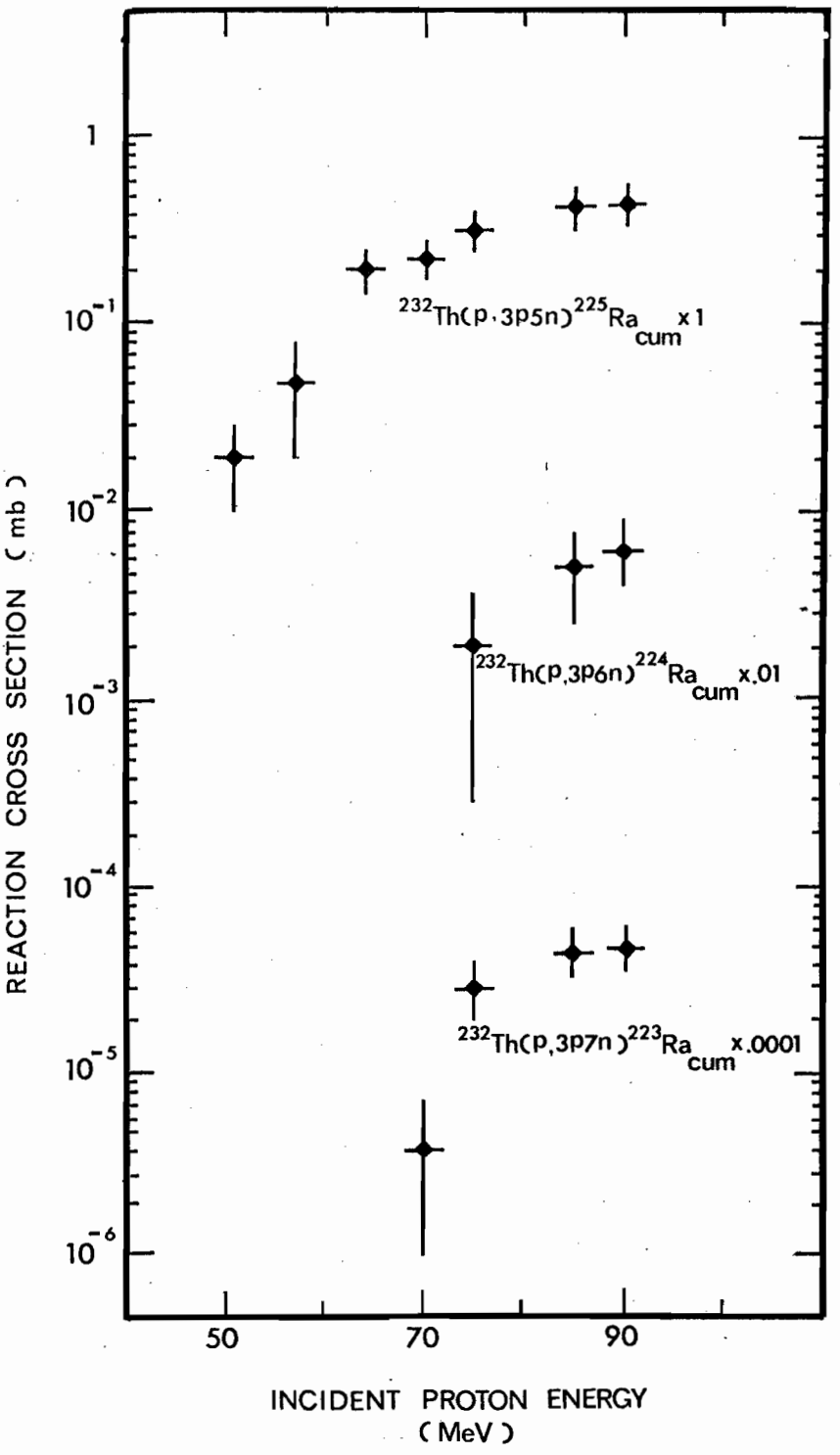
REACTION CROSS SECTION (mb)
1
10^{-1}
10^{-2}
10^{-3}
10^{-4}
10^{-5}
10^{-6}
$^{232}Th(p,3p5n)^{225}Ra_{cum}$ x 1
$^{232}Th(p,3p6n)^{224}Ra_{cum}$ x.01
$^{232}Th(p,3p7n)^{223}Ra_{cum}$ x.0001
50
70
90
INCIDENT PROTON ENERGY
(MeV)

except those near the reaction threshold. The detection limit is calculated to be 0.02 mb mainly because of the estimation of the (p,2p8n) cross section mentioned in the last section.

The uncertainty associated with (p,3pXn) reaction cross sections is higher than that in (p,pXn) reactions since there is low activity (low cross sections) in radium counting, which in turn means high statistical random error. No previous measurement has been made on (p,3pXn) reactions with proton energies less than 90 MeV. However, Lefort's group measured a set of data at higher proton energy (Le61), 150 MeV; their result, around 2 mb, does agree with the increasing trend of the excitation functions with increasing proton energy.

E4. General trend of measured excitation functions

From the experimental excitation functions of ^{232}Th-(p,pXn)Th with X = 1, 4-6, there are several common phenomena observed: (1) the experimental reaction threshold increases about 7 MeV with increasing X, namely 12 MeV for X = 1, 34 MeV for X = 4, 40 MeV for X = 5, and 47 MeV for X = 6; (2) a sharp rise of the excitation function between the reaction threshold and the edge of a plateau is encountered for each X, covering an energy range about 15 MeV wide; and (3) a generally flat plateau which decreases only slowly on the high energy side is encountered for each X, no peak exists

in the plateau region. Accordingly, one can reasonably estimate the behavior of the excitation functions of ^{232}Th-(p,pXn)Th with X other than those measured in this work.

For cumulative results on radium, no attempt has been made to separate francium and radon since these radium precursors have relatively short half-lives. However, cumulative results on radium can be represented as independent cross sections as well, without any substantial error; furthermore, the ^{232}Th(p,3pXn)Ra reactions investigated in this work can be regarded as the reactions of ^{232}Th(p,αp(X-2)n)Ra; these can be justified from the summary in Table 05.

The reaction threshold, defined as the sum of all separation energies and the Coulomb barrier height of all outgoing neutrons and/or charged particles, is calculated for each spallation reaction pertinent to radium and listed in the table. Also tabulated is the experimental threshold obtained by extrapolating data points back to infinitesimal in the excitation function. Take the case of ^{225}Ra as an example: below 50 MeV no detectable cross section (< 0.01 mb) was measured, therefore the ^{232}Th(p,2α)^{225}Fr reaction with a threshold near 22 MeV has too small a cross section to be measured; between 50 and 90 MeV the experimental excitation function of ^{225}Ra rises smoothly, which probably implies reactions like the ^{232}Th(p,α3pn)^{225}Rn with threshold at 70 MeV and the ^{232}Th(p,3p5n)^{225}Ra with threshold at 80 MeV have again too small a cross section to be measured.

Table 05

Calculated and experimental

reaction thresholds of interest.

Spallation reaction products isobar	Reaction mode		Calculated reaction threshold (MeV)	Experimental reaction threshold (MeV)
	(p,5p5n)	^{223}Rn	113.3	
	(p,2αpn)		45.7	
223	(p,4p6n)	^{223}Fr	102.5	~ 60
	(p,2α2n)		35.0	
	(p,3p7n)	^{223}Ra	88.6	
	(p,αp5n)		57.7	
	(p,5p4n)	^{224}Rn	107.3	
	(p,2αp)		39.7	
224	(p,4p5n)	^{224}Fr	97.8	< 60
	(p,2αn)		30.5	
	(p,3p6n)	^{224}Ra	83.9	
	(p,αp4n)		52.9	
	(p,5p3n)	^{225}Rn	102.8	
	(p,α3pn)		70.4	
225	(p,4p4n)	^{225}Fr	91.4	~ 50
	(p,2α)		22.2	
	(p,3p5n)	^{225}Ra	80.0	
	(p,αp3n)		48.0	

The only reaction mode remaining in the proton energies up to 90 MeV is then the $^{232}Th(p,\alpha p3n)^{225}Ra$ with calculated and experimental thresholds matching each other. From the similar arguments, the cumulative results on ^{224}Ra and ^{223}Ra may be taken to be the independent cross sections of the $^{232}Th(p,\alpha p4n)^{224}Ra$ and the $^{232}Th(p,\alpha p5n)^{223}Ra$, respectively.

III

THEORETICAL PREDICTION OF THE $^{232}Th(p,X)$ REACTIONS

Calculation of the ^{232}Th(p,Spallation) and (p,Fission) reactions at proton energies to 100 MeV is performed by using the fission-added Pre-equilibrium / Exciton Model program code. The results of this theoretical calculation are then compared to the total fission cross sections, together with seventeen excitation functions. Among the latter, seven were measured in this work.

A. The Spallation Data

Generally speaking, for each spallation excitation function, the experimental results obtained from different investigators agree with one another. However, there is some scatter data, in particular the (p,3n) and (p,6n) results from (Me56).

Meinke, Wick and Seaborg (Me56) measured the excitation functions of (p,3n) and (p,6n) reactions using an electrostatically deflected proton beam at 348 MeV with thickly stacked foil targets. As many as 10 000 mg/cm^2 copper were used as intermediate absorbers to reduce proton energy down to the desired range, namely from 348 to 20 MeV. Their results disagree with all other investigations both in energy and in cross section. They admitted that both the energy and cross section they calculated from experiments were very questionable, and therefore they suggested that "calculated energy values are only approximate, particularly at the lower

end of the energy scale", due to "initial energy spread and straggling of the beam"; furthermore, "cross sections can only be considered the maximum value" because of the "questionable chemical yield and attenuated beam intensity". Hence, their excitation functions are normalized on both energy and cross section to the result of the (p,3n) reaction investigated by Tewes (Te55), as hinted by Seaborg's group themselves. Although the normalized data improve the agreement with those results measured by other investigators considerably, there is still some disagreement especially at proton energies between 40 and 60 MeV. This is mainly because of the inherent problems just mentioned above. Hence, the normalization should not be taken seriously.

B. Prediction of the ^{232}Th(p,X) Reactions

Comparison between the experiments and calculation using the model described previously are made and discussed individually in the following sections. Because of the Monte Carlo approach to the calculation, it must be recognized that there is also a statistical error associated with the theoretical predictions. This is particularly the case for calculating the cross sections of complex reactions such as (p,XαYpZn) with large values of X, Y, and Z, where cross sections are as low as a fraction of a milibarn. These correspond to events occuring with a probability, at most,

of one out of every 15 000 cases. It should also be noticed that no normalization of calculated results to experimental data is needed since absolute cross sections are calculated directly and the only parameter is, as mentioned in the first chapter, the ratio of a_f/a_n.

B1. The total fission cross sections

The calculation is compared to the total fission cross sections, measured from among (Te52), (Mc54), (Te55), (St56), (Ch63), (Fr68), (Ch71), and (Ea76). The results are illustrated in Figure 07. At energies above 25 MeV, the experimental total fission cross sections are best reproduced by assuming $a_f/a_n = 1.05$; calculation with higher or lower values of the ratio of a_f/a_n overestimate or underestimate the total cross sections, respectively. In the lower energy region, calculation with $a_f/a_n = 1.10$ in general gives a better prediction than the one with 1.05. However, in considering the widely scattered data points in the low energy region, e.g., 21-92 mb at 9.5 MeV and 350-850 mb at 18 MeV, the calculation will always achieve a good fit on at least some experimental data, providing that $a_f/a_n \geq 1.05$. That is to say, no specific value of the ratio of a_f/a_n is concluded in the low energy region because of the scattered experimental data. In all, the parameter may be narrowed down to the range $1.05 \leq a_f/a_n \leq 1.10$ and treated independently of incident proton energy.

Figure 07

Comparison between experiments and calculation
on total fission cross sections
of the $^{232}Th(p,Fission)$ reaction

- experimental data -

▼ : after (Te52)

◆ : after (Te55)

■ : after (St56)

✱ : estimated from (Be69) and (Cr69)

● : after (Ch63)

▲ : after (Fr68)

⊡ : after (Ch71)

⊙ : after (Ea76)

◀ : after (Mc54)

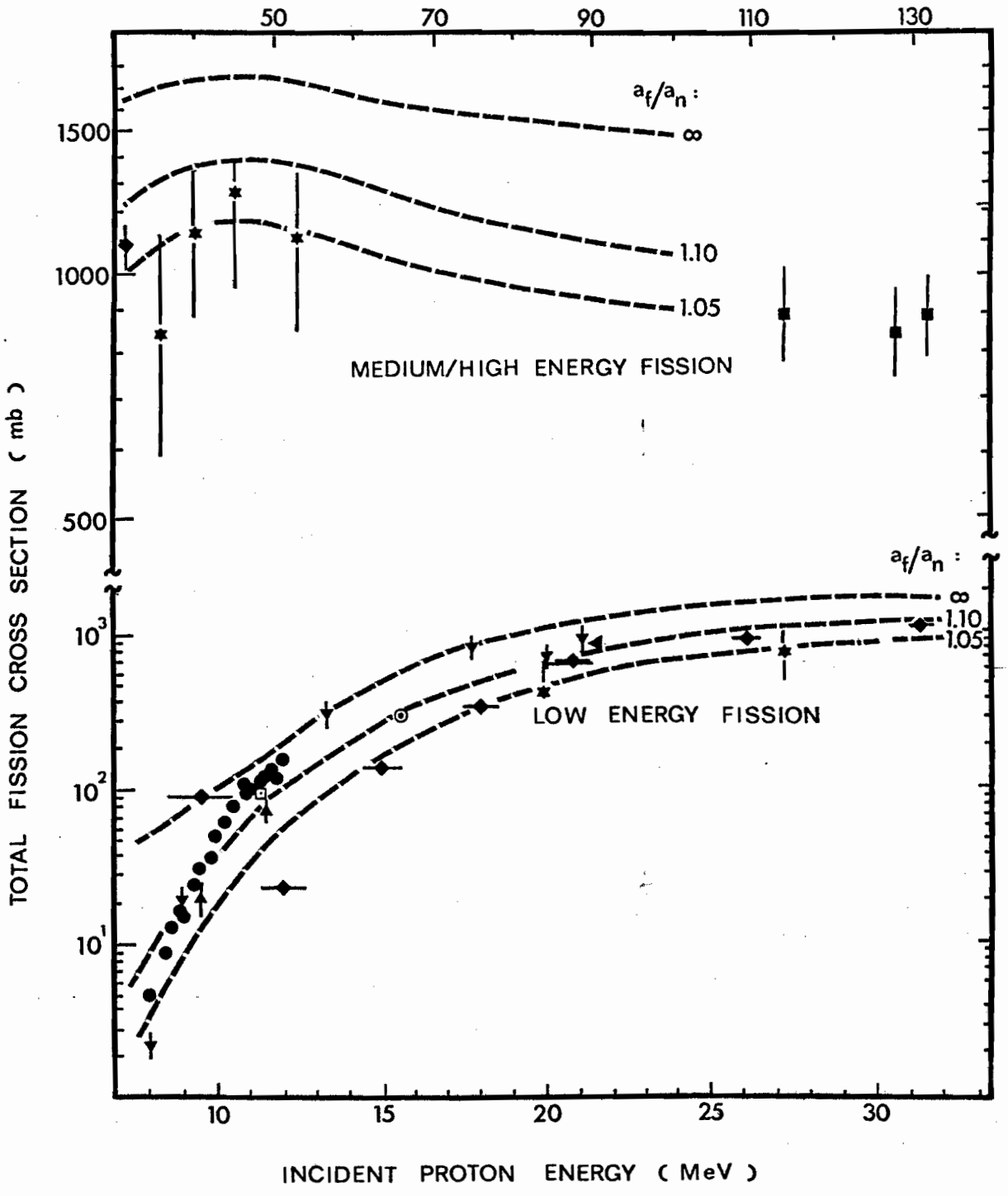
50
70
90
110
130
1500
1000
500
a_f/a_n :
∞
1.10
1.05
MEDIUM/HIGH ENERGY FISSION
10^3
10^2
10^1
LOW ENERGY FISSION
10
15
20
25
30
TOTAL FISSION CROSS SECTION (mb)
INCIDENT PROTON ENERGY (MeV)

B2. The cross sections of the ^{232}Th(p,Xn)Pa reactions

The calculation is compared to the excitation functions of (p,Xn) reactions with X = 1, 3, 5-7, measured from among (Te52), (Te55), (Me56), (Le61), (Br62), (Le62), and (Su74). The comparison is summarized graphically in Figure 08. All the five excitation functions are fitted excellently by the calculation with a_f/a_n = 1.05 except perhaps the (p,3n) and (p,5n) reactions at proton energies above 50 MeV. In this energy region, the calculation overestimates the (p,3n) and (p,5n) data, measured by (Br62), by a factor of two. A calculation proceeding on the basis of a_f/a_n = 1.10 yields a worse result. An increase of the ratio of a_f/a_n by only 5%, which in turn increases the fission probability slightly, results in a severe underestimate of the data of (p,7n) and (p,6n) by factors of 20 and 10, respectively, while the (p,5n) cross sections are still underestimated by a factor of two. In the (p,3n) reaction, this calculation improves the prediction slightly but still overestimates the experimental data by 40%. Therefore, we observe that the calculation with a_f/a_n = 1.10 yields a larger degree of underestimation on the experimental data of (p,Xn) with increasing X. This is because at large values of X, more chances of fission competition appear in the deexcitation chain of the excited nucleus; in other words, the probability of spallation is severely depleted.

The calculation of (p,n) cross sections is insensitive

Figure 08

Comparison between experiments and calculation in the $^{232}Th(p,Xn)Pa$ reactions

- experimental data -

◀ : after (Te52)

▶ : after (Te55)

● : normalized (Me56)

▲ : after (Le61)

■ : after (Br62)

▼ : after (Le62)

◆ : after (Su74)

- calculated points -

○ : based on $a_f/a_n = 1.05$

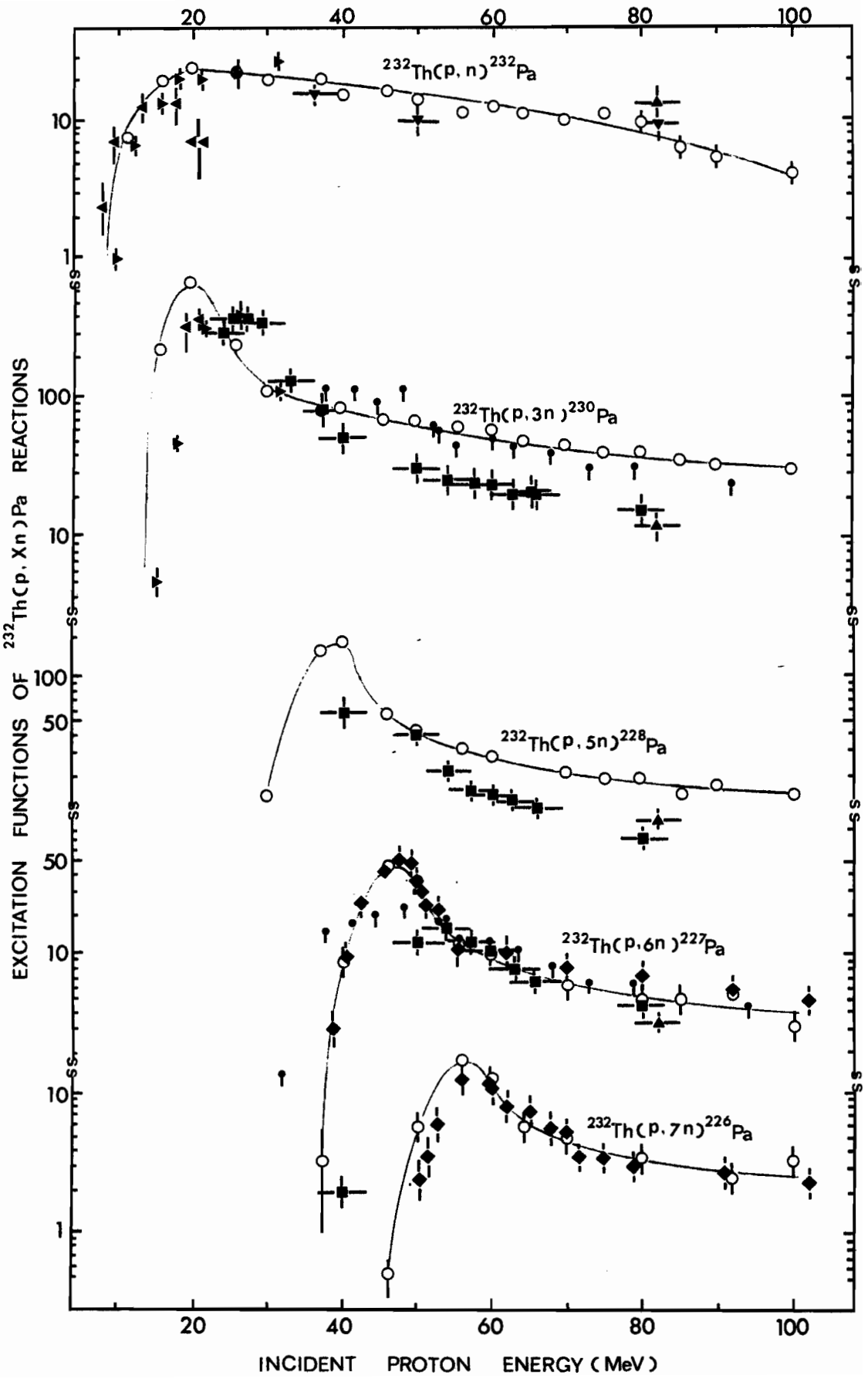
EXCITATION FUNCTIONS OF ^{232}Th(p, Xn)Pa REACTIONS
INCIDENT PROTON ENERGY (MeV)
^{232}Th(p, n)^{232}Pa
^{232}Th(p, 3n)^{230}Pa
^{232}Th(p, 5n)^{228}Pa
^{232}Th(p, 6n)^{227}Pa
^{232}Th(p, 7n)^{226}Pa
20
40
60
80
100
1
10
50
100

to the variation of the ratio of a_f/a_n at energies above 20 MeV since the outgoing neutron in the (p,n) reactions is directly knocked out by the incident proton in the pre-equilibrium stage where fission does not compete with other decay modes.

Despite the unsatisfactory fit to the (p,3n) and (p,5n) data at proton energies above 50 MeV using $a_f/a_n = 1.05$, a point of great importance is the general agreement with all experimental data of (p,Xn) reactions, in particular the impressive fits to (p,6n) and (p,7n) data. The excited compound nucleus formed in these reactions must deexcite to the reaction products by sequential emission of X neutrons and for each and every emission in the evaporation stage, fission competes with other decay modes. Any error in the formulation of fission would be magnified in the cross section calculation by successive application of the Γ_f/Γ_i, especially for those high energy data where the fissioning charge, mass, and its excitation energy are widely distributed. It is felt that the achievement of such a good fit without adjusting the parameters from case to case is particularly gratifying.

It is highly unlikely that a calculation with $a_f/a_n = 1.05$ could not fit the (p,3n) and (p,5n) data while reproducing both the data of simple reactions like (p,n) and the data of complex reactions like (p,7n). In fact, the only discrepancy in the fit of (p,Xn) data arises from the experimental data from (Br62). By comparing the (p,3n) and (p,6n) data from

various investigations, we find at the peak of these experimental excitation functions neither the energy nor the cross section of the results from (Br62) agree with those of (Te55) and (Su74); the latter are fitted very well by the calculation. Because theoretical prediction fits the peaks of all experimental excitation functions of (p,Xn) reactions, it is therefore reasonable to believe that the experimental data of (p,3n), (p,5n), and (p,6n) reactions measured by (Br62) may be incorrect in the determination of proton energy and furthermore, using a monitor, in the magnitude of the reaction cross sections. If the data of (Br62) were shifted 10 MeV to the lower end of the proton energy scale and the cross sections were multiplied by a factor of two, the data could be reproduced as well as other experimental results.

B3. <u>The cross sections of the ^{232}Th(p,pXn)Th reactions</u>

The calculation with $a_f/a_n = 1.05$ is compared to the excitation functions of the (p,pXn) reactions with X = 1, 4-6, mainly measured in this work with some sporadic data from (Le61) and (Le62). The fit of the calculation is shown in Figure 09. Except for the (p,pn) reaction discussed below at low energy region, the theoretical prediction on the experimental results is strikingly good. The discrepancy observed in the (p,pn) reaction in the low energy region is attributed to the (p,d) reaction which is beyond the scope of the Exciton Model used in this work. Indeed, the differ-

Figure 09

Comparison between experiments and calculation in the $^{232}Th(p,pXn)Th$ reactions

- experimental data -

◇ : corrected (Le61), (Le62)

◆ : this work

- calculated points -

○ : based on $a_f/a_n = 1.05$

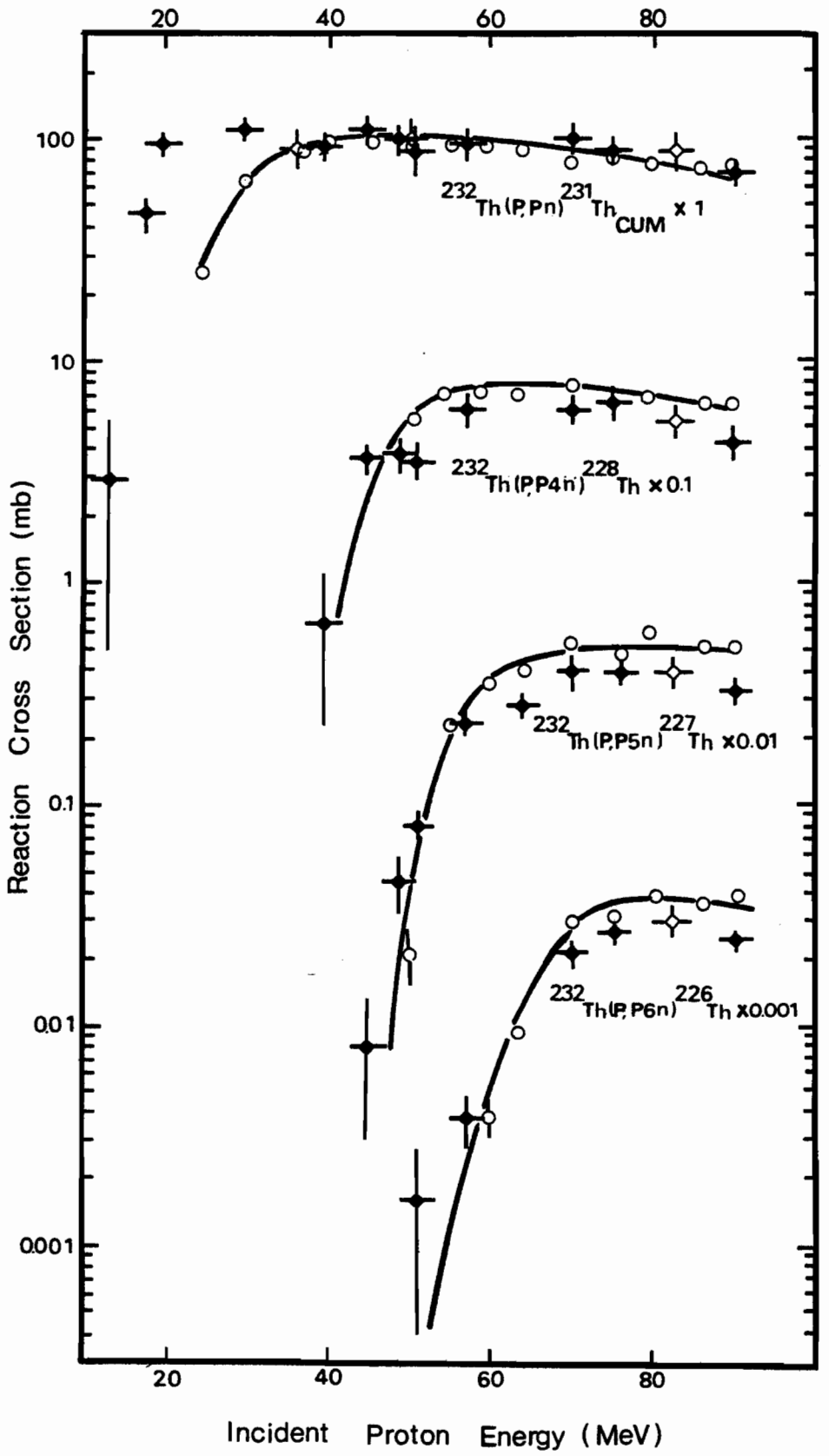
20
40
60
80
100
10
1
0.1
0.01
0.001
Reaction Cross Section (mb)
232Th(P,Pn)231Th CUM x 1
232Th(P,P4n)228Th x0.1
232Th(P,P5n)227Th x0.01
232Th(P,P6n)226Th x0.001
Incident Proton Energy (MeV)

ence may be assigned as a prediction of the cross sections of the (p,d) reaction as discussed in (Ga77A).

The calculated (p,pn) cross sections are relatively insensitive to the variation of the ratio of a_f/a_n since the outgoing proton and neutron leave the excited nucleus predominantly in the pre-equilibrium stage where fission does not compete with other decay modes, that is to say, the (p,pn) reaction may be treated as a fast, inelastic scattering reaction.

Similarly to the case of (p,6n), a calculation based on $a_f/a_n = 1.10$ underestimates the experimental excitation function of the (p,p6n) reaction, involving the multi-neutron emission process, by a factor of two. However, the same 5% rise in the calculation of (p,6n) cross sections underestimates the experimental data by a factor of 10, as mentioned in the last section. This is because unlike the more fissionable isotopes of protactinium in the deexcitation chain of the (p,6n) reaction, the excited nuclei in the deexcitation chain of the (p,p6n) reaction left behind by the first outgoing proton, are the isotopes of the less fissionable thorium; therefore, the (p,p6n) spallation reaction is less depleted by fission than that of the (p,6n) reaction.

Kavanagh and Bell (Ka61) and Lebeyec and Lefort (Le67) found that, at the high energy tails of the excitation functions of (p,pXn) reactions at bismuth-gold region, the cross sections are independent of the X and of the order of 100 mb.

In the present work, the measured cross sections of the ^{232}Th(p,pXn)Th reactions decrease with increasing X; this is due to the fact that in the ^{232}Th(p,pXn)Th reactions with large values of X, the excited nuclei along the deexcitation chain have noticeably larger values of Z^2/A; therefore, the probability of spallation becomes smaller owing to the significant emergence of fission competition.

The theoretical prediction based on $a_f/a_n = 1.05$ yields a general agreement on all (p,pXn) data; coupled with the successful fit on (p,Xn) data mentioned in the last section, it is felt that the treatment of fission in the program code, involving different fissioning charges and masses, is generally supported.

B4. The cross sections of the ^{232}Th(p,2pXn)Ac reactions

In order to fit the experimental data involving the emission of individual nucleons as well as preformed alpha particles, an improved version of the nucleon-alpha scattering dynamics by Gadioli, Gadioli-Erba, and Ferrero (Ga78A) is kept in the calculation. A calculation based on $a_f/a_n = 1.05$ is compared to the experimental data of the (p,2pXn) reactions with X = 3-7, measured by Gauvin (Ga62,63). Since the calculation of the (p,2pXn) cross sections is less than 5 mb, corresponding to, at most, one out of every 300 events in the Monte Carlo calculation, the statistical error becomes apparent. Ten thousand cascades have been run at each incident

proton energy pertinent to this work with an average 25% statistical error associated with the calculated value. The result of the fit is illustrated in Figure 10.

For all the five experimental excitation functions, the fit at proton energies above 70 MeV is excellent; however, at lower energies, especially around the peaks of the excitation functions, the fit is not so good. The calculation underestimates the peak position for all the five reactions by 5 to 10 MeV and overestimates the peak cross section, except perhaps that of the (p,2p3n) reaction, by a factor of two. According to the interpretation of (Ka76), the peak in the excitation function of the (p,2pXn) reaction may be attributed to the (p,α(X-2)n) process, involving emission of a preformed alpha particle from the excited nucleus. Even in the high energy tail of the excitation function the alpha-emission process still plays a significant role. For example, at 90 MeV bombarding energy, the (p,αn) reaction counts for 40% of the (p,2p3n) case while the (p,α5n) reaction counts for 95% of the (p,2p7n) case. It is therefore impossible to fit the high energy tail well while obtaining a bad fit for the low energy peak.

The experimental data of (p,2pXn) reactions were measured in the internal proton beam at the Synchrocyclotron d'Orsay where cross sections of the (p,Xn) reactions, badly fit by the present calculation, were investigated by (Br62). In the previous section a suggestion was made that the energy

Figure 10

Comparison between experiments and calculation in the $^{232}Th(p,2pXn)Ac$ reactions

- experimental data -

■ : after (Ga62)

● : after (Ga63)

- calculated points -

o : based on $a_f/a_n = 1.05$

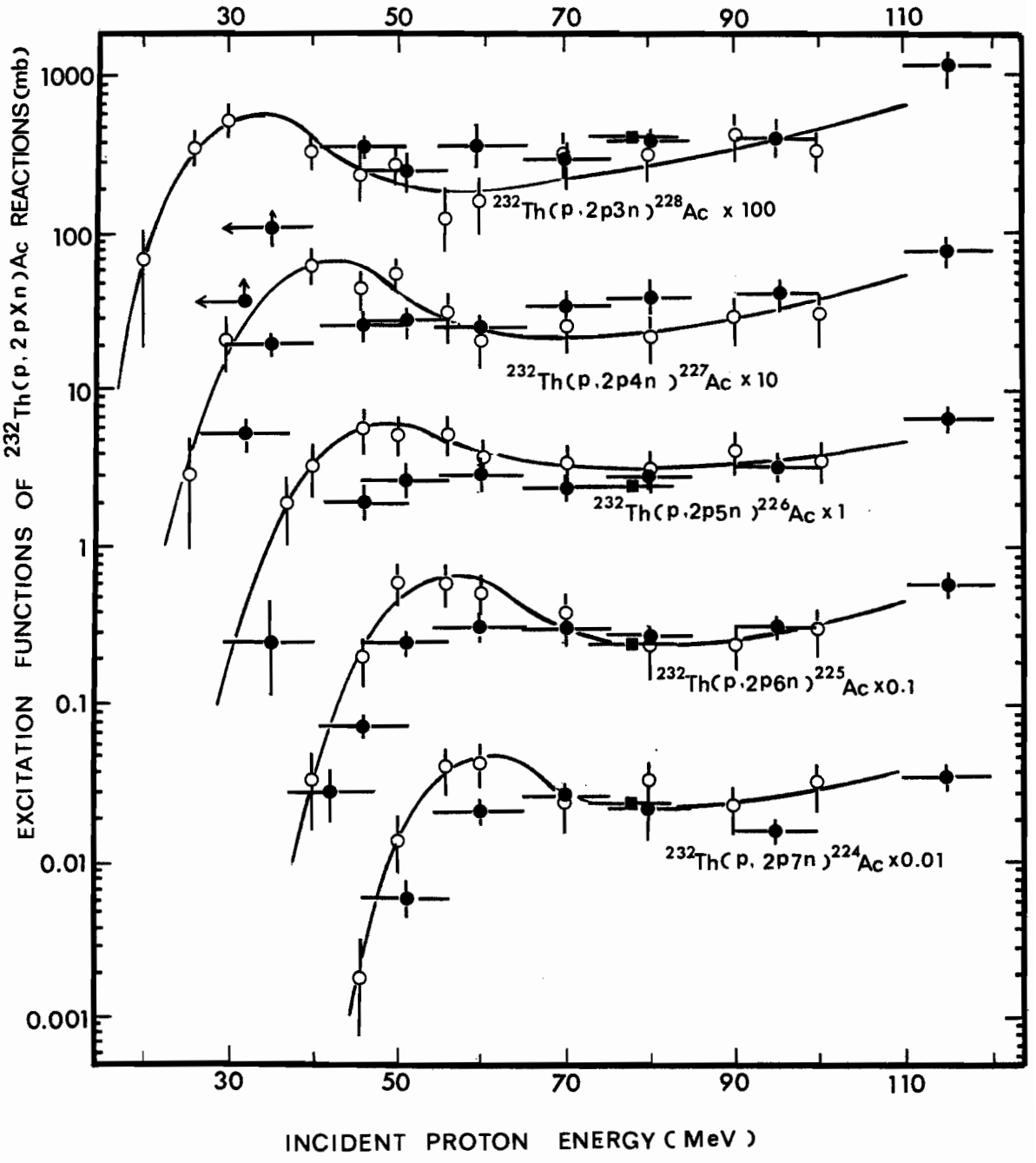
30
50
70
90
110
1000
100
10
1
0.1
0.01
0.001
EXCITATION FUNCTIONS OF ^{232}Th(p,2pXn)Ac REACTIONS(mb)
^{232}Th(p,2p3n)^{228}Ac x 100
^{232}Th(p,2p4n)^{227}Ac x 10
^{232}Th(p,2p5n)^{226}Ac x 1
^{232}Th(p,2p6n)^{225}Ac x0.1
^{232}Th(p,2p7n)^{224}Ac x0.01
INCIDENT PROTON ENERGY (MeV)

determined in the internal beam in the Synchrocyclotron d'Orsay be treated with reservation. Here the same suggestion is carried over to the (p,2pXn) reactions. If the data points below 70 MeV were shifted about 10 MeV toward the lower end of the proton energy scale, fits to the experimental data would be as good as those in the high energy tail.

The calculations of the (p,2pXn) cross sections are relatively insensitive to the variation of the ratio of a_f/a_n. This should not be interpreted as implying that all outgoing neutrons and charged particles leave the excited nucleus in the pre-equilibrium stage where fission does not compete at all. Rather, the insensitivity arises mainly because the actinium isotopes with their high fission barrier encountered along the neutron evaporation chain in the ^{232}Th(p,2pXn)Ac reactions seldom undergo fission.

B5. The cross sections of the ^{232}Th(p,3pXn)Ra reactions

The calculation based on $a_f/a_n = 1.05$ is compared to the excitation functions of the (p,3pXn) reactions with X = 5-7, which were measured in this work. As many as 80 000 cascades were run by Gadioli and Gadioli-Erba (Ga79) in the high incident proton energy region to calculate this reaction which occurs with a frequency of about once in every 3 000 events. The calculation has an average 45% statistical uncertainty. The fit of the (p,3pXn) data is illustrated in Figure 11.

Figure 11

Comparison between experiments and calculation in the $^{232}Th(p,3pXn)Ra$ reactions

◆ : experimental data in this work

o : calculation based on $a_f/a_n = 1.05$

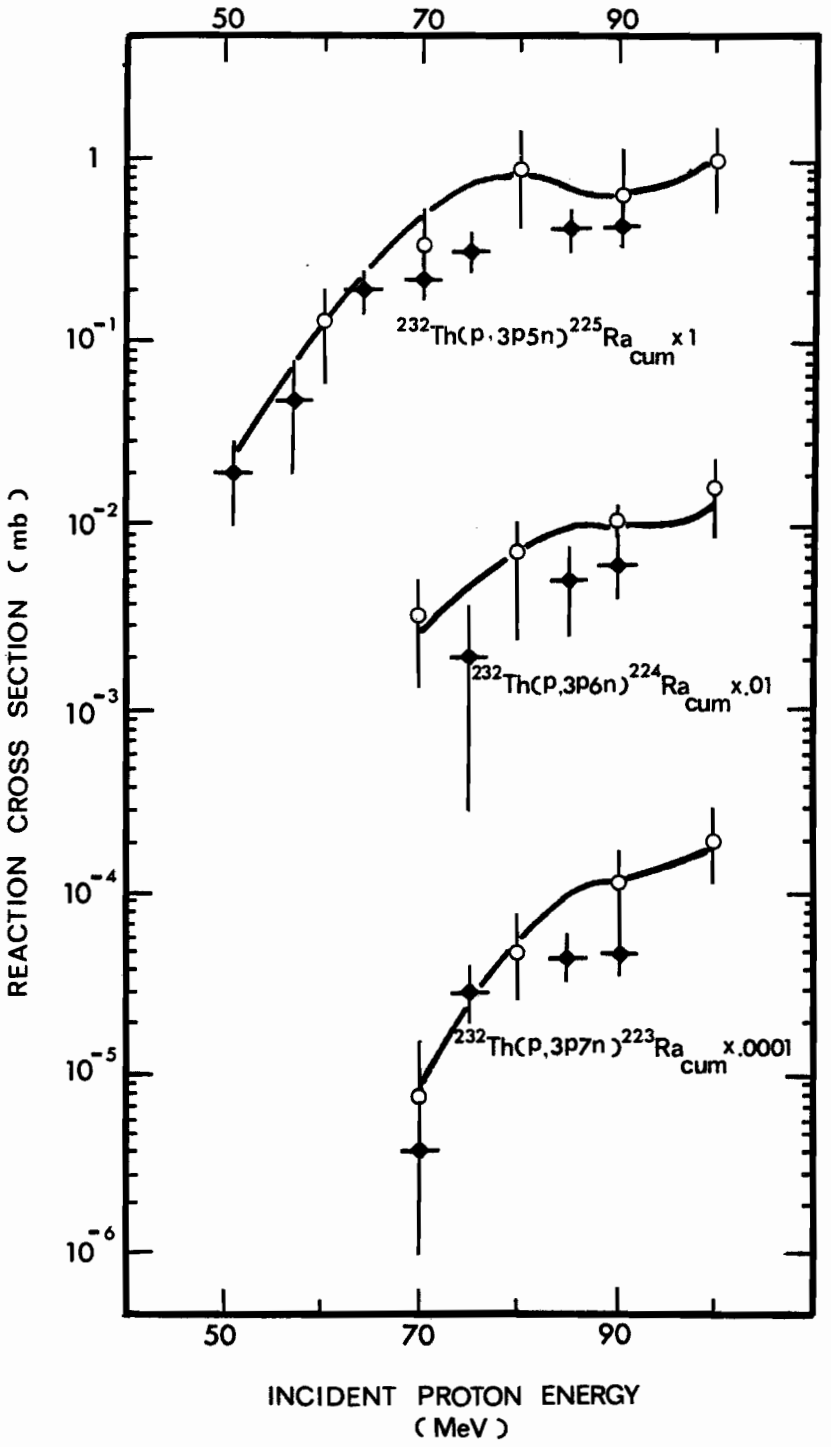
50
70
90
1
10^{-1}
10^{-2}
10^{-3}
10^{-4}
10^{-5}
10^{-6}
REACTION CROSS SECTION (mb)
$^{232}Th(p,3p5n)^{225}Ra_{cum}$ x 1
$^{232}Th(p,3p6n)^{224}Ra_{cum}$ x.01
$^{232}Th(p,3p7n)^{223}Ra_{cum}$ x.0001
50
70
90
INCIDENT PROTON ENERGY
(MeV)

The theoretical prediction on (p,3pXn) data is excellent, especially in view of the low cross sections in this calculation. The alpha peak of the (p,3p5n) reaction is calculated to lie near 80 MeV bombarding energy. If the McGill Synchrocyclotron could offer a proton beam energy up to 120 MeV, alpha peaks might well have been observed experimentally in all the three excitation functions of the (p,3pXn) reactions.

Similar to the previous section, a calculation based on different values of the ratio of a_f/a_n yields the same prediction for the (p,3pXn) cross sections; the reason is similar as well. Therefore, the radium isotopes formed along the neutron evaporation chain of the (p,αp(X-2)n) reactions have very low fission probability.

C. Summary of the Predictions

The agreement between the calculation based on a_f/a_n = 1.05 and experimental results of seventeen excitation functions of the ^{232}Th(p,Spallation) reactions and the total cross sections of the ^{232}Th(p,Fission) process is extraordinarily good, especially for those complex reactions in which many particles are emitted. In these complex reactions the theory of fission is tested most severely, the competition of fission and other decay modes are checked many times over a wide range of excited muclides and excitation energies. Any error in the treatment of fission would therefore be

magnified consecutively and yield an escalating error in the calculated cross sections. For example, the disagreement between the calculated cross sections of the (p,6n) reaction and experimental data at 90 MeV is about 20%; this suggests an average error in the treatment of the fission of about 3%. While it is hardly believed that a simple approach with only a single parameter to the highly complex problem of fission competition is really valid at a 3% uncertainty level, the fact remains that the calculation does reproduce a broad range of experimental data with this high accuracy.

The fit of the theoretical calculation to the experimental data is indeed very good, lending a solid confidence to the treatment of the fission. The competition among fission and other decay modes as well as the characteristics of the individual ^{232}Th(p,Fission) remain to be examined more closely. This will be done in the next chapter.

IV

FISSIONABILITY AND

FISSION CROSS SECTIONS

A. Fission Probability

The term most commonly used in discussing the competition of fission process and particle emission is the "fissility", P_f. It is defined as the fractional probability that a nucleus fissions and is expressed as:

$$P_f = \frac{\Gamma_f}{\Gamma_f + \Gamma_n + \Gamma_p + \Gamma_\alpha} \qquad (07)$$

where individual width Γ_i has been defined in Eqs. (01) and (02). In Figure 12 the ratio of $\Gamma_{\text{charged particle}}/\Gamma_{\text{neutron}}$ is plotted against the excitation energy for various fissioning nuclides encountered in the ^{232}Th(p,Fission) reaction. At excitation energies below 30 MeV, this ratio is small, never greater than 0.001, therefore Eq. (07) is sometimes simplified to include only neutron emission and fission:

$$P_f \simeq \frac{\Gamma_f}{\Gamma_f + \Gamma_n} = (1 + \frac{\Gamma_n}{\Gamma_f})^{-1} \qquad (08)$$

Here the competition between neutron emission and fission, $\frac{\Gamma_n}{\Gamma_f}$, is given the name "fissionability" and historically this is the main focus of discussions of fission. However, the approximation in Eq. (08) does not hold in the high excitation energy region. For instance, at excitation energies > 50 MeV the ratio of the charged particle width to neutron width of some fissioning nuclides is greater than

Figure 12

The ratio of $\Gamma_{\text{charged particle}}/\Gamma_n$ with

$220 \leqslant$ fissioning mass $\leqslant 233$

$87 \leqslant$ fissioning charge $\leqslant 91$

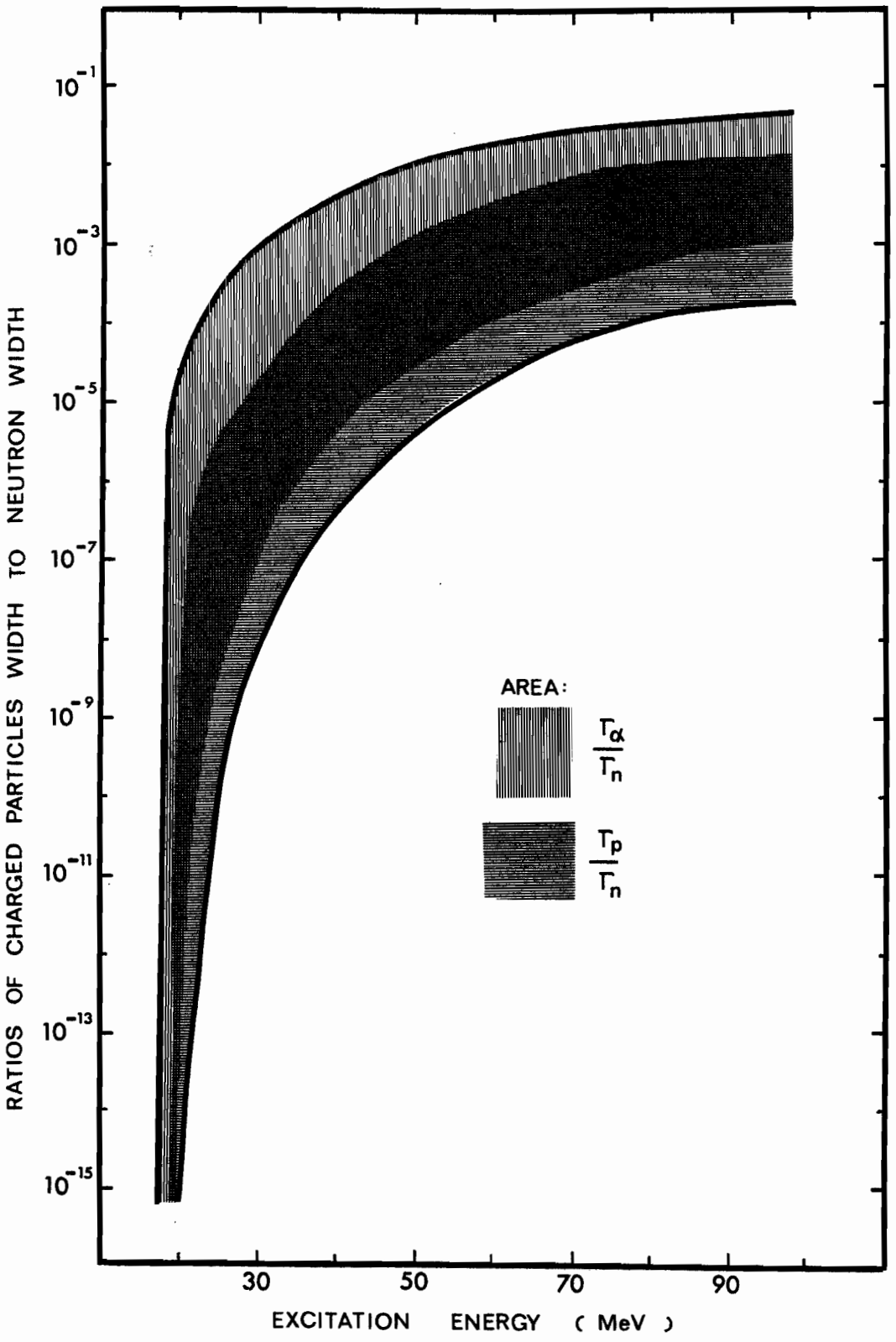
RATIOS OF CHARGED PARTICLES WIDTH TO NEUTRON WIDTH
10^{-1}
10^{-3}
10^{-5}
10^{-7}
10^{-9}
10^{-11}
10^{-13}
10^{-15}
AREA:
$\frac{\Gamma_\alpha}{\Gamma_n}$
$\frac{\Gamma_p}{\Gamma_n}$
30
50
70
90
EXCITATION ENERGY (MeV)

1% and therefore competition of charged particle emission to fission is not negligible in this excitation energy region.

A1. The fission barrier

The most sensitive factor in calculating the fissionability and fissility, as reflected in Eqs. (02), (07), and (08), is the fission barrier, B_f. For most of the nuclei undergoing fission, the fission barrier is unknown. Myers and Swiatecki (My66) have found that the best way of reproducing the limited experimental data of B_f is obtained by adding a semi-empirical ground state shell correction, ΔE_{sh}, to the Liquid Drop Model (LDM) fission barrier height, B_f^{LDM}. The fission barriers adopted in this work, derived by Gadioli, Gadioli-Erba, and Moroni (Ga78), are essentially a modified version of Myers' semi-empirical equation:

$$B_f = B_f^{LDM} - \Delta E_{sh} + \Delta_{GS} - \Delta_S \qquad (09)$$

where Δ_{GS} = ground state pairing energy,

Δ_S = saddle point pairing energy.

The first term in the equation, B_f^{LDM}, is the fission barrier evaluated on the basis of the LDM (Co63). Qualitatively speaking, this term decreases with increasing fissioning charge Z_F and decreasing fissioning mass A_F. The second term, ΔE_{sh}, maximizes its negative value at closed-shell nuclei and becomes close to zero for fissioning nuclei with semi-closed

shell. The remaining terms, Δ_{GS} and Δ_{S}, reflect an even-odd effect on the fission barrier but do not exist in Myers' treatment.

The calculated fission barriers from (Ga78) are compared to the experimental B_f within the ranges of $82 \leqslant Z_F \leqslant 93$ and $207 \leqslant A_F \leqslant 240$. The result of this comparison is illustrated in Figure 13. On the average, the calculated B_f are in good agreement with all experimental B_f; the average percentage difference between measured B_f and calculation is about 5%, which is well within the uncertainty of the experimental data.

For each given Z_F, calculated values of B_f form a unique V-shaped curve as increases A_F, with the notch located at $A_F \sim 226$. This is because ΔE_{sh} in Eq. (09) is minimized near $A_F \sim 226$, corresponding to a half-filled neutron shell, and is maximized at both extremes, corresponding to nuclei near the N = 126 and 152 closed-shells. In addition, the even-odd effect is also seen in these V-shaped curves. This is due to the correction on pairing energy, as reflected by Δ_{GS} and ΔS in Eq. (09).

The characteristics of the barrier B_f as a V-shaped function of A_F are carried over to the predicted fissility and fissionability, which will be discussed in the following sections.

A2. Fission probability as a function of Z^2/A

From the earliest recognition of the relationship between

Figure 13

The fission barriers

with $82 \leqslant Z_F \leqslant 93$ and $207 \leqslant A_F \leqslant 240$

• : calculated barrier, after (Ga78)

o : experimental barrier, after (My77)

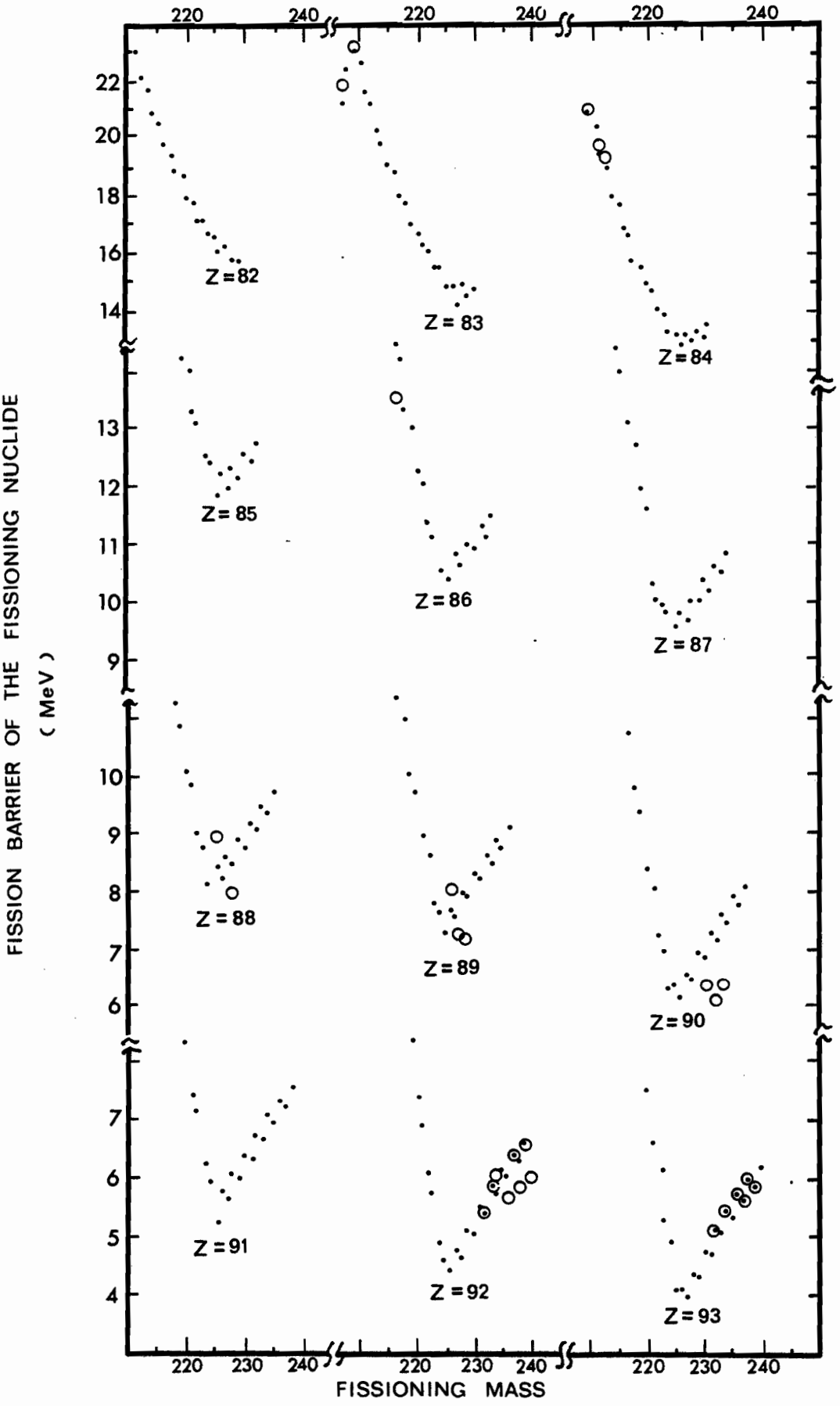
FISSION BARRIER OF THE FISSIONING NUCLIDE
(MeV)
FISSIONING MASS
Z = 82
Z = 83
Z = 84
Z = 85
Z = 86
Z = 87
Z = 88
Z = 89
Z = 90
Z = 91
Z = 92
Z = 93

fissioning nuclei and a highly excited and distorted Liquid Drop Model, the "fissility parameter", $x = \frac{Z^2}{50.13A}$, representing the ratio of the Coulomb to twice the surface energies in the distorted fissioning nucleus, had been known to be a principal factor in determining the fissionability (Bo39). As a simplified approach to the highly complex process of fission, the value of Z^2/A was quite often taken as the only factor upon which the fissionability depended.

Although no explicit Z^2/A dependence is evident in the theoretical calculation in this work, each variable except those energy related factors in Eqs. (01) and (02) is indeed a function of either Z or A or both. At a given E^*, the fissility P_f can be calculated on the basis of Eqs. (01), (02), and (07). Representative values of the P_f at $E^* = 100$ MeV are plotted as a function of Z^2/A and illustrated in Figure 14, covering a range of $32 < Z^2/A < 40$ and including heavy elements from francium to neptunium.

For each heavy element shown in the figure, there is a clearly defined convex curve for the fissility, the peak value of the curve increasing with increasing Z. The left wings of these curves, representing those very long-lived nuclides which are frequently used as fission targets, overlap one another and form a general upward belt of increasing fissility with the value of Z^2/A, thus retaining the historical dependence of the P_f on Z^2/A. In each convex curve, the fissility increases from the neutron rich side, or from

Figure 14

Calculated fissility as a function of Z^2/A at E^* = 100 MeV

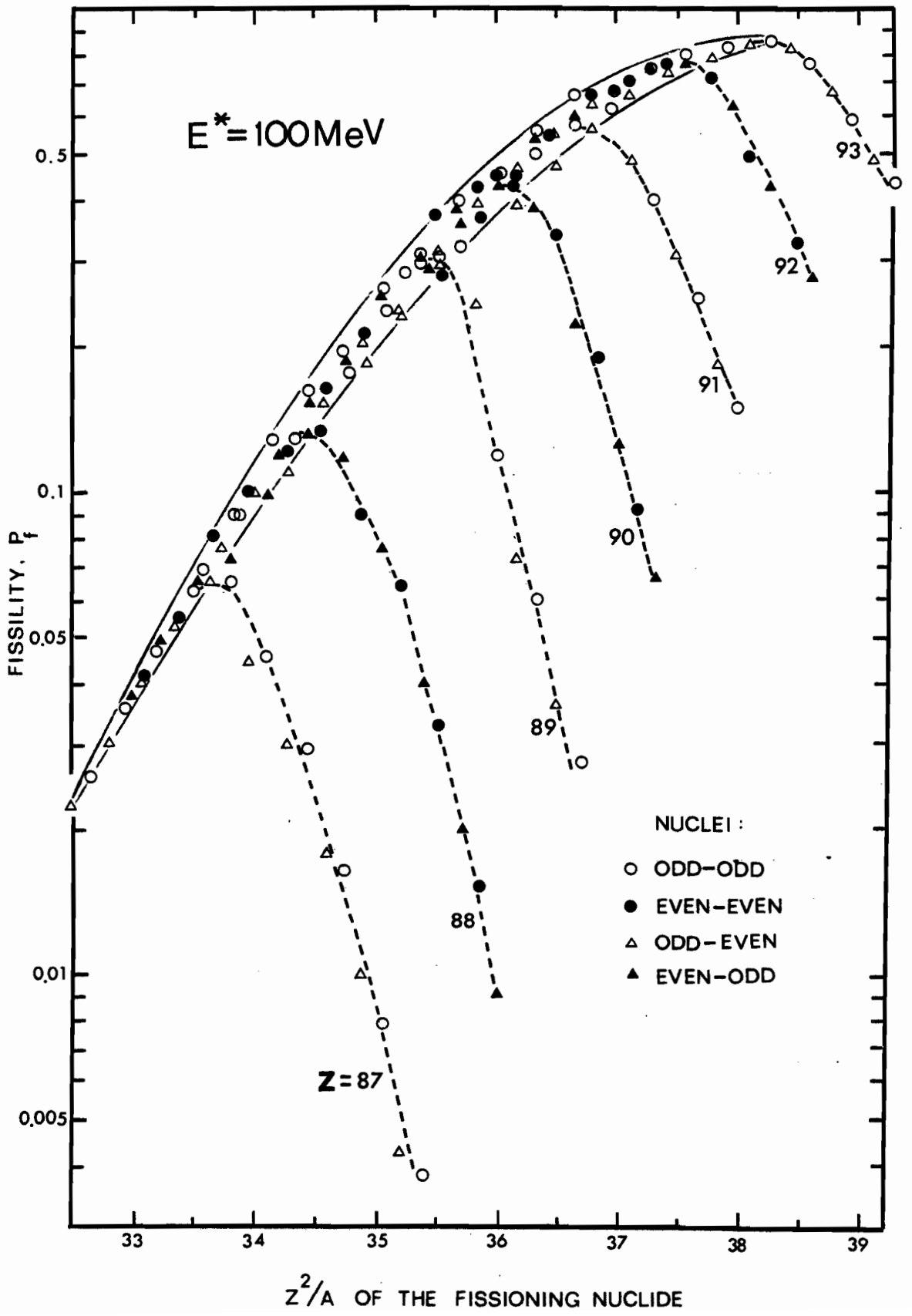
E*=100MeV
FISSILITY, Pf
0.5
0.1
0.05
0.01
0.005
93
92
91
90
89
88
Z=87
NUCLEI :
ODD-ODD
EVEN-EVEN
ODD-EVEN
EVEN-ODD
33
34
35
36
37
38
39
Z²/A OF THE FISSIONING NUCLIDE

the small Z^2/A value, reaches a peak and then decreases towards the neutron deficient side, or to the large Z^2/A value. This trend holds for all elements at all E^* and can be attributed to the competition between the neutron binding energy and fission barrier height.

The most sensitive term in determining the fissility is the exponential term of

$$\exp\left[\, 2\sqrt{a_f[E^* - (B_f + \Delta_S)]} - 2\sqrt{a_n[E^* - (B_n + \Delta_n)]}\,\right]$$

as reflected in Eqs. (01) and (02), or more clearly, related to the difference of $(B_n + \Delta_n)$ to $(B_f + \Delta_S)$. The effective neutron binding energy, $B_{n\,eff} \equiv B_n + \Delta_n$, defined as the neutron binding energy with the correction on the pairing energy for neutron level density, increases with increasing Z^2/A when it moves toward the neutron deficient nuclei; the effective fission barrier height, $B_{f\,eff} \equiv B_f + \Delta_S$, defined in Eq. (02), maintains the V-shaped characteristic of decreasing Z^2/A when it moves toward the neutron rich nuclei. Hence, the difference of $(B_n - B_f)_{eff}$ first increases, then decreases after passing through a maximum, with increasing Z^2/A, which is in turn the behavior of the fissility shown in the figure.

A more subtle illustration is shown in Figure 15 where the fissionability is plotted against A_F at some selected E^*. Calculated points are seen to define fairly distinct V-shaped curves for each element. More interestingly, the minimum in

Figure 15

Calculated fissionability as a function of A_F

(a) at E^* = 30 MeV

(b) at E^* = 60 MeV

(c) at E^* = 90 MeV

(d) reproduced from (Va58)

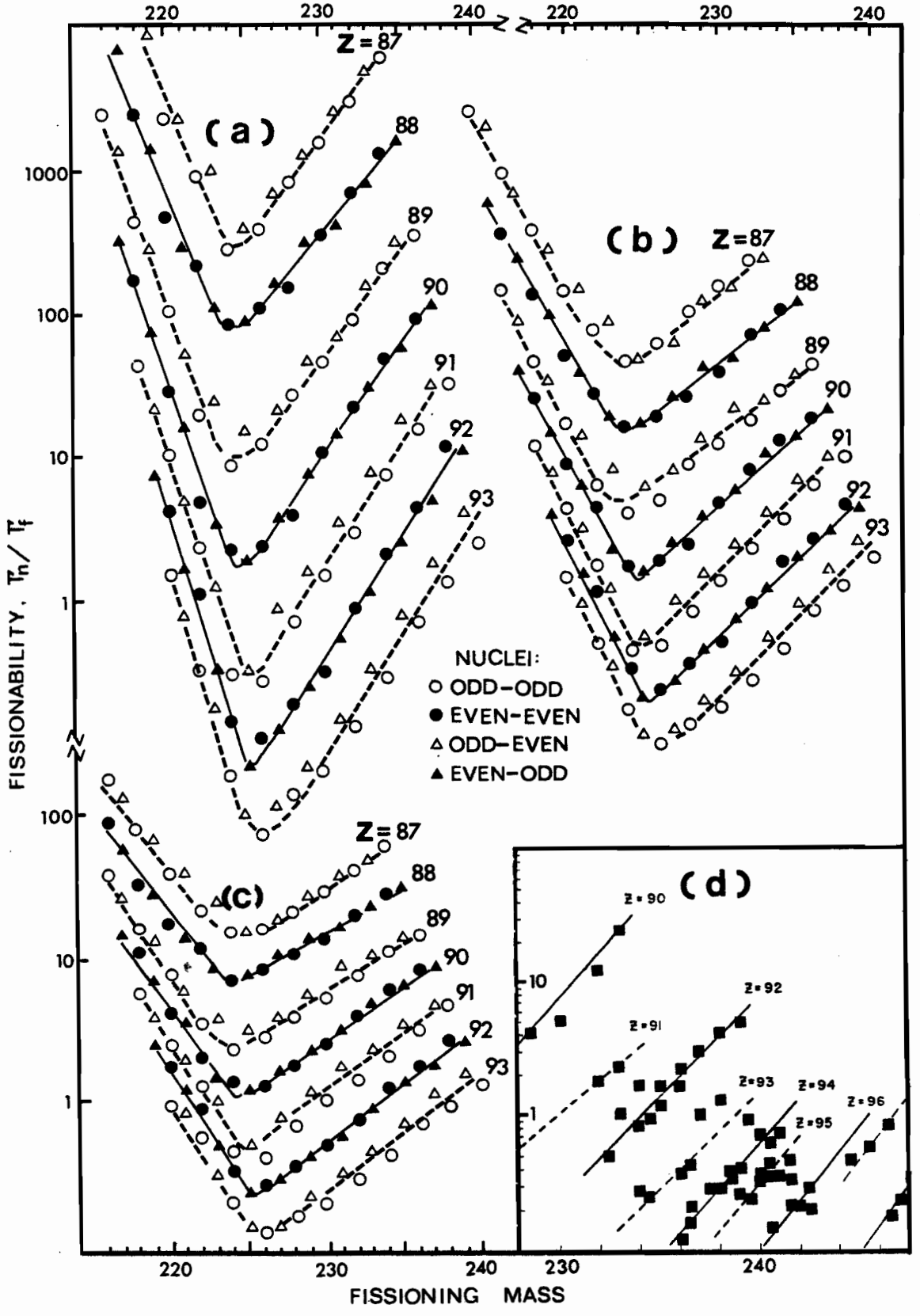
(a)
(b)
(c)
(d)
Z=87
88
89
90
91
92
93
NUCLEI:
ODD-ODD
EVEN-EVEN
ODD-EVEN
EVEN-ODD
FISSIONABILITY, Γ_n/Γ_f
FISSIONING MASS
220
230
240
1000
100
10
1
Z=90
Z=91
Z=92
Z=93
Z=94
Z=95
Z=96

each curve is found at $A_F \sim 226$. This is again due to the behavior of the fission barrier B_f (refer to Figure 13). Furthermore, the value of the fissionability for odd-odd isotopes lies systematically below the adjacent odd-even nuclide on the right wing of the V-shaped curve; indeed the two may be said to lie along two different lines. For the odd-odd isotopes, no correction of Δ_S is required; however, for neutron emission the residual nuclide becomes odd-even and a correction of Δ_n is required. This reduces the neutron density of final states hindering the release of a neutron. Therefore, the odd-odd nuclide tends to be more fissionable and on the average emit fewer neutrons, that is to say, a lower Γ_n/Γ_f value. The opposite trend is held for odd-even nuclides with a result of higher Γ_n/Γ_f value. This effect is less apparent in the left wing of the V-shaped curves and the less fissionable isotopes of francium and actinium, mainly because these nuclides have fewer protons and neutrons and subsequently smaller corrections on Δ_S and Δ_n.

The left wings of all of the V-shaped curves correspond to nuclides on the very neutron deficient side, e.g., $^{216-224}$Th and $^{218-225}$U. Not a single nuclide of this kind has ever been used as an experimental target for a fission study because of its non-availability. Experimental data of the fissionability only exist for the right wings of these curves; the best known plot of the experimental fissionability was

made by Vandenbosch and Huizenga (Va58) and reproduced in Figure 15(d). Although the calculated fissionability in Figure 15(a) is in agreement with these experimental data, it should not be directly compared since their approach to the experimental plot is quite different from the present calculation which yields an exact value of fissionability for each specific fissioning nuclide with a precise E^*. They calculated an average fissioning mass by accounting for the average pre-fission neutrons from many sources, having different targets, projectiles, and excitation energy. Furthermore, experimental fissionabilities were averaged from different measurements at different E^*, implicitly indicating that the fissionability was independent of E^*, at least in the quoted $E^* \leqslant 23$ MeV region. In all, their plot may only be treated as an average fissionability vs. average fissioning mass over a wide range of E^*. As will be seen in later sections, excitation energy is also an important factor in determining fissionability and therefore cannot be neglected at even low E^*; furthermore, using some grand average value among some other averages to draw on the complex fission problem clearly leads to an incomplete picture.

A3. Fission probability as a function of E^*

As mentioned in the first chapter, the dependence of fissionability on excitation energy E^* had been a point of

debate for many years. Part of the reason for the continuing controversy is that until now no complete set of excitation functions were available to examine this problem.

From Eqs. (01) and (02), fissionability is taken to be a function of excitation energy explicitly. If, rather, the fissionability has a constant value with respect to E^*, the most obvious effect on the calculated fit would be a general overestimate of the peaks of complex reactions such as (p,7n) at high E^* region, and a general underestimate fo the peaks of simple reactions such as (p,n) at low E^*. This would be owing to a lower value of fissionability with respect to the average at low E^* and vice versa.

Dependence of the fissionability on E^* has already been noted in Figure 15 where the V-shaped curves flatten with increasing E^*. The fissility P_f of isotopes of thorium and protactinium with fissioning masses A_F pertinent to the present work are plotted against E^* and illustrated in Figure 16. Also indicated among the curves are the A_F and the value of $(B_n - B_f)_{eff}$. At $E^* \leq 40$ MeV, fissilities either converge to infinitesimal or close to unity, depending upon whether the $(B_n - B_f)_{eff}$ is less or greater than zero. Furthermore, for a given E^*, the fissility is higher if the $(B_n - B_f)_{eff}$ is greater since the fission is more favored due to the relatively high neutron binding energy.

As shown in the figure, at $E^* > 40$ MeV, fissilities increase with increasing E^* and tend to level off to unity

Figure 16

Calculated fissility as a function of E^*

(a) at thorium

(b) at protactinium

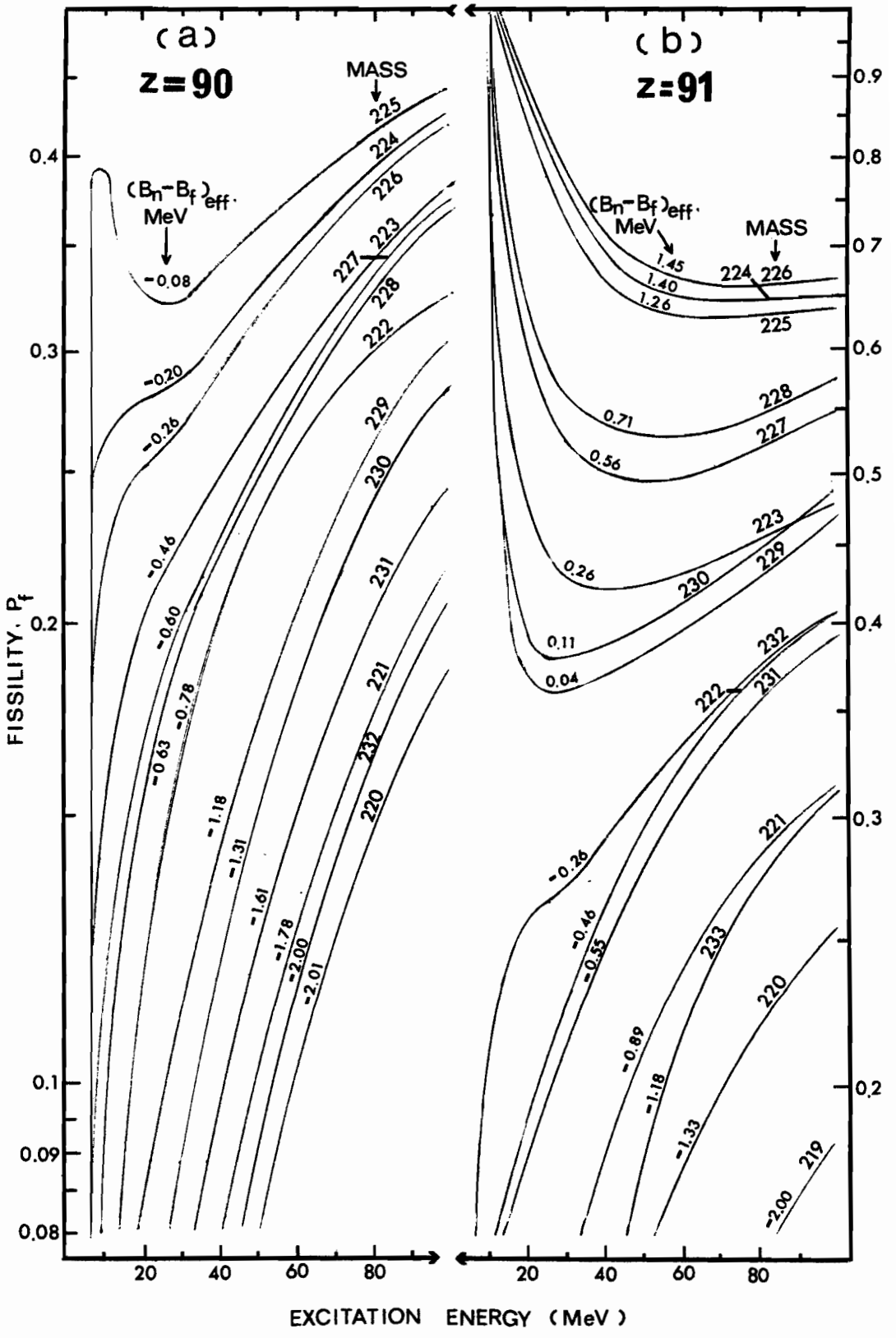
(a)
z=90
MASS
225
224
226
223
227
228
222
229
230
231
221
232
220
(Bn-Bf)eff.
MeV
-0.08
-0.20
-0.26
-0.46
-0.60
-0.63
-0.78
-1.18
-1.31
-1.61
-1.78
-2.00
-2.01
(b)
z=91
(Bn-Bf)eff.
MeV
MASS
1.45
1.40
1.26
224
226
225
0.71
228
227
0.56
223
0.26
230
229
0.11
0.04
232
222
231
-0.26
221
-0.46
-0.55
233
-0.89
220
-1.18
-1.33
219
-2.00
FISSILITY, Pf
0.4
0.3
0.2
0.1
0.09
0.08
0.9
0.8
0.7
0.6
0.5
0.4
0.3
0.2
20
40
60
80
EXCITATION ENERGY (MeV)

at very high E^*. At $E^* > 100$ MeV, fissility P_f can be simplified as $P_f \simeq \left[1 + \text{constant} \cdot \sqrt{E^*} \exp\left(\frac{\sqrt{E^*}}{-4}\right)\right]^{-1}$; indeed if the excitation energy is high enough, e.g., in the GeV region, the simplified P_f becomes unity or 100% fission.

The regular dependence of the fissility on $(B_n - B_f)_{eff}$ is consistent with the observations of the convex and V-shaped curves in Figures 14 and 15, respectively. For the thorium isotopes the highest $(B_n - B_f)_{eff}$ value is -0.08 MeV, corresponding to the fissioning nucleus ^{225}Th, which is indeed the turning points of those curves pertinent to thorium isotopes. Similarly, the highest $(B_n - B_f)_{eff}$ value among protactinium isotopes is +1.45 MeV at the fissioning nucleus ^{226}Pa; therefore all curves related to protactinium turn over at around $A_F = 226$.

As shown in Figure 16(b), isotopes of Pa with $223 \leqslant A_F \leqslant 230$ have positive values of $(B_n - B_f)_{eff}$; therefore the fissilities of these nuclides lie close to unity at an excitation energy equivalent to the effective neutron binding energy. On the other hand, the fissilities of the remaining protactinium isotopes, having negative values of $(B_n - B_f)_{eff}$, converge to infinitesimal at excitation energy equivalent to the effective fission barrier. For thorium isotopes, as shown in Figure 16(a), all fissilities converge to infinitesimal at excitation energy equivalent to the effective fission barrier. This is because the values of $(B_n - B_f)_{eff}$ of the thorium isotopes are all negative.

B. Fission Information

In the previous chapter the theoretical calculation has been demonstrated to predict highly successfully seventeen experimental excitation functions of the ^{232}Th(p, Spallation) reactions with incident proton energies to 100 MeV. The program code which has been used, however, does not evaluate the detail of the fission. In order to obtain the individual fission information, a modified version of Gadioli's program code is made to store the fissioning nuclide, its excitation energy, and the fission cross sections. Calculation based on the modified code were performed with 5 000 cascades with incident proton energies to 85 MeV.

To avoid misunderstanding, a brief example of the ^{232}Th(p,nF) fission is given. The probability that ^{233}Pa, excited by a 45 MeV incident proton on the target ^{232}Th, goes to fission is about 17.5% (refer to Figure 16(b)). The remaining 82.5% ^{233}Pa then goes to neutron emission while charged particle emission has a relatively negligible probability (refer to Figure 12). The surviving excited nuclide after the first chance fission and followed by the first evaporated neutron is then ^{232}Pa, excited to the order of 40 MeV. The probability of that ^{232}Pa fissioning is now 26.1%. Therefore, the overall probability of the (p,nF) happening is 82.5% x 26.1% = 21.6%. If the called random

number in the calculation falls into this 21.6% region, an event of (p,nF) fission, one pre-fission neutron, an excitation energy associated with fission of E^*_F = 40 MeV, and a fissioning nuclide ^{232}Pa are stored. Accordingly, the details of fission can be calculated from the probability of each individual surviving fission in a series of competing nuclides at their respective excitation energies along the deexcitation chain.

Weighted results over all fission events, including the average numbers of pre-fission neutrons, the total fission cross sections, the average fissility, the average fissioning charge, and mass are listed in Table 06.

B1. The average fission information

The pre-fission neutrons are defined as those emitted in both the pre-equilibrium and evaporation stages before the excited nucleus fissions. For instance, if there are two neutrons emitted in the "long" evaporation stage after one neutron emitted in the "short" pre-equilibrium stage and finally the (p,3nF) fission occurs, there are totally three pre-fission neutrons counted. The average number of pre-fission neutrons per fission, $\bar{\nu}_{pre}$, is therefore the weighted average over all (p,Fission) events.

As listed in the table, no pre-fission neutron has been calculated in the 8 MeV case, that is to say, the only fission mode is the (p,F) reaction, having the fissioning

Table 06

Calculated result of the average information of the ^{232}Th(p,Fission) reaction.

Incident proton energy, MeV	8	20	30	40	50	60	70	85
Average pre-fission neutrons	0.0000	1.0699	1.7200	2.0742	2.3260	2.3251	2.3869	2.4170
Total fission cross section, mb	3.4	426.4	909.6	1135.4	1164.5	1092.4	1005.3	965.0
Average fissility, %	6.20	35.63	54.01	65.26	65.47	64.91	62.45	61.29
Average fissioning charge	91.000	91.000	91.000	90.994	90.976	90.945	90.897	90.807
Average fissioning mass	233.00	231.93	231.28	230.92	230.65	230.62	230.51	230.39
Average excitation energy for fissioning nuclide, MeV	13.21	16.53	20.95	26.33	32.00	39.73	46.60	48.78

compound nucleus $^{233}Pa = p + ^{232}Th$. As the bombarding energy increases, the number of the pre-fission neutrons also increases. At incident proton energies above 50 MeV, the numbers of pre-fission neutrons become roughly constant although increasing slowly on the high energy side. This is because the (p,XnF) fissions with small values of X predominate in all kinds of fission modes.

The calculated total fission cross sections, a summation of those from individual (p,XαYpZnF) fission, have been used to determine the best value of the only parameter in the present calculation, the ratio of a_f/a_n (refer to Figure 07).

The average fissility, calculated as the fraction of the total fission cross sections to the total reaction cross sections, increases steadily with increasing incident proton energy, then levels off at energies above 40 MeV at around 63%. This indicates two thirds of the total reactions go to fission.

The average fissioning charge is 91, protactinium, at incident proton energies below 40 MeV. It implies that only the (p,XnF) fissions count in this energy region since excited nuclides other than the protactinium isotopes in the deexcitation chain are not likely to fission. On the high energy side, the average fissioning charge gradually decreases with increasing incident proton energy but remains near 91. This indicates the (p,XnF) fissions are still predominant throughout the energy region although some more

complex fissions like (p,XαYpZnF) with much lower cross sections emerge at these high energies.

The average fissioning mass for the 8 MeV case is 233 since the excitation energy is barely enough to initiate the only fission mode, the (p,F). At higher incident proton energies, more fission modes become available and therefore the average fissioning mass decreases with increasing incident proton energy. At incident proton energies between 40 and 85 MeV, the average fissioning mass decreases from 230.9 to 230.4; this indicates the predominant (p,XnF) fissions are heavily concentrated among those with $X < 6$, corresponding to fissioning nuclides $^{233-227}Pa$.

The last row in the table gives information on the average excitation energy associated with fission at various incident proton energies. In the 8 MeV case, the average excitation energy associated with the only fission mode, the (p,F), is simply the sum of the incident proton energy, corrected to the center of the mass (CM) system from the lab system, and the proton binding energy of the $^{232}Th + p$ system. Indeed, for each and every (p,F) fission there is one and only one excitation energy associated with fission. However, this unique energy distribution does not hold for fission modes other than (p,F) which involve pre-fission particle emission. In the 85 MeV case, there are 23 fission modes; the average 48.8 MeV excitation energy associated with fission cannot reflect the actual energy distribution since

fission can happen at whatever excitation energy is available for fission owing to the Monte Carlo approach.

A representative result of the calculated fissioning charge, mass and cross sections for individual (p,XαYpZnF) fission modes is listed in Table 07. In the highest proton energy case, the fissioning masses of protactinium, thorium, and actinium, corresponding to the (p,XnF), (p,pXnF), and (p,αXnF) / (p,2pXnF) fission modes, respectively, have been obtained. However, this should not be interpreted as indicating that no fission occurs in nuclides with $Z_F \leqslant 87$ in the present studies. The lowest fission cross section listed in the table is about 0.3 mb, corresponding to the event of one out of 5 000 reactions, which is the limit of the present calculation. If more cascades were run in this work, the more complex fission mode of (p,XαYpZnF) with large values of X, Y, and Z, corresponding to the fissioning nuclides with $Z_F \leqslant 87$, might have appeared in the calculation with cross sections < 0.3 mb.

B2. The fissioning spectra

The fissioning spectrum of the (p,XαYpZnF) fission, defined as the excitation energy distribution for the fissioning nucleus, is the direct reflection of the kinetic energies of the pre-fission particles of X alphas, Y protons, and Z neutrons. For instance, the pre-fission neutron in (p,nF) fission at 90 MeV excitation energy may take away

Table 07

Theoretical calculation of the fissioning nuclides and cross sections of the $^{232}Th(p,Fission)$ reaction.

Fission mode	Fissioning nuclide	Fission cross sections (mb) at E_p (MeV) 8	20	40	60	85
(p,F)	^{233}Pa	3.35	114.50	194.37	151.37	115.46
(p,nF)	^{232}Pa	-	170.38	266.13	225.87	174.74
(p,2nF)	^{231}Pa	-	141.30	204.82	200.47	157.36
(p,3nF)	^{230}Pa	-	0.23	232.34	195.73	135.64
(p,4nF)	^{229}Pa	-	-	175.56	117.84	89.08
(p,5nF)	^{228}Pa	-	-	56.08	89.06	64.25
(p,6nF)	^{227}Pa	-	-	-	44.36	32.59
(p,7nF)	^{226}Pa	-	-	-	10.16	16.76
(p,8nF)	^{225}Pa	-	-	-	-	4.66
All (p,XnF)	Pa	3.35	426.41	1129.30	1034.86	790.54
(p,pF)	^{232}Th	-	-	4.18	12.19	31.66
(p,pnF)	^{231}Th	-	-	1.39	16.59	33.83
(p,p2nF)	^{230}Th	-	-	0.35	13.88	34.76
(p,p3nF)	^{229}Th	-	-	-	5.07	20.48
(p,p4nF)	^{228}Th	-	-	-	6.34	29.18
(p,p5nF)	^{227}Th	-	-	-	0.34	6.21
(p,p6nF)	^{226}Th	-	-	-	-	9.62
(p,p7nF)	^{225}Th	-	-	-	-	1.24
All (p,pXnF)	Th	—	—	5.92	54.41	166.98

... cont'd

Table 07 - cont'd

Fission mode	Fissioning nuclide	Fission cross sections (mb) at E_p (MeV) 8	20	40	60	85
(p,αF)	^{229}Ac	-	-	0.35	1.02	1.86
(p,αnF)	^{228}Ac	-	-	-	1.02	1.24
(p,α2nF)	^{227}Ac	-	-	-	0.68	1.86
(p,α3nF)	^{226}Ac	-	-	-	0.34	1.55
(p,α4nF)	^{225}Ac	-	-	-	-	0.31
(p,α5nF)	^{224}Ac	-	-	-	-	0.62
All (p,αXnF)	Ac	—	—	0.35	3.06	7.44
(p,Fission)	——	3.35	426.41	1135.57	1092.33	964.96

30 MeV as its kinetic energy (this could happen if the neutron leaves the excited ^{233}Pa in the pre-equilibrium stage), or the outgoing neutron may take away about 4 MeV as its kinetic energy, equivalent to twice the nuclear temperature of the excited ^{233}Pa (this could happen if the neutron leaves the excited ^{233}Pa in the evaporation stage). After the neutron emission, the remaining excitation energy associated with the fissioning nuclide ^{232}Pa, less the first pre-fission neutron binding energy, is therefore 54 MeV for the former and 80 MeV for the latter. Hence, excitation energy could be widely distributed.

For each incident proton energy, the fissioning excitation energy spectra of all fission modes have been binned into 18 energy sections in the present calculation. Results for those fission modes with large cross sections are shown in Figure 17, including fission modes of (p,XnF) with X = 1-6 and (p,pXnF) with X = 0-4. Also shown in the figure are the integrated cross sections in millibarns for each fission mode.

Most of the 53 fissioning spectra shown in the figure have widely distributed excitation energies. For instance, the calculated fissioning spectrum of (p,nF) at 85 MeV incident proton energy, as shown in Figure 17(1A), has excitation energies ranging from 9 MeV to 82 MeV. It certainly should not be represented by a single, average value.

There are several similarities among the (p,XnF) fis-

Figure 17

Spectra of the excitation energy associated with the fissioning nuclides in the $^{232}Th(p,Fission)$ reaction

(XY) assignment:

X = incident proton energy,	Y = fission mode
X = 1: at 85 MeV	Y = A: (p,nF)
X = 2: at 70 MeV	Y = B: (p,2nF)
X = 3: at 55 MeV	Y = C: (p,3nF)
X = 4: at 40 MeV	Y = D: (p,4nF)
X = 5: at 25 MeV	Y = E: (p,5nF)
X = 6: at 75 MeV	Y = F: (p,6nF)
X = 7: at 65 MeV	Y = G: (p,pF)
X = 8: at 45 MeV	Y = H: (p,pnF)
	Y = K: (p,p2nF)
	Y = L: (p,p3nF)
	Y = M: (p,p4nF)

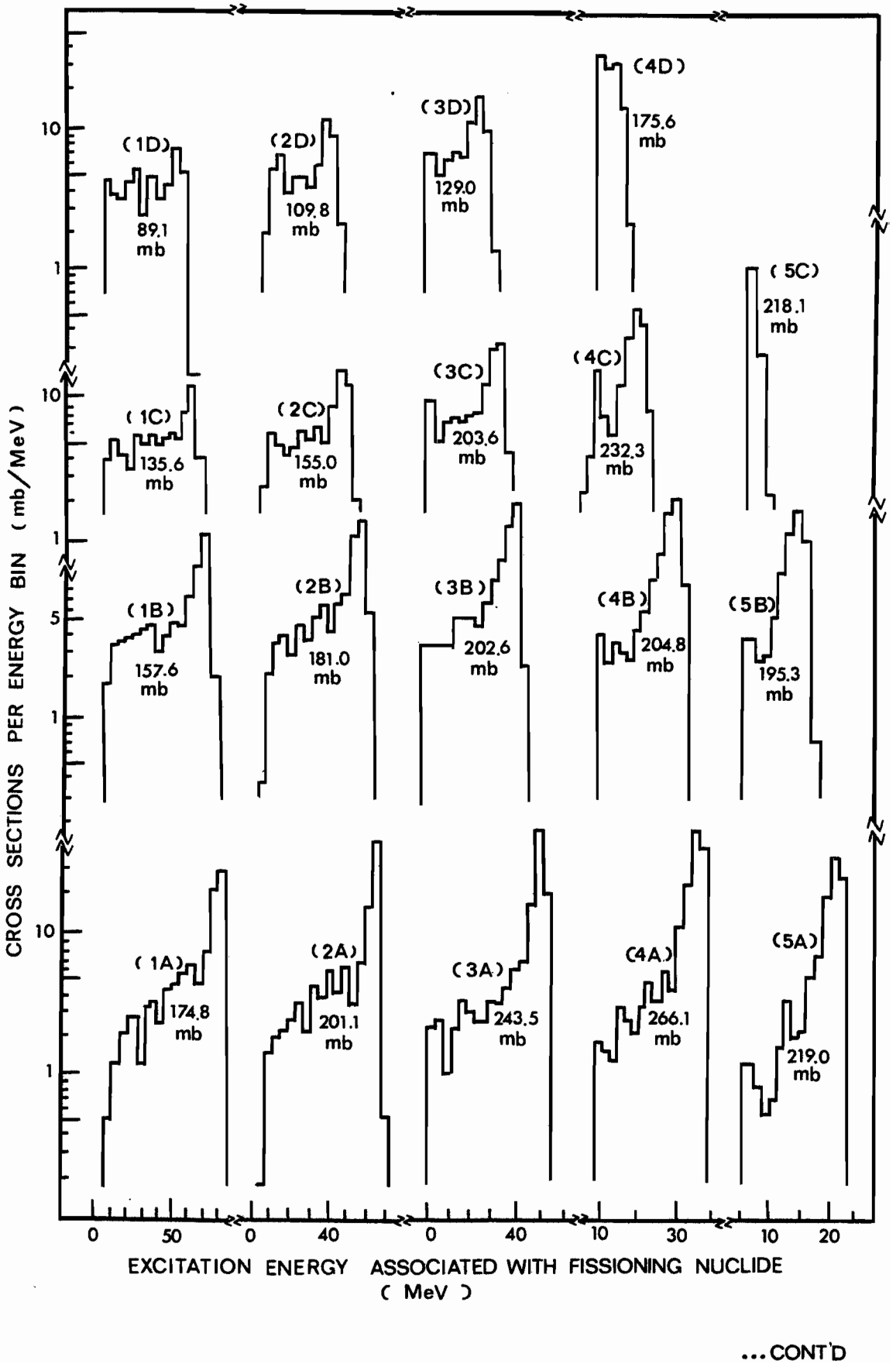
(1D)
89.1 mb
(2D)
109.8 mb
(3D)
129.0 mb
(4D)
175.6 mb
(5C)
218.1 mb
(1C)
135.6 mb
(2C)
155.0 mb
(3C)
203.6 mb
(4C)
232.3 mb
(1B)
157.6 mb
(2B)
181.0 mb
(3B)
202.6 mb
(4B)
204.8 mb
(5B)
195.3 mb
(1A)
174.8 mb
(2A)
201.1 mb
(3A)
243.5 mb
(4A)
266.1 mb
(5A)
219.0 mb
CROSS SECTIONS PER ENERGY BIN (mb/MeV)
EXCITATION ENERGY ASSOCIATED WITH FISSIONING NUCLIDE
(MeV)

...CONT'D

FIGURE-17 (CONT'D)

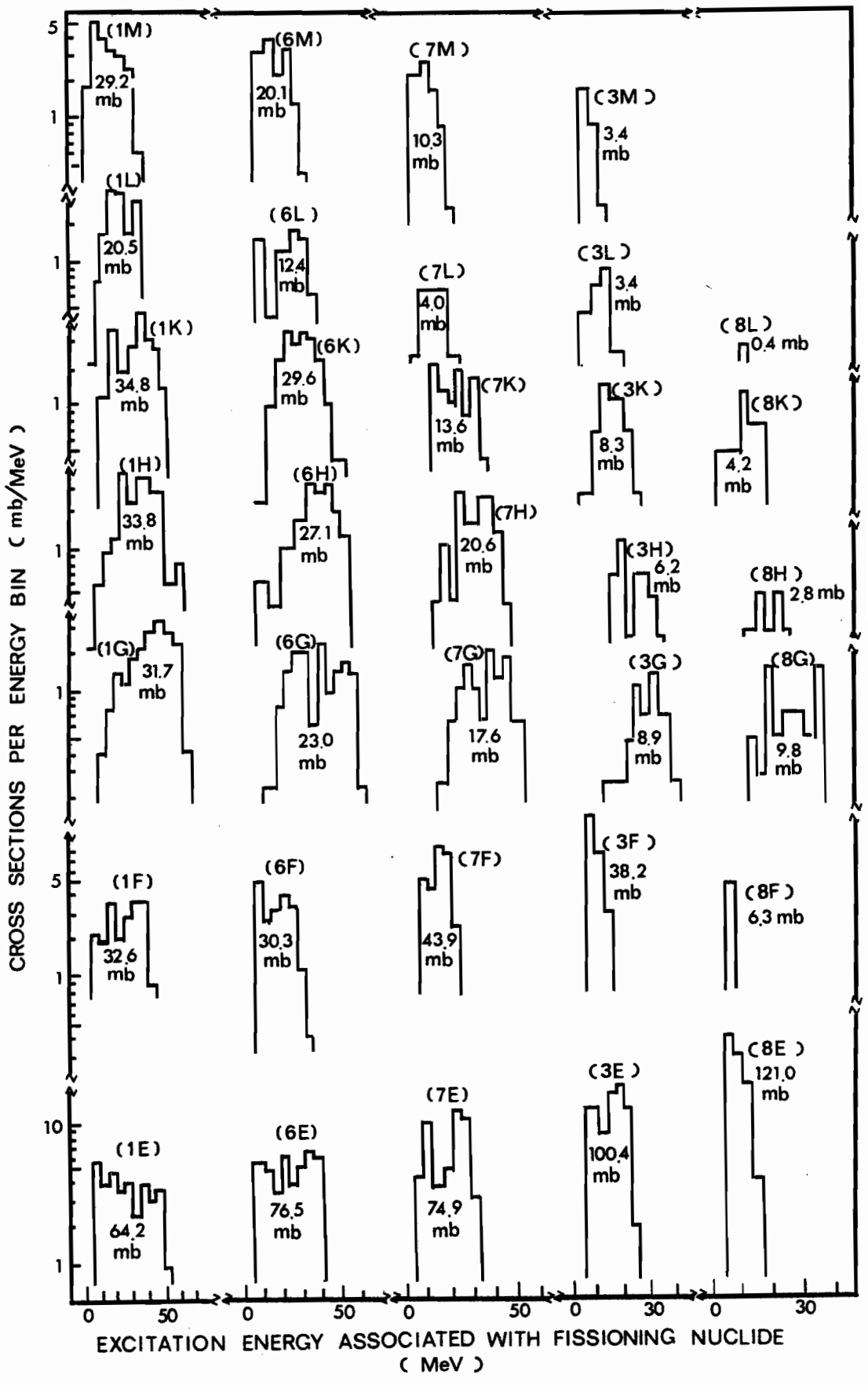

sioning spectra with X = 1-4 in the figure. First, each spectrum peaks at the highest excitation energy available for fission. Secondly, the peak area in each spectrum represents those fission events having the least amount of kinetic energy carried away by those pre-fission neutrons. Thirdly, each spectrum has a tail on the low excitation energies side; this is mainly because the fissility P_f decreases with decreasing E^* (refer to Figure 16(b)). Finally, the tail area in each spectrum represents those fission events having a large amount of kinetic energy carried away by those pre-fission neutrons.

For the (p,5nF) and (p,6nF) spectra, the characteristics mentioned above are reversed and the peak shows up at low excitation energies with a tail at high excitation energies. This is because the fissilities of the fissioning ^{228}Pa and ^{227}Pa, respectively, increase with decreasing E^*.

Unlike the peak-tail type of the (p,XnF) fissioning spectra, those of the (p,pXnF), involving an outgoing proton before fission, are generally flat. In the case of (p,pF) fission, the outgoing proton can be treated as an inelastic scattered particle and the remaining ^{232}Th survives long enough to go into the evaporation stage where fission starts competing with other decay modes. The flatness implies the kinetic energy of the inelastic scattered proton can be anywhere from zero to the highest available energy. Again because the fissility of the fissioning ^{232}Th decreases expo-

nentially with decreasing E^* (refer to Figure 16 (a)), the spectrum of (p,pF) fission has a tail at low excitation energies. For (p,pXnF) fissioning spectra with X = 1-4, these observed trends also hold despite the emergence of the emission of X pre-fission neutrons. At each given incident energy, the (p,pXnF) fissioning spectrum rises roughly about 10 MeV lower than that of the (p,p(X-1)nF) fission; the 10 MeV difference is attributed to the emission of the extra pre-fission neutron.

In all, the conclusion is made that as long as the excitation energy is greater than the effective fission barrier, fission can occur and there is therefore a widely distributed spectrum for all kinds of (p,Fission) reactions.

C. Summary of the Pre-fission Calculation

The theoretical calculation in this work yields quantitative details about the ^{232}Th(p,Fission) reactions. The identity of the fissioning nuclide, its excitation energy, the numbers of pre-fission neutrons, and the fission cross sections for each fission mode have been evaluated. Although the calculated result of fission is difficult to be measured directly by experiment, the result may be considered as reliable as the theoretical calculation of the spallation reactions, which gave a strikingly good fit to the experimental data. This is because in each and every step in the calcula-

tion, fission and spallation are interlocked with each other. A further support of this interlocking is discussed below.

The proton induced spallation reaction on the heavy but less fissionable target, ^{209}Bi, has been investigated by Lebeyec and Lefort (Le67). They found the ratio of the cross sections of the (p,7n) to (p,p6n) reactions at 85 Mev incident proton energy, both involving seven emitted particles, is close to unity. However, in the present work, the same ratio on the more fissionable thorium target is $\sigma(p,7n) / \sigma(p,p6n) = 3$ mb / 30 mb = 0.1 , only one tenth of that found in the bismuth region. Since both bismuth and thorium have fairly similar nucleon binding energies and Coulomb barriers for proton emission, we expect the ratio for thorium to be about the same as that in bismuth. The difference in the two cases is that the only deexcitation channel opened in the less fissionable bismuth is spallation, but in the thorium case both fission and spallation are probable. Therefore, the fission cross section affects the ratio. The last competition between fission and spallation happens at ^{227}Pa and ^{227}Th for $^{232}Th(p,7n)^{226}Pa$ and $^{232}Th(p,p6n)^{226}Th$, respectively; if it goes to fission, the fission modes, corresponding to the respective spallation reactions, are (p,6nF) and (p,p5nF). The fission cross sections of these fission modes are 33 mb and 6 mb (refer to Table 07), respectively. Therefore, one can account for the experimental facts. If the fission is included in the thorium case, we find the ratio

in thorium is indeed unity:

$$\frac{\sigma(p,7n) + \sigma(p,6nF)}{\sigma(p,p6n) + \sigma(p,p5nF)} = \frac{3\ mb + 33\ mb}{30\ mb + 6\ mb} = 1$$

The "missing" portion in the spallation ratio of thorium is actually the "loss" to fission.

The grand average of the fission calculation, such as the average fissioning charge, mass, its excitation energy, and fission cross sections, is the average over many widely distributed events. For instance, at 85 MeV of incident proton energy the average fissioning nuclide and its excitation energy are $^{230.4}90.8$ and 48.8 MeV, respectively. These represent 23 different fission modes comprising 166 excitation energy bins with ranges of $89 \leqslant Z_F \leqslant 91$, $224 \leqslant A_F \leqslant 233$, and $8\ MeV \leqslant E^*_F \leqslant 90\ MeV$. Hence, the true picture of fission, in particular of high energy fission, cannot be drawn simply by taking the grand average values.

Based on the details of the fission calculation, an attempt has been made to explore the post-fission behavior, including the calculation of post-fission neutrons, nuclear charge distribution, and symmetric to asymmetric ratio in fission. These will be discussed both qualitatively and quantitatively in the following chapters.

V

CALCULATION OF POST-FISSION NEUTRONS

Based on the calculated information for the fissioning nuclide, its excitation energy, and the fission cross section, an attempt was made to evaluate the post-fission neutron yield. A brief discussion of the fission process is given in the following section.

A. Fission Process

When the energetic proton strikes the target nuclide, either spallation or fission may occur. For the ^{232}Th(p, Fission) reaction, there may be some pre-fission nucleons leaving the excited nucleus during the deexcitation process. After the emission of the pre-fission nucleons and particles, the remaining nucleus is elongated and contracted by the Coulomb and surface energies of the fissioning nucleus, respectively.

When the fissioning nucleus is elongated slightly beyond the "saddle point" configuration, the Coulomb repulsion forces drive the fissioning nucleus apart. The fissioning nucleus then reaches the "scission point" where the highly deformed fissioning nucleus splits into at least two "primary fragments". For a "binary fission" involving a release of two primary fragments, the light and heavy fragments are designated as (Z'_L, A'_L) and (Z'_H, A'_H), respectively. In spite of many investigations which have been done in the past forty years, the basic question in fission is still open:

is the process from saddle point toward the scission point fast or slow? It is here that the different postulates of the post-fission charge distributions arise. As mentioned in the first chapter, if the motion between the two points is fast, the charge distribution follows the UCD postulate; if slow, it follows the MPE hypothesis.

At the instant of scission, or immediately thereafter while the two primary fragments are still close together, some light nuclei, primarily alpha particles, may be emitted. The chances of light-nuclei accompanying fission are found to increase slowly with increasing Z^2/A value of the fissioning nuclide (Lo67) and/or the excitation energy (Th66). The probability of this kind of fission in ^{232}Th(p,Fission) reactions, interpolated from their results, is estimated below 0.5% of each binary fission in this work. On the other hand, there is a possibility that the fissioning nucleus may split into three fragments of comparable mass and hence called "ternary fission". Previous experiments indicated that the probability of ternary fission is both excitation energy and fissioning nucleus dependent (Ya68). The ratio of ternary to binary fission events in ^{232}Th(p, Fission) reactions is estimated around 10^{-7}. Hence, fissions other than binary may be ignored in the present calculation owing to their low frequency.

In a time period of about 10^{-20} second after scission, the primary fragments reach their maximum kinetic energy (Ya68).

Some of the outgoing neutrons are emitted within this period. Whether these neutrons are emitted at scission or in the short post-fission period is very difficult to verify experimentally. In the present work these neutrons, usually designated as "scission neutrons" or "central neutrons", are treated as being emitted from the primary fragment, rather than the fissioning nuclide.

Under all these simplified situations the sum of the two fission fragment charges and masses, $Z'_L + Z'_H$ and $A'_L + A'_H$, are equal to the fissioning charge Z_F and mass A_F, respectively. In this work the primed quantities refer to the primary fragments, and those subscripted L and H to light and heavy masses, respectively.

Most of the outgoing neutrons, however, are emitted from the fully accelerated fragments. Fraser (Fr52) showed that experimental data indicate most of the outgoing neutrons are emitted at times shorter than 4×10^{-14} second after scission, as expected from evaporation theory. All kinds of outgoing neutrons which are emitted from fully accelerated primary fragments then are called "fragment neutrons". Collectively, scission and fragment neutrons are referred to as "prompt neutrons".

Similar to the evaporation calculation in the spallation reaction, charged particle emission in the post-fission deexcitation stage has to be considered. However, experimental data compiled by Vandenbosch and Huizenga (Va73)

showed that charged particles emitted in fission appear predominantly at right angles to the primary fragment tracks. Hence, charged particles are emitted preferentially at scission, rather than evaporated in the post-fission period. In the present calculation, prompt neutron emission is considered as the only deexcitation mode as long as the excitation energy is greater than the neutron binding energy.

After the emission of all prompt neutrons, the fragment finally loses the remaining excitation energy by the "prompt gammas". Maier-Leibnitz, Armbruster, and Specht (Ma65) compiled fission data and showed that approximately 10^{-11} second after scission, prompt gammas appear. Comparison of the average lifetime with the Weisskopf estimate for $\sim$ 1 MeV gamma indicates that only M1 and E2 radiations are important for the majority of the prompt gammas. After the gamma emission, the cooled fragments are then referred to as "secondary fragments" or "independent fission products". The light and heavy independent fission products are designated as (Z_L, A_L) and (Z_H, A_H), respectively. The unprimed quantities in this work refer to the independent fission products. The following properties of fragments and products are therefore maintained:

$$Z'_L = Z_L, \quad Z'_H = Z_H, \quad A_H = A'_H - \nu_H, \quad \text{and} \quad A_L = A'_L - \nu_L$$

where ν_L and ν_H are the numbers of prompt neutrons associated with light and heavy fragments, respectively.

The independent products are in most cases radioactive and the final stage of the fission process is the radioactive decay of the independent products, accompanied by "delayed gammas", to the stable end products. Some radioactive decays in mass chains 85-90, 92-94, 98-99, and 134-144 lead to a level which is neutron-unstable (Wa69). Hence, "delayed neutrons" may be emitted from the neutron-unstable nuclides. The radioactive half-lives of these nuclides, ranging from 10^{-1} to 10^{2} second, control the emission period of delayed neutrons. The sum of prompt and delayed neutrons is defined as "post-fission neutrons", including all neutrons emitted after scission. Since the number of delayed neutrons is low, about 1% of the prompt neutrons (Ke57), it is not counted in the present calculation; the prompt neutrons evaluated in this work are therefore considered to comprise the post-fission neutrons.

B. Calculation of Properties of the Primary Fragments

The total excitation energy of the two primary fragments, E^*_T, may be calculated from the following equation:

$$E^*_T = E^*_F + \Delta M - E_K \qquad (10)$$

with $\Delta M = M(Z_F,A_F) - M(Z'_L,A'_L) - M(Z'_H,A'_H)$

where E^*_F = excitation energy associated with the fissioning nucleus with charge Z_F and mass A_F,

E_k = the total kinetic energy for the primary fragments,

$M(Z,A)$ = mass excess of nucleus with charge Z and mass A in MeV.

Here the E_k is actually derived from the Coulomb repulsion forces between the light and heavy fragments at scission.

Immediately after the scission, E^*_T can be further split into:

$$E^*_T = E^*_L + E^*_H \tag{11}$$

where E^*_L and E^*_H are the internal excitation energy associated with the respective primary fragments. This internal excitation energy is used for post-fission neutron evaporation, using the same theory of evaporation discussed in earlier chapters. In order to calculate the prompt neutrons $\nu_{L,H}$ as a function of primary fragment mass $A'_{L,H}$, each and every energy term in Eqs. (10) and (11) must be evaluated; these are discussed in the following sections.

B1. Mass difference at fission, ΔM

The total excitation energy carried away by primary fragments, E^*_T, is determined by E^*_F, ΔM, and E_k, as reflected in Eq. (10). To calculate the E^*_T, the energy terms ΔM and E_k must first be evaluated. The leading term E^*_F on the right hand side of the equation has been evaluated in

the last chapter. The second term ΔM is the mass difference in MeV between the fissioning mass $M(Z_F,A_F)$ and the primary fragment masses $M(Z'_L,A'_L)$ and $M(Z'_H,A'_H)$. The mass formula adopted in the present calculation is the most recent one derived by Myers (My77), which is based on the Droplet Model with shell and pairing energy corrections. In order to simplify the calculation, all shape factors in the mass equation are taken as unity.

The fissioning mass $M(Z_F,A_F)$ can be calculated directly using the mass equation. The fragment mass, however, has to be averaged over a range of nuclear charges, Z, since for each primary fragment mass chain there is a charge distribution. The distribution of nuclear charge is assumed to be Gaussian in the proton energies pertinent to this work. Hence, the fragment mass can be evaluated by the following equation:

$$M(Z',A') = \sum_Z p(Z) \cdot M(Z,A') \qquad (12)$$

with

$$p(Z) = \frac{1}{\sqrt{\pi C}} \cdot \exp\left[-(Z - Z_p)^2/C\right]$$

where $p(Z)$ = fractional chain yield of fragment having charge Z in mass chain A',

C = Gaussian distribution constant = 1.4.

The $C = 1.4$ is taken from the latest result of ^{232}Th(p,Fission)

reaction data, estimated by Eaker and Choppin (Ea76). Using the two extreme postulates of charge distribution, namely the UCD and MPE, the most probable charge $Z_p(A')$, defined in the first chapter, is evaluated. The calculated average fragment mass is found to be relatively insensitive to the $Z_p(A')$ based on different postulates. This is because the Gaussian distribution tends to wash out the effect of different values of $Z_p(A')$.

Representative results of the mass difference ΔM for some fissioning nuclides, ranging from ^{232}Th to ^{240}Pu, are plotted against the A_H' and illustrated in Figure 18(a). Also shown in the figure are calculated mass differences for thermal neutron induced fissions on ^{233}U and ^{239}Pu from Milton (Mi62) who used a rather simple Liquid Drop Model mass equation derived from Cameron (Ca57). The present calculation of ΔM on ^{234}U and ^{240}Pu is actually a refinement of Milton's evaluations of ΔM on $^{233}U(n_{th},F)$ and $^{239}Pu(n_{th},F)$, respectively. The even-odd effect in the present calculation is clearly reflected in the figure, while the smooth curves from Milton do not include the pairing energy correction. In this figure, all curves and calculated points show a peak in ΔM near $A_H' \sim 132$ and a fall-off in ΔM on the high A_H' side; this is because of the maximum shell correction for those fragments with N = 82 closed-shell in the former and a fairly large, negative shell correction for those very asymmetric fragments with semi-closed neutron shells in the latter.

Figure 18

Calculated ΔM and E_k in the present work

(a) calculated ΔM at scission

(b) synthetic E_k for the $^{232}Th(p,Fission)$

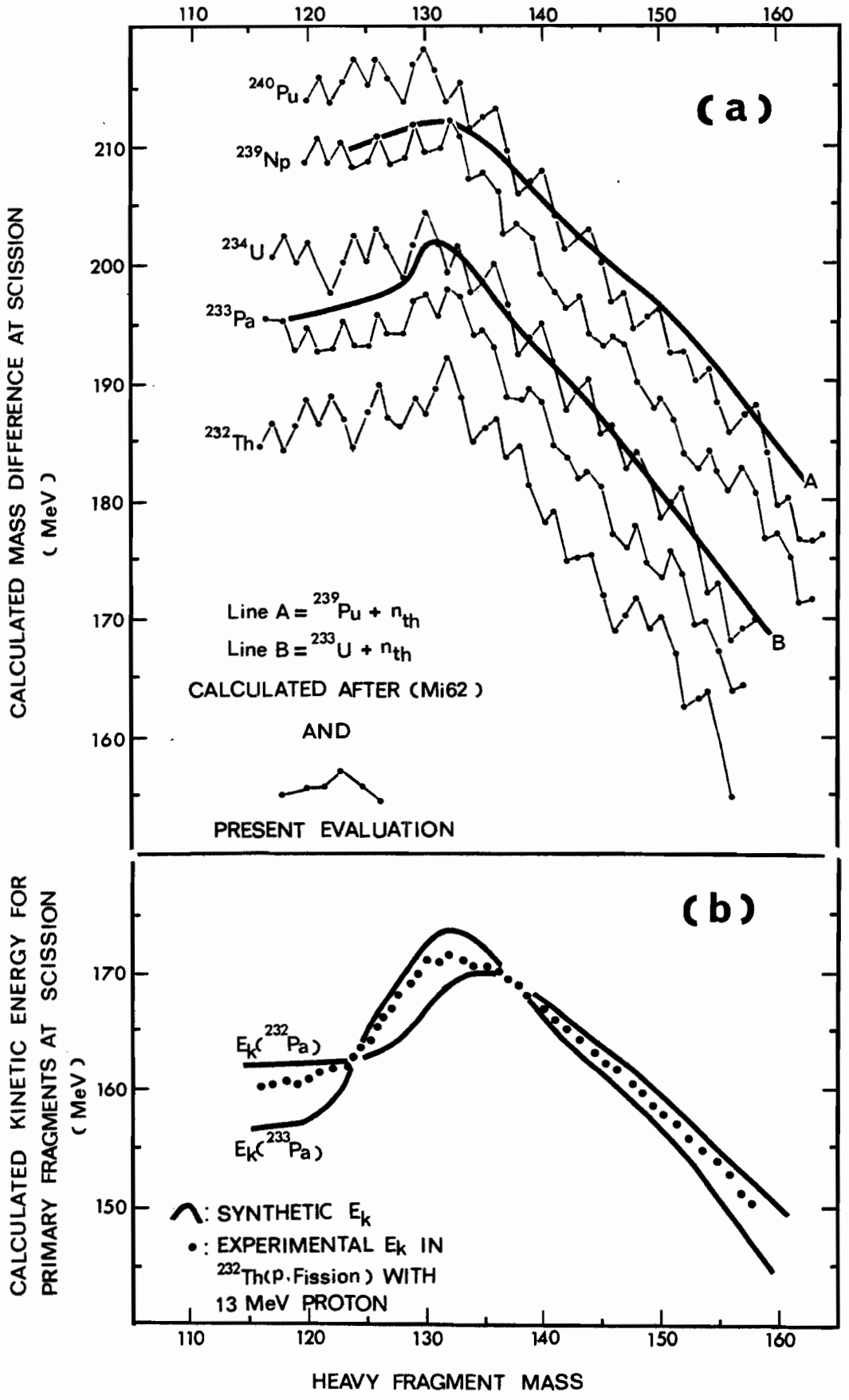
(a)
CALCULATED MASS DIFFERENCE AT SCISSION
(MeV)
110
120
130
140
150
160
210
200
190
180
170
160
240Pu
239Np
234U
233Pa
232Th
A
B
Line A = 239Pu + nth
Line B = 233U + nth
CALCULATED AFTER (Mi62)
AND
PRESENT EVALUATION
(b)
CALCULATED KINETIC ENERGY FOR PRIMARY FRAGMENTS AT SCISSION
(MeV)
170
160
150
Ek(232Pa)
Ek(233Pa)
: SYNTHETIC Ek
• : EXPERIMENTAL Ek IN
232Th(p,Fission) WITH
13 MeV PROTON
110
120
130
140
150
160
HEAVY FRAGMENT MASS

B2. Total kinetic energies for the primary fragments, E_k

Quite a number of fission experiments confirmed that the $\bar{E}_k$, the total kinetic energy averaged over all fragment masses, is nearly independent of the excitation energy. Furthermore, experimental results indicated a fairly systematic variation of the $\bar{E}_k$ with the $Z^2_F/A_F^{1/3}$; this is understandable since the kinetic energy of the primary fragments at infinite distance is equal to the Coulomb repulsion forces at scission, using $Z^2_F/A_F^{1/3}$ as the Coulomb energy parameter. Viola (Vi66) concluded that an empirical formula can fit experimental data of $\bar{E}_k$ over the range of $800 < Z^2_F/A_F^{1/3} < 1650$:

$$\bar{E}_k = 0.1071 \cdot Z^2_F/A_F^{1/3} + 22.2 \text{ MeV} \qquad (13)$$

In addition to the dependence of the $\bar{E}_k$ on Z_F and A_F, the total kinetic energy is also found to be a function of fragment mass. Experimental plots of $E_k(A'_L,A'_H)$ vs. A'_H for fissioning nuclides heavier than ^{226}Ac, as shown by Britt et al. (Br63A) and Croall and Cuninghame (Cr69), generally yield a dip in E_k for a symmetric mass division, a prominent peak in E_k for fission leading to $A'_H \sim 132$, and a decrease of E_k at $A'_H > 132$. An example of an $E_k(A'_L,A'_H)$ vs. an A'_H plot of the ^{232}Th(p,Fission) with 13 MeV protons (Cr69) is reproduced in Figure 18(b). The fall-off in E_k for very asymmetric mass division leading to high A'_H value has a

slope similar to that of the mass difference shown in Figure 18(a), suggesting that simple energetic limitations have become relevant for these mass splits. The peak of E_k at $A_H' \sim 132$ strongly suggests that the shape of these fragments become essentially spherical, resulting in a shorter distance between the two charge centers of fragments at scission, which in turn yields high E_k.

The effect of increasing excitation energy is to decrease the characteristic structure of $E_k(A_L',A_H')$ vs. A_H' mentioned above. This is not because the excitation energy destroys the shell effect but because at high excitation energy multi-chance fission with several other fissioning nuclei is introduced. This argument is further backed by the decrease of characteristic structure of $E_k(A_L',A_H')$ vs. A_H' observed for fissioning nuclei lighter than ^{226}Ra (Un69). Based on these experimental data, a universal synthetic function of $E_k(A_L',A_H')$ is constructed in order to evaluate the total kinetic energy for the primary fragment pair (A_L',A_H') from fissioning nuclide (Z_F,A_F). The synthetic kinetic energy distributions of the fissioning nuclides ^{233,232}Pa, corresponding to the (p,F) and (p,nF) fissions in this work are plotted against A_H' and also illustrated in Figure 18(b); the weighted average of the two synthetic curves is designed to match the experimental data shown in the same plot.

Since the magnitude of the E_k and the mass difference ΔM at scission are essentially independent of E^*_F, the energy

contributed from the fissioning nucleus alone is therefore $\Delta M - E_k$. This quantity, ranging from 10 to 30 MeV, is dependent upon the A'_L, A'_H, Z_F, and A_F. Adding the term E^*_F to $\Delta M - E_k$, the resultant becomes the total excitation energy at scission and is subsequently transferred to the internal excitation energy of the primary fragments. These energies give rise to the prompt neutrons and prompt gammas as the deexcitation of fragments occurs.

B3. Internal excitation energy of the primary fragments, $E^*_{L,H}$

In the present calculation, the E^*_T is divided such that the internal excitation energy $E^*_{L,H}$ is proportional to its mass:

$$E^*_T/A_F = E^*_L/A'_L = E^*_H/A'_H \qquad (14)$$

This is equivalent to an assumption of thermal equilibrium at the scission point. If the neutron binding energies for each fission fragment is the same, the prompt neutron distribution should be observed as a linear function of primary fragment mass A' with the assumption. However, this assumption may be invalid for spontaneous fission and very low energy fission such as the (n_{th},F) reaction. Measurements of the prompt neutron distribution in these fissions showed a unique "saw-tooth" characteristic (Va73). With increasing

excitation energy, the strong saw-tooth variation of the prompt neutron distribution is fairly rapidly washed out. Bishop et al. (Bi70) found that U(p,Fission) with 10 MeV protons yields a distinct saw-tooth curve for the prompt neutron distribution; however, at around 20 MeV of incident proton energy, the saw-tooth character disappears and the curve becomes relatively linear. This is presumably because the shell effect is washed away at high excitation energy involving multi-chance fission, resulting in a tendency toward thermal equilibrium at scission. The fact remains that at proton energies pertinent to this work, the thermal equilibrium assumption is supported by the experimental observation in (Bi70).

B4. Prompt gamma ray energy, E_γ

After the internal excitation energy $E^*_{L,H}$ is assumed, the prompt gamma ray energy $E_{\gamma_{L,H}}$ must be deducted from it in order to obtain the net energy available for the evaporation of prompt neutrons.

Experimental results, as summarized by Vandenbosch and Huizenga (Va73), show that the total prompt gamma ray energies are dependent upon neither the excitation energy nor the identity of the fissioning nucleus. This is because the prompt gamma emission occurs only at the last stage of deexcitation of the fission fragment, losing all memory about the pre-fission identity. There are typically about eight

prompt gammas per fission with an average energy about 1 MeV/gamma, resulting in a total prompt gamma ray energy of approximately 8 MeV (Va73). This is due to the sum of the remaining excitation energies for each fission fragment being too small to overcome the average 8 MeV neutron binding energy and neutron kinetic energy, thereafter appearing as the energy for gamma ray emission.

The prompt gamma ray energy $E_{\gamma_{L,H}}$ has been found to be a function of fragment mass in thermal neutron induced fission and spontaneous fission. Similar to the prompt neutron distribution in very low energy fission, a saw-tooth character is also observed in the prompt gamma distribution. However, there are no prompt gamma yields measured at high excitation energy; whether this saw-tooth character is washed out at high excitation energy is not known. The gamma ray energy distribution is assumed in the present calculation as:

$$E_{\gamma_L}/A_L = E_{\gamma_H}/A_H \qquad (15)$$

with

$$E_{\gamma_L} + E_{\gamma_H} = 8 \text{ MeV}$$

Since there is no experimental support for the idea in Eq. (15), one may argue that other versions of the E_γ distribution, in particular a synthetic saw-tooth function,

may give a better prediction. Although the present assumption of the E_γ distribution may not be the best one, the error in the energy dissipated by gamma rays in a single fragment cannot be more than 2 MeV. In considering this small uncertainty, it is believed that the present treatment of E_γ is sufficient and further refinement is not necessary.

B5. Neutron binding energy, B_n

To evaporate a prompt neutron in the deexcitation of a fission fragment, the internal excitation energy $E^*_{L,H}$ must be large enough to overcome the binding energy of the least bound neutron of the fission fragment. During the deexcitation of the fragment, there is a competition among neutron emission, charged particle evaporation, and gamma ray emission. The chance of charged particle evaporation is assumed to be zero for the reasons given in the previous section; gamma ray emission is also assumed to be zero during the neutron evaporation stage since the time period required for the observed prompt gamma emission is much longer than that of prompt neutron emission. Hence, as long as the internal excitation energy is greater than the neutron binding energy, prompt neutron emission is considered as the only deexcitation mode.

Early investigators frequently applied an average neutron binding energy $\overline{B}_n$ for estimating the prompt neutron yield; for instance, $\overline{B}_n$ = 7 MeV was suggested by Levy (Le57).

Using the average $\bar{B}_n$ can avoid the complexity of B_n calculation since the nuclear charge distribution in the fragment mass chain must be evaluated first. However, an average $\bar{B}_n$ may lead to an erroneous prediction of the prompt neutron yield. Since the excited fission fragments are mainly neutron rich and far from beta stability, the average $\bar{B}_n$ is then greater than the actual binding energy of the primary fragment.

In order to take account of the variation of B_n on fragment mass and charge, the binding energy is calculated in this work, using the same mass equation as in Eq. (12). Since the most probable charge of that particular fragment mass chain is not necessarily an integer, the even-odd correction inherent in this equation is the weighted average between the nearest two integers of Z_p. The B_n evaluated by this equation is therefore more realistic than any suggested $\bar{B}_n$ value.

To ensure the accuracy of the B_n value and the correctness of the shape dependence, a library of B_n for those fragments near the N = 82 closed-shell is used in the present work. This B_n library, covering a range of $48 \leqslant Z_p \leqslant 57$ and $130 \leqslant A' \leqslant 141$, is compiled with data from Myers (My77) and activated whenever the value of Z_p and A' of fission fragment falls in the library range. Under these kinds of treatments, the neutron binding energies used are estimated to have an uncertainty of less than 0.5 MeV.

B6. Kinetic energy of the prompt neutrons, KE_n

The average kinetic energy of prompt neutrons observed experimentally is approximately 2 MeV for very low energy fission (Va73). This approximately corresponds to twice the nuclear temperature of the fission fragment. Similar to the treatment of evaporation discussed in earlier chapters, the kinetic energy of the prompt neutron is taken as:

$$KE_n(A') = 2T = 2\sqrt{\frac{E^*(A')}{a_n(A')}} \qquad (16)$$

where the neutron level density parameter a_n is essentially taken from the result of Lang (La61) and $E^*(A')$ is the internal excitation energy in fission fragment A'. It is thought that the method used here to determine KE_n is sufficient enough to reproduce the 2 MeV kinetic energy observed in experiments.

C. Calculation of the Numbers of Prompt Neutrons

From Eqs. (10) to (16) one finds the prompt neutron yield is mainly dependent upon the E^*_F, ΔM, E_k, and B_n. The prompt neutron yield may become large if a large value of $E^*_F + \Delta M - E_k$ and a small B_n are encountered in the de-excitation of primary fragments or vice versa.

The prompt neutron yield for each primary fragment can be evaluated using the fission information calculated in the

last chapter and equations discussed in the last section. An example of the calculation is given below.

In the ^{232}Th(p,Fission) with 85 MeV incident proton energy, one of the 166 bins of input information is (Z_F, A_F, E^*_F, σ_F) = (91, 232, 81.30 MeV, 20.28 mb), representing the (p,nF) fission with 20.28 mb probability having 81.30 MeV associated with the fissioning nuclide $^{232}_{91}$Pa (refer to Figure 17(1A)). A calculation of the mass division of (A'_L,A'_H) = (76,156) is implemented, where $A_F = A'_L + A'_H$. The mass difference calculated from Eq. (10) yields ΔM = 164.82 MeV. The total kinetic energy of the primary fragments is evaluated from the synthetic formula and found to be E_k = 147.47 MeV. Therefore, the total excitation energy becomes $E^*_T = E^*_F + \Delta M - E_k$ = 98.65 MeV. The internal excitation energy is divided using Eq. (14), resulting in $E^*_L = E^*_T \cdot A'_L/A_F$ = 32.32 MeV and E^*_H = 66.33 MeV. The prompt gamma ray energies are estimated using Eq. (15), yielding E_{γ_L} = 2.62 MeV and E_{γ_H} = 5.38 MeV. The net energy available for prompt neutron emission hence becomes $E^*_{L,H} - E_{\gamma_{L,H}}$, or 29.7 MeV and 60.95 MeV for the light and heavy fragments, respectively. By using the estimated B_n and KE_n values in the deexcitation process of the primary fragment, the following numbers of prompt neutrons are obtained:

$$\nu_L(A'_L = 76) = 3.03; \qquad \nu_H(A'_H = 156) = 6.63;$$

and $$\nu_L + \nu_H = 9.66.$$

The actual prompt neutron yield at $A'_H = 156$ is weighted among all other yields calculated from each individual bin of input information on the basis of σ_F. The weighted prompt neutron yield in this example is $\bar{\nu}_H(A'_H = 156) = 4.48$.

C1. The numbers of prompt neutrons in the ^{232}Th(p,Fission) reaction

The prompt neutron yield for each primary fragment with mass ranging from 76 to 167 is calculated for the ^{232}Th(p, Fission) reactions to 85 MeV. Results are illustrated in the upper part of Figure 19, where the incident proton energy is also labelled. The uncertainties associated with the calculation, including the estimated error in ΔM, E_k, KE_n, B_n, E_γ, and input information of fission, are about 15% in the 8 MeV case and about 30% in the 85 MeV case. As shown in the figure, the prompt neutron distributions at different incident proton energies, except perhaps the 8 MeV case, display some common patterns: (1) for each primary fragment, the prompt neutron yield increases with increasing incident proton energy; this is due to the increase in E^*_F; (2) for each case the prompt neutron yield in primary fragment mass region $A'_L < 90$ and $A'_H > 140$ tends to level off; this is because the energy contributed from the fissioning nucleus, $\Delta M - E_k$, decreases when the mass division becomes very asymmetric (refer to Figure 18 (a) and (b)) and hence gives a smaller E^*_T for prompt neutron emission; (3) for each case

Figure 19

Prompt neutron distribution as a function of primary fragment mass

•: calculation of $^{232}Th(p,Fission)$ in this work

▲: experimental data of $^{238}U(p,Fission)$, after (Bi70)

◆: experimental data of $^{230}Th(\alpha,Fission)$, after (Br64)

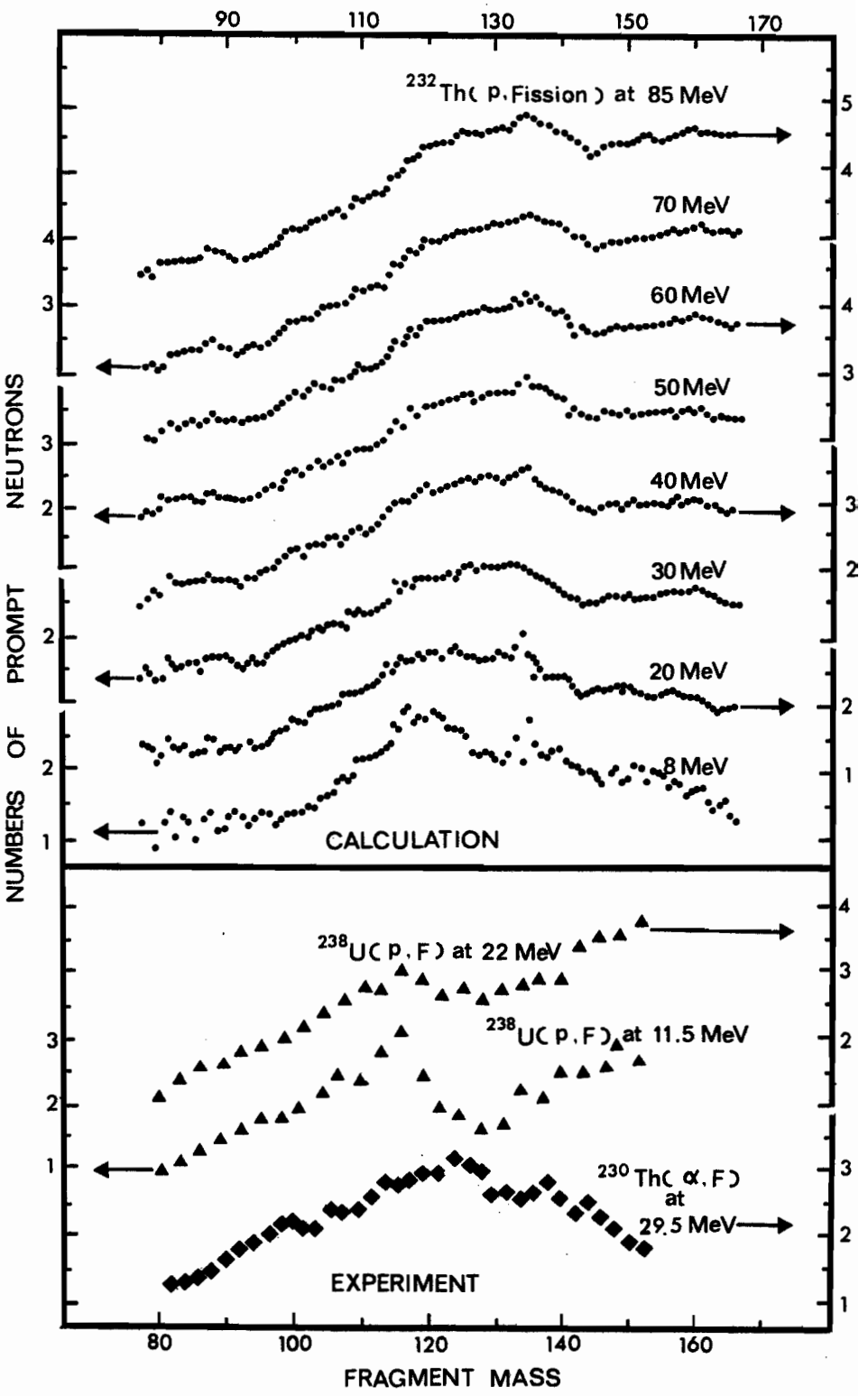
90
110
130
150
170
^{232}Th(p, Fission) at 85 MeV
70 MeV
60 MeV
50 MeV
40 MeV
30 MeV
20 MeV
8 MeV
CALCULATION
NUMBERS OF PROMPT NEUTRONS
^{238}U(p, F) at 22 MeV
^{238}U(p, F) at 11.5 MeV
^{230}Th(α, F) at 29.5 MeV
EXPERIMENT
80
100
120
140
160
FRAGMENT MASS

the prompt neutron yield generally increases with increasing primary fragment mass in the region of $90 \leqslant A' \leqslant 140$; this is mainly because of the assumption of thermal equilibrium in the total excitation energy split at scission; and (4) the prompt neutron yield, regardless of incident proton energies, peaks at $A'_H \sim 135$; this is because of the low B_n for those fragments having extra neutrons outside of the N = 82 closed-shell; another peak related to the N = 50 closed-shell, to a lesser extent, is also observed in the figure near $A'_L \sim 86$.

Unlike the situation in high energy bombardments, the prompt neutron distribution in the 8 MeV case keeps a saw-tooth shape, having its peak at symmetric mass division, that is, at $A'_H = A'_L \simeq 116$. This is because the dip in E_k at the symmetric mass division of the only fissioning nuclide ^{233}Pa is quite deep (refer to Figure 18(b)), which in turn gives a large E^*_T for prompt neutron evaporation.

There is no direct fit of the predicted prompt neutron distributions as a function of primary fragment mass in the $^{232}Th(p,Fission)$ reaction since no experimental measurement has been done. However, some measured prompt neutron distributions in other fission reactions are reproduced in the lower part of Figure 19 in order to make a comparison of the shape and magnitude of the distribution curves. The experimental data include the prompt neutron distribution of $^{230}Th(\alpha,Fission)$ with 29.5 MeV alpha, measured by Britt and

Whetstone (Br64) and ^{238}U(p,Fission) with 11.5 MeV and 22 MeV protons, measured by Bishop et al. (Bi70).

The saw-tooth character in the prompt neutron distribution as a function of primary fragment mass of the ^{238}U(p, Fission) with 11.5 MeV is clearly observed. However, at 22 MeV, the saw-tooth character is washed out. This experimental fact reappears in the present calculation of the prompt neutron distribution of ^{232}Th(p,Fission) at 8 MeV and 20 MeV. The increase in the prompt neutron yield with increasing fragment mass is also observed in the ^{238}U(p, Fission) with 22 MeV protons and ^{230}Th(α,Fission) with 29.5 MeV alpha.

On the other hand, the experimental shape and magnitude of the prompt neutron distribution of ^{230}Th(α,Fission) with 29.5 MeV alphas, representing a compound nucleus ^{234}U excited to 24.1 MeV, is very similar to the calculated result of ^{232}Th(p,Fission) with 30 MeV protons, corresponding to a compound nucleus, ^{233}Pa, excited to 35 MeV. The similarity implies the total excitation energy E^*_T available for prompt neutron evaporation is about the same. In order to obtain the same E^*_T in two different cases with different E^*_F, the term $\Delta M - E_k$, according to Eq. (10), has to balance the difference in E^*_F. Since the E_k are about the same for both fissioning nuclides ^{234}U and ^{233}Pa, we expect the ΔM of ^{234}U to be greater than that of ^{233}Pa by an amount of 35 - 24 = 11 MeV throughout the fragment mass region. We indeed

observe this amount of mass difference ΔM (refer to Figure 18(a)), indicating the present calculation is consistent with experimental data.

C2. The numbers of post-fission neutrons in the $^{232}Th(p,$ Fission) reaction

The total numbers of post-fission neutrons, ν_{post}, is the sum of post-fission neutrons from both light and heavy primary fragments. As mentioned earlier, delayed neutrons are not considered due to their relatively small contribution and hence prompt neutrons are identical to the post-fission neutrons in the present calculation.

A brief example of the present calculation has been given at the beginning of this section for one of the input bins of information of ^{232}Th(p,Fission) at 85 MeV; for a mass division leading to $A_H' = 156$, the total number of prompt neutrons in that particular example is found to be 9.66. Weighted over all input bins on the basis of σ_F, the ν_{post} at a mass division leading to $A_H' = 156$ is found to be 6.92. Results of the calculated ν_{post} of ^{232}Th(p,Fission) reactions at different incident proton energies are plotted against the heavy fragment A_H' and illustrated in the upper part of Figure 20. The labelled value $\bar{\nu}_{post}$ is the average number of post-fission neutrons per fission and will be discussed later.

Again, the experimental results of the post-fission

Figure 20

Post-fission neutron distribution

as a function of heavy fragment mass

•: calculation of ^{232}Th(p,Fission) in this work

▲: experimental data of ^{238}U(p,Fission), after (Bi70)

◆: experimental data of ^{230}Th(α,Fission), after (Br64)

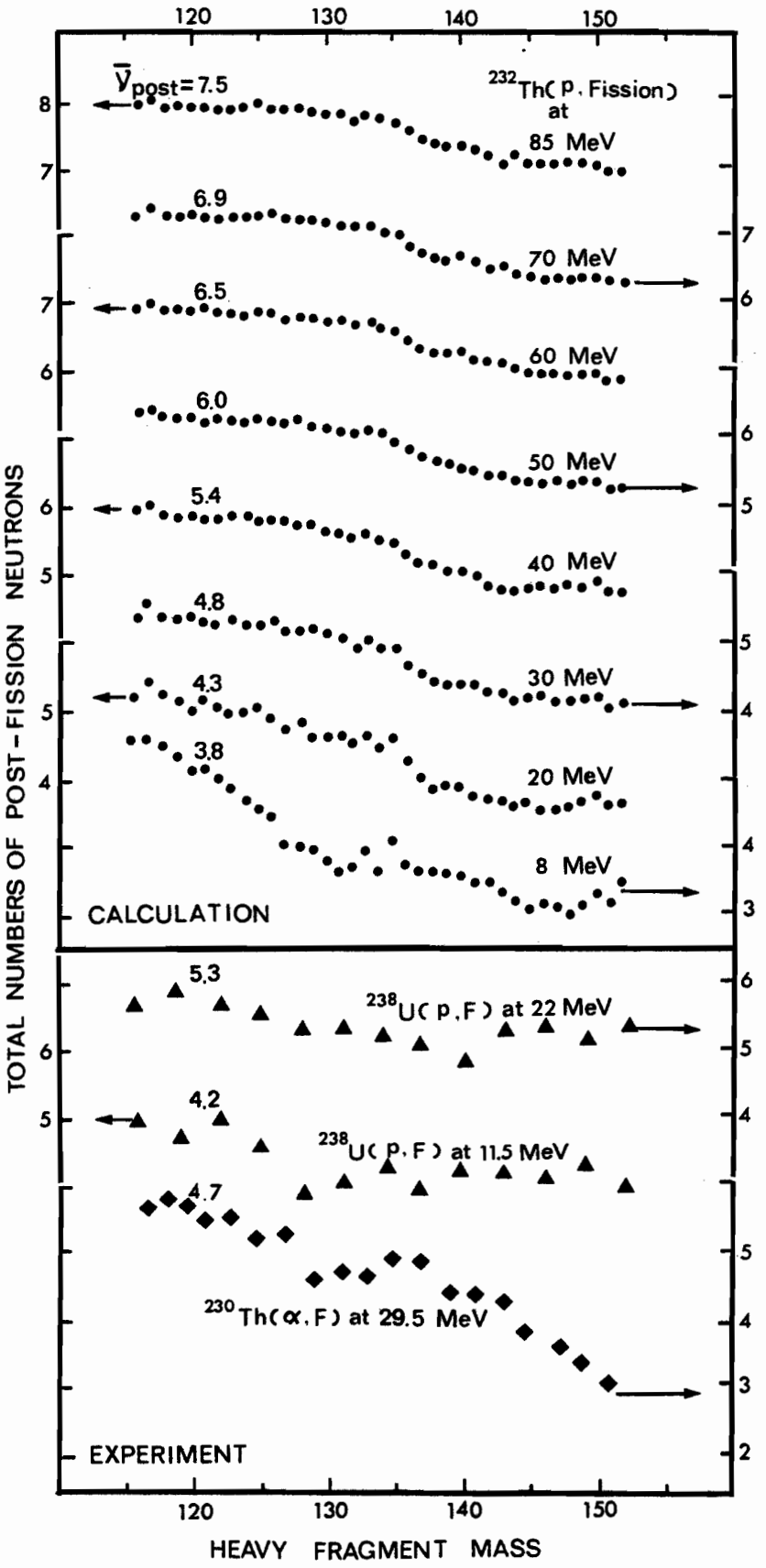
120
130
140
150
$\bar{\nu}_{post}$=7.5
^{232}Th(p, Fission) at
85 MeV
6.9
70 MeV
6.5
60 MeV
6.0
50 MeV
5.4
40 MeV
4.8
30 MeV
4.3
20 MeV
3.8
8 MeV
CALCULATION
5.3
^{238}U(p,F) at 22 MeV
4.2
^{238}U(p,F) at 11.5 MeV
4.7
^{230}Th(α,F) at 29.5 MeV
EXPERIMENT
TOTAL NUMBERS OF POST-FISSION NEUTRONS
HEAVY FRAGMENT MASS

neutron distribution as a function of heavy fragment mass of the $^{238}U(p,Fission)$ and $^{230}Th(\alpha,Fission)$ reactions are reproduced in the lower part of Figure 20. In general, both the calculated and experimental ν_{post} decrease with increasing A'_H; in other words, ν_{post} in symmetric mass division is slightly greater than that in asymmetric mass division. This is mainly because the term ΔM in the symmetric mass division region is greater than that in the asymmetric mass division region (refer to Figure 18(a)) which in turn gives a larger E^*_T for post-fission neutron evaporation.

Just as with comparison to the prompt neutron distribution, the present calculation of the ν_{post} of $^{232}Th(p,Fission)$ still maintains the basic trends, in particular the shape and magnitude, of those found in other heavy element fissions.

The average number of post-fission neutrons per fission, $\bar{\nu}_{post}$, can be evaluated by weighing each ν_{post} value by its fragmental mass yield. Croall and Cuninghame (Cr69) have measured the mass yield for primary fission fragments in $^{232}Th(p,Fission)$ with incident proton energies to 53 MeV. Their mass yield curves are reproduced in Figure 21. In order to evaluate the $\bar{\nu}_{post}$ at incident proton energies pertinent to this work, the mass yields for primary fragments are either directly taken or interpolated from Figure 21, up to and including 45 MeV incident proton energy. For those evaluations involving higher incident proton energies, the shapes of the mass yield curves are assumed to be the same

Figure 21

Fragmental mass yield curves for the $^{232}Th(p,Fission)$ reactions with protons to 53 MeV, after (Cr69)

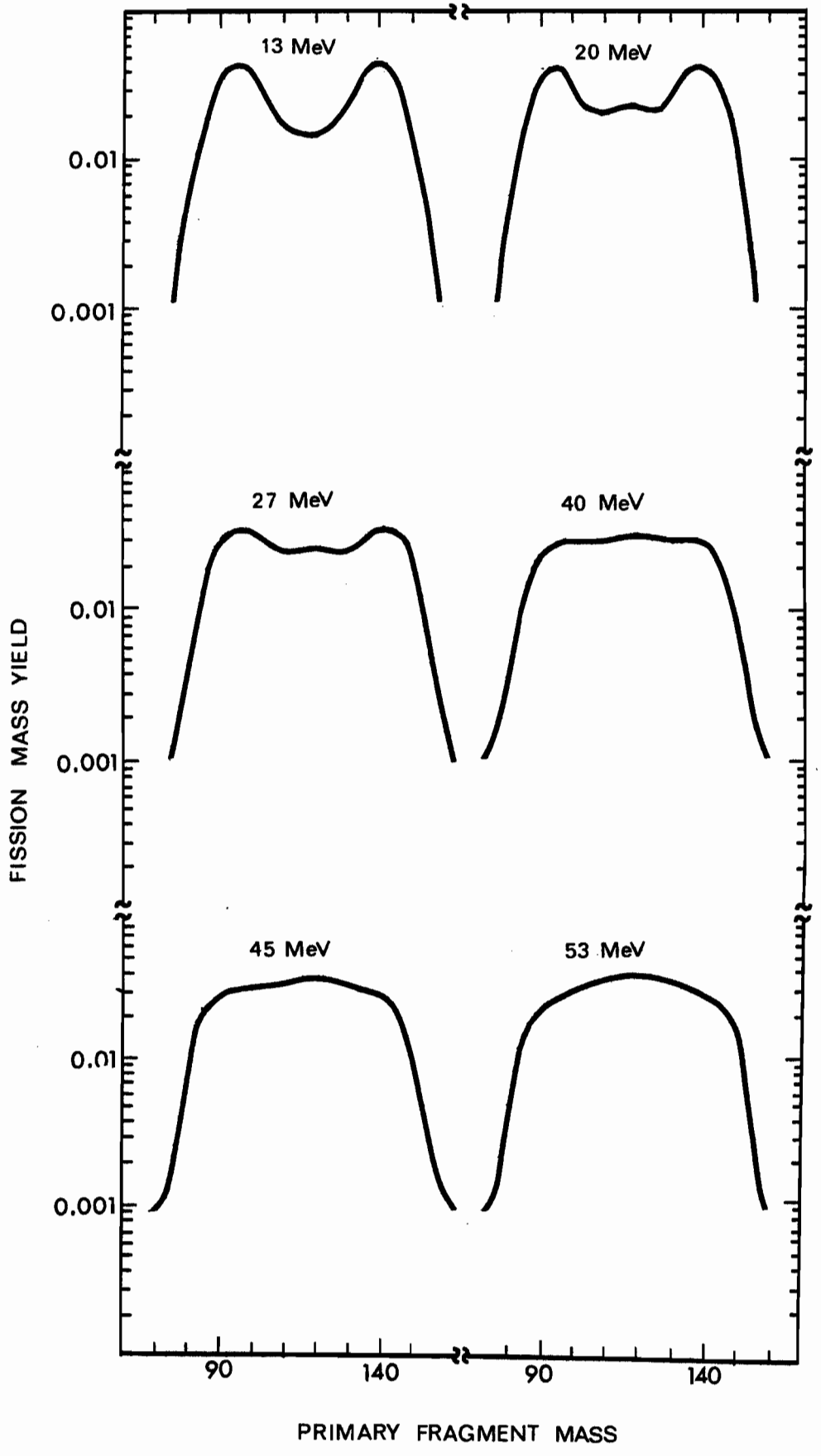
13 MeV
20 MeV
27 MeV
40 MeV
45 MeV
53 MeV
0.01
0.001
0.01
0.001
0.01
0.001
FISSION MASS YIELD
90
140
90
140
PRIMARY FRAGMENT MASS

as the experimental result in the 53 MeV case. This assumption is supported by two experimental facts. First, the measured total fission cross sections are relatively constant throughout this proton energy region (refer to Figure 07), and second, the cumulative cross sections for each fission product, measured by Yaffe and co-workers in (Pa58A), (Fo66), (Mc71), (Di78), and (Di79), are found relatively insensitive to the variation of proton energies providing it is greater than 50 MeV. These observations imply both the shape and magnitude of the mass yield curve for the fission product are relatively constant in this energy region. The mass yield curves for primary fragments, although not exactly the same as that of fission products, are therefore similar to one another in this energy region.

Based on the mass yield curves discussed above, the $\bar{\nu}_{post}$ is estimated at different incident proton energies; it ranges from 3.75 neutrons in the 8 MeV case to 7.54 neutrons in the 85 MeV case. In order to make a comparison to those experimental $\bar{\nu}_{post}$ in other heavy element fissions, all calculated and experimental $\bar{\nu}_{post}$ are labelled to the respective distributions in Figure 20. The consistency found in the prompt neutron distributions between the experimental result of ^{230}Th(α,Fission) with 29.5 MeV alpha and the predicted values of ^{232}Th(p,Fission) with 30 MeV protons reappears in the comparison of $\bar{\nu}_{post}$. Here the experimental $\bar{\nu}_{post}$ is found to be about 4.7 neutrons/fission in the

former and the calculated $\bar{\nu}_{post}$ results to be about 4.8 neutrons/fission in the latter, which is indeed in good agreement.

The average number of pre-fission neutrons per fission, $\bar{\nu}_{pre}$, have been discussed and calculated in the last chapter. The $\bar{\nu}_{pre}$ and $\bar{\nu}_{post}$ at different incident proton energies are listed in Table 08 and illustrated in Figure 22. The last column in the table shows the average total neutron yield per fission $\bar{\nu}_{total}$, which is the sum of $\bar{\nu}_{pre}$ and $\bar{\nu}_{post}$. As mentioned in the last chapter, the $\bar{\nu}_{pre}$ increases with increasing incident proton energy to 50 MeV, mainly because more fission channels are continuously becoming available. At higher bombarding energy, the $\bar{\nu}_{pre}$ levels off to about 2.5 neutrons/fission; this indicates that (p,XnF) fissions with X = 0-6 predominate. The pre-fission neutron curve is cut off at around 9 MeV, equivalent to the threshold of the (p,nF) fission where the first pre-fission neutron appears. The $\bar{\nu}_{post}$, however, increases steadily with increasing incident proton energy. This is because the E^*_F also increases steadily. The post-fission neutron curve has to be cut off at the experimental fission threshold of 3 MeV, found by Choppin, Meriwether, and Fox (Ch63). The $\bar{\nu}_{total}$, as shown in the plot, therefore increases with increasing incident proton energy.

Table 08 and Figure 22

Calculated numbers of fission-related neutrons
in the $^{232}Th(p,Fission)$ reaction

Table-08

Incident proton energy (MeV)	Average numbers of pre-fission neutron/fission $\bar{\nu}_{pre}$	Average numbers of post-fission neutron/fission $\bar{\nu}_{post}$	Average number of total neutrons/fission $\bar{\nu}_{total}$
8	0.00	3.75	3.75
20	1.07	4.30	5.37
30	1.72	4.79	6.51
40	2.07	5.42	7.49
50	2.33	5.96	8.29
60	2.32	6.53	8.85
70	2.39	6.93	9.32
85	2.42	7.54	9.96

Figure-22

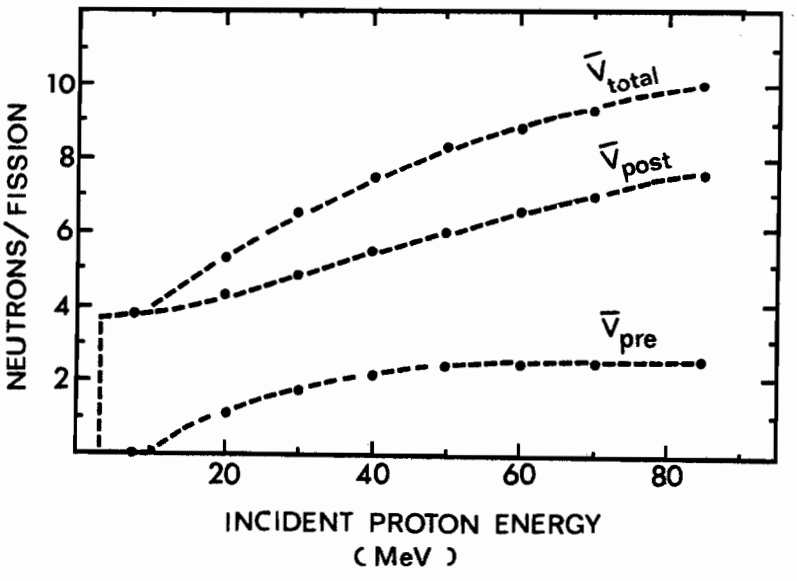

D. Summary of the Post-fission Neutron Calculation

Details of the pre- and post-fission neutron distributions of the ^{232}Th(p,Fission) with incident proton energies to 85 MeV have been calculated. Results of the predictions of the shape and magnitude of the distribution are found to be in good agreement with experimental data for other heavy element fissions, lending confidence to the present treatment of post-fission deexcitation.

The calculation of post-fission properties is very sensitive to the use of the mass equation. The fissioning nucleus mass, the primary fragment masses, and the neutron binding energy are all determined by the mass equation in order to calculate the prompt neutron yield. The mass equation adopted in this work is the one derived by Myers (My77) on the basis of the Droplet Model, a refinement of the Liquid Drop Model. It has been reflected in Figure 18(a) that a relatively simple Liquid Drop Model mass equation in some cases gives as much as 8 MeV difference in ΔM to the present calculation; this corresponds to a difference of about 1.1 prompt neutrons evaluated later. Hence, using the Droplet Model mass equation, rather than a simplified one, is considered to be necessary in this work in order to keep the precision throughout the calculation.

The evaluation of the prompt neutron yield is indispensable for the prediction of nuclear charge distribution

in fission. The present treatment of post-fission deexcitation is therefore carried over to the next chapter.

VI

CALCULATION OF

NUCLEAR CHARGE DISPERSION IN FISSION

The three different postulates of nuclear charge distribution in fission, namely, the Equal Charge Displacement (ECD) rule, the Unchanged Charge Distribution (UCD) postulate, and the Minimum Potential Energy (MPE) hypothesis, have been briefly discussed in the first chapter. The most probable charge Z_p based on each postulate has been calculated and compared to the experimental data for both thermal neutron induced fission and ^{232}Th(p,Fission) reaction in this work.

A. The Postulates

Nuclear charge distribution is perhaps one of the least understood aspects of the fission process. Three postulates have been successful in interpreting some but not all experimental results. These are the ECD, MPE, and UCD.

(1) ECD rule. This postulate (G149) assumes that the most probable charge Z_p for each primary fragment A' in binary fission is equally distant from the most stable charge along isobar A', $Z_A(A')$:

$$Z_A(A'_L) - Z_p(A'_L) = Z_A(A'_H) - Z_p(A'_H)$$

or (17)

$$Z_p(ECD) = \frac{1}{2} \cdot [Z_A(A') - Z_A(A_F - A') + Z_F]$$

The original proposal of the ECD rule implied that the nuclear charge division occurs at the scission point and that primary fragment masses should be applied to the equation. Owing to the early day confusion of "fragment" and "product", however, the formulation of the ECD rule outlined in (G149) was actually based on a nuclear charge division at the post-fission stage where observed fission products were applied. The empirically derived ECD rule, having nuclear charge division at either primary fragments or fission products, is arbitrary in nature. The former may be understood as a permanent rearrangement of nucleons achieved well before the scission point during the fission process. The latter, however, requires even a pre-arrangement of the numbers of prompt neutrons and fission product pair before fission happens; this is highly unlikely to happen since fission is a random process. Owing to the unrealistic physical implication of the latter, the ECD rule used in this work, unlike many evaluations in the literature, is the former, as reflected in Eq. (17).

(2) MPE hypothesis. The concept of the MPE suggests (Wa48) that fission is a slow process from saddle to scission point such that nuclear charge rearrangement has taken place at scission. Under this circumstance, the most probable charge Z_p will arise from that division in which the potential energy at scission is minimized:

$$\frac{\partial}{\partial Z}PE(A'_L,A'_H)\Big|_{min} = \frac{\partial}{\partial Z}M(Z,A') + \frac{\partial}{\partial Z}M(Z_F - Z,\ A_F - A') + \frac{\partial}{\partial Z}\frac{Z \cdot (Z_F - Z) \cdot e^2}{\bar{D}} = 0 \qquad (18)$$

where e^2 = electrostatic constant = 1.44 MeV-fm,

$\bar{D}$ = average distance between the two charge centers of primary fragments at scission.

(3) UCD postulate. The UCD postulate (Go48,49) predicts that the most probable charges Z_p for both primary fragments are determined by maintaining the same neutron to proton ratio as that of the fissioning nucleus. In other words, charge is divided between the primary fragments as it is in the fissioning nucleus:

$$(N'/Z_p)_L = (N'/Z_p)_H \quad \text{or} \quad Z_p(UCD) = A' \cdot Z_F/A_F \qquad (19)$$

The physical meaning of the UCD postulate is an assumption that the fission process between saddle and scission is too fast to allow charge rearrangement to take place, the completely opposite prediction to the MPE hypothesis.

Among the three postulates, a calculation of $Z_p(UCD)$ is the simplest as long as the fissioning nuclide (Z_F,A_F) and primary fragments (A'_L,A'_H) are provided. Others require use of a mass equation to solve for either the most stable charge Z_A (in the ECD calculation) or the differential

equation (in the MPE calculation). Furthermore, the average $\overline{D}$ has to be evaluated in the Z_p(MPE) calculation.

A1. The most stable charge, Z_A

Glendenin, Coryell, and Edwards (Gl51) were among the first to evaluate the values of Z_A using the Bohr-Wheeler (Bo39) mass equation. Their calculated Z_A, by ignoring shell correction, is essentially a continuous function of mass, A, and cannot predict the effect of shells occurring near the mass region involving proton and neutron closed-shells.

To eliminate the shell-crossing difficulty, Coryell later (Co53) empirically established the values of Z_A. In his treatment the Z_A(A) function is assigned and becomes distinct lines in different mass regions, with a sharp discontinuity at the shell edge. His empirical Z_A data have been frequently used for the calculation of Z_p(ECD) in the last quarter century.

Chu et al. (Ch71A) have used a least-squares computer program to fit the experimental isobaric mass excess given by Garvey et al. (Ga69) to a parabola and have determined the value of Z_A, corresponding to the minimum of the mass parabola. Their result is generally in good agreement with Coryell's empirical data. The main discrepancy between the experimentally evaluated Z_A and the empirically assigned Z_A is near mass region A $\sim$ 156, where no discontinuity of Z_A(A) is observed in the former but a discontinuity ascribed as

a Z = 64 sub-shell effect is observed in the latter. In both cases, two values of Z_A are given for several mass regions, corresponding to either side of the proton or neutron closed shell.

In this work, however, none of these sets of Z_A data are used. Since the Droplet Model mass equation has been built in to the present computing code, the value of Z_A is directly evaluated by finding the minimum of mass in isobar A. The calculated Z_A is plotted as a function of both numbers of neutrons and protons and illustrated in Figure 23(a); also shown there are Coryell's empirical Z_A lines and stable isotopes in the related mass region. As expected, the calculated value of the most stable charge is observed to lie among stable isotopes at each isobar line. Furthermore, the calculated Z_A do agree quite well with Coryell's empirical Z_A data, except near mass region $A \sim 156$ where no discontinuity of Z_A is evaluated in this work, indicating that the calculated Z_A is consistent with the experimental Z_A obtained in (Ch71A). This is expected since the Droplet Model mass equation used in this work is also constructed on the basis of the experimental masses.

The calculated Z_A curves, as seen in the figure, are continuous around masses involving P,N = 50 and N = 82 closed-shells; hence, they avoid the problems of double values and substantial increases of Z_A (about 1.4 charge unit) at the discontinuity. In fact, the calculated Z_A data

Figure 23

Values of Z_A and $\bar{D}$ used in this work

(a) Z_A values

: present calculation

: empirical data, after (Co53)

• : stable isotopes

(b) $\bar{D}$ values

: present evaluation

● : ^{230}Th(p,Fission) at 8 MeV, after (Br63A)

■ : ^{226}Ra(α,Fission) at 27.1 MeV, after (Br63A)

◆ : ^{226}Ra(^{3}He,Fission) at 23.4 MeV, after (Br63A)

▼ : ^{226}Ra(d,Fission) at 14 MeV, after (Br63A)

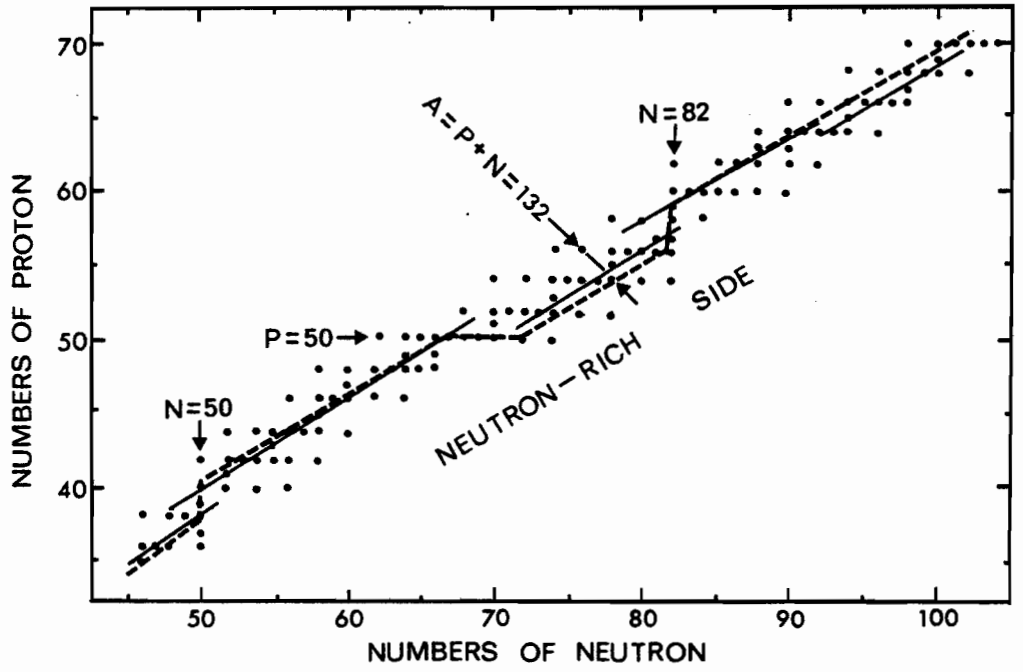

FIGURE-23(a)

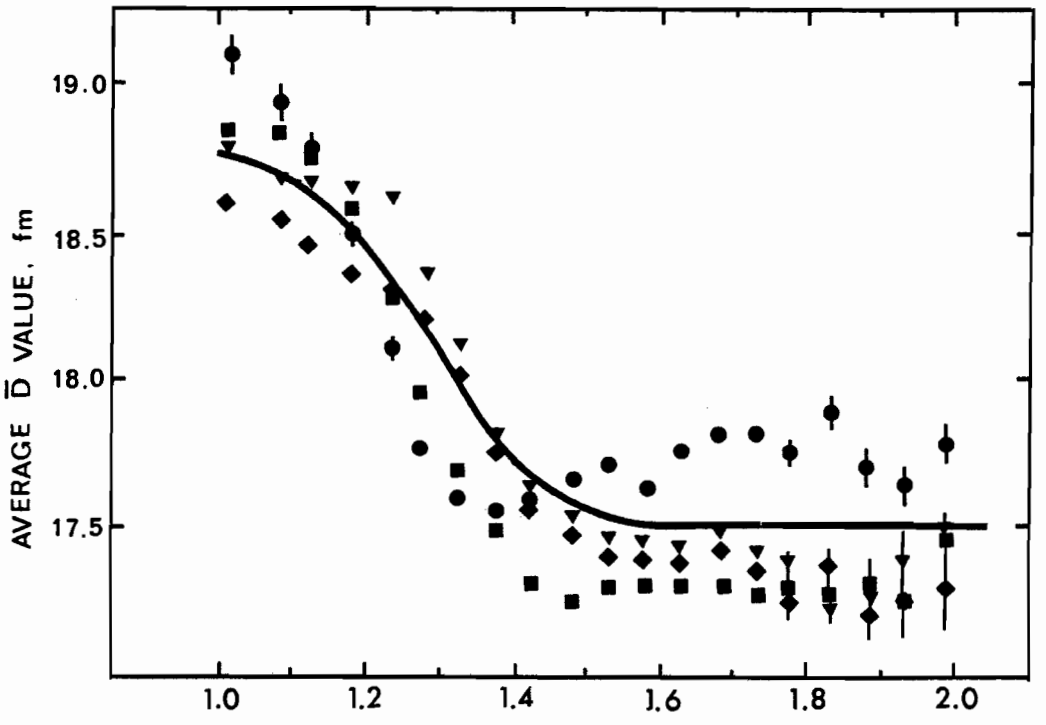

FIGURE-23(b)

near mass regions involving closed-shells are more realistic. This is because only those Z_A data of neutron-rich primary fragments are required in this work, corresponding to the lower part of Figure 23(a) where the calculated Z_A curve (or the lower line of Coryell's double Z_A) passes through. Hence, the present treatment of the most stable charge Z_A for ECD calculation retains both the reality and the experimental fact.

A2. The average $\bar{D}$ value

Britt, Wegner, and Gursky (Br63A) evaluated the value of $\bar{D}$, the average distance between the two charge centers of primary fragments at scission in heavy element fissions. They found the $\bar{D}$ value to be relatively independent of the choice of nuclear charge and a rather slowly varying function of the mass division (A_L', A_H'), ranging from 19.1 fm for symmetric mass division to 17.2 fm for very asymmetric mass division. Furthermore, they concluded that the $\bar{D}$ value is also relatively independent of the fissioning nuclides within the range of $89 \leqslant Z_F \leqslant 91$ and $228 \leqslant A_F \leqslant 231$. Results of their $\bar{D}$ values as a function of fragment mass ratio A_H'/A_L' are reproduced in Figure 23(b). Following their observation, a universal $\bar{D}$ curve is constructed empirically in this work, passing through the majority of experimental data given by (Br63A). This synthetic $\bar{D}$ curve, also shown in the figure, is only a function of the fragment mass ratio A_H'/A_L'.

Considering the small variation of the $\overline{D}$ value to the mass split, no more than 10% at most, the present treatment of the average distance between the two primary fragments at scission is believed adequate enough for the MPE calculation.

B. Experimental Z_p Data

Important information that one would like to have about the fission process is the division of nuclear charge between the primary fragments at scission. Unfortunately, to determine this is a difficult experimental problem and the available data are very limited. The reasons for the difficulty are the extremely short lifetime of the primary fragment from the experimental point of view and the fact that most of the fission products deexcited from the primary fragments have very short half-lives which hinder post-fission radiochemical work. Despite this difficulty, some independent fission chain yields of those shielded and semi-shielded fission products may be measured and subsequently used for evaluating the charge dispersion in each fission product chain.

Based on their experimental results on fission product chain yields, Glendenin, Coryell, and Edwards (G151) first suggested that the independent yield for fission products with charge Z in mass chain A, P(Z), is distributed along

a Gaussian curve having distribution constant C:

$$P(Z) = (\pi C)^{-\frac{1}{2}} \cdot \exp\left(-(Z - Z_p)^2/C\right) \qquad (20)$$

where Z_p is mathematically the maximum of the Gaussian function and physically the most probable charge for those primary fragments which may subsequently evaporate prompt neutrons, leading to the fission product having mass A. Hence, the experimental Z_p for each fission product mass chain may be obtained once the Gaussian function is constructed.

In this chapter, two sets of experimental data of Z_p are compared to the present calculation. They are the data of the ^{232}Th(p,Fission) reaction with proton energies pertinent to this work and those from thermal neutron induced fission. The former are chosen owing to the closely related post-fission calculation in this work. The latter are chosen mainly because of the well-established fact that the experimental Z_p in thermal neutron induced fissions can be fit by the ECD rule (as the rule was originally designed) but not by the UCD postulate; whether the present calculation can reproduce these experimental data becomes a serious test of the post-fission treatment in this work.

B1. Experimental Z_p data in the (n_{th},F) reactions

Wahl et al. (Wa62) measured and compiled the independent and cumulative chain yields of fission products in ^{233,235}U,

$^{239}Pu(n_{th},F)$ reactions. They used the mass yield data to construct the Gaussian functions at fission product masses 91 and 139-143 of $^{235}U(n_{th},F)$ reaction; then they averaged the distribution constant C among the Gaussian curves, yielding $\overline{C} = 0.94 \pm 0.15$. With the assumption that $\overline{C}$ is applicable to other Gaussian functions from different fissioning nuclides and different fission product masses, they found that most of the Z_p values obtained by this assumption correlate quite well with the experimental chain yields. More recent data by Fowler and Wahl (Fo74) on several chains can also be reproduced by a Gaussian distribution with this average constant $\overline{C}$.

Owing to the unreliability of part of the experimental fission chain yields, however, some editing work has to be done on the experimental Z_p data in (Wa62) on the basis of more recent data compiled also by Wahl and co-workers in (Wa69) and (Fo74). Two kinds of Z_p data are dropped: those having a major discrepancy with the experimental chain yields and those constructed on a single, small chain yield (less than 10^{-3}%). The remaining Z_p data are listed in Table 09 and will be compared to the calculation based on different charge distribution postulates.

B2. Experimental Z_p data in the $^{232}Th(p,Fission)$ reaction

The experimental Z_p data in the $^{232}Th(p,Fission)$ reaction with incident proton energies to 87 MeV have been

Table 09

Experimental Z_p data of the $^{233,235}U, ^{239}Pu(n_{th},F)$ reactions, after (Wa62).

Fission product mass chain	Experimental Z_p	Fission product mass chain	Experimental Z_p
$^{235}U(n_{th},F)$		$^{233}U(n_{th},F)$	
78	31.02 ± 0.17	82	32.61 ± 0.22
89	35.42 ± 0.12	128	50.20 ± 0.23
90	35.84 ± 0.10	130	50.64 ± 0.18
91	36.32 ± 0.09	131	51.04 ± 0.05
92	36.81 ± 0.04	140	54.84 ± 0.16
93	37.39 ± 0.10		
94	37.84 ± 0.15	$^{239}Pu(n_{th},F)$	
95	38.40 ± 0.19		
96	38.20 ± 0.24	96	38.54 ± 0.20
97	38.65 ± 0.27	97	39.16 ± 0.17
128	50.19 ± 0.23	128	50.35 ± 0.22
131	50.77 ± 0.08	130	50.72 ± 0.18
132	51.26 ± 0.30	131	50.94 ± 0.06
138	53.45 ± 0.10		
139	53.82 ± 0.14		
140	54.34 ± 0.03		
141	54.97 ± 0.04		
142	55.36 ± 0.04		
143	55.92 ± 0.10		
144	56.40 ± 0.28		
150	58.74 ± 0.18		

reported by Yaffe's research groups in (Pa58A), (Fo66), (Be69), (Mc71), (Ho73), (Di78), and (Di79), covering fission product mass regions 75-79, 90-98, and 130-146.

Pate, Foster, and Yaffe (Pa58A) have measured some independent and cumulative cross sections of fission product mass chains 130-135 in the ^{232}Th(p,Fission) with proton energies to 87 MeV. They converted the cross section data into charge dispersion curves by means of the mass yield data available in (Te52). Two assumptions were made in (Pa58A) to construct the charge dispersion curves: (1) in each fission product mass chain the fractional chain yield is Gaussian-distributed, and (2) all Gaussian functions at the same bombarding energy have the same Gaussian distribution constant C, indicating that C is applicable to all fission product mass chains at all fissioning nuclides pertinent to their work. They plotted the Gaussian curves against Z_A, hence the value of Z_p for each fission product mass at a given proton energy was deduced from the plot. Only those Z_p associated with A_H = 132 are taken for this work since these fission products represent the mid-point of the investigated mass region 130-135.

Forster, Porile, and Yaffe (Fo66) have measured some independent and cumulative cross sections for fission product mass chains 133 and 135 in the ^{232}Th(p,Fission) reaction. Based on the same assumptions as in (Pa58A), they evaluated the values of Z_p at A_H = 133 and 135 with C = 0.95, 1.20,

and 1.45. They found the evaluated Z_p data to be relatively insensitive to a variation of the constant C, leading to a free choice of any set of the data. The values of Z_p with C = 1.45 are taken for this work because Eaker and Choppin (Ea76) found that the experimental fragmental chain yield data can best be fit with Gaussian curves having C = 1.41 in the ^{232}Th(p,Fission) reaction with 17.6 MeV protons.

Benjamin et al. (Be69) have measured some independent and cumulative cross sections at fission product mass chains 130-138 in the ^{232}Th(p,Fission) with incident protons at energies 20-85 MeV. In addition to those assumptions made by (Pa58A), they also assumed that: (1) the mass yield curve at mass region 130-138 is reasonably flat at proton energies pertinent to their work; and (2) the N/Z_p values for different product mass chain A are the same. The Gaussian curves were plotted against N/Z of the fission product rather than the $Z-Z_A$ used in (Pa58A) to avoid shell discontinuities of Z_A. Hence, the Z_p data are deduced from the experimentally obtained value of N/Z_p which represents the maximum of the Gaussian curve. The Z_p data at mass chain 136 are taken for this work since it represents the mid-point of that high fractional chain yield mass region, namely, A_H = 134-138.

McGee, Rao, and Yaffe (Mc71) have measured some independent and cumulative cross sections at fission product mass chains 90-98 in the ^{232}Th(p,Fission) with incident proton energies to 85 MeV. Based on all the assumptions made

by (Be69), they plotted the Gaussian curves but only the Z_p value at fission product mass chain 96 was listed. Their Z_p is taken for this work.

Holub and Yaffe (Ho73) have measured some independent and cumulative cross sections for fission product mass chains 139-144 in the ^{232}Th(p,Fission) with incident proton energies to 83 MeV. As mentioned in the second chapter (refer to Figure 04), however, their result was quite different from the more recent data. Diksic (Di78) measured again those cross sections in the mass region 141-146 with protons at energies 45-85 MeV and subsequently evaluated the Z_p values. The Z_p data for fission product mass chain 144, which were determined in his later investigation (Di79), are used in this work.

Diksic et al. (Di79) have measured some independent and cumulative cross sections for fission product mass chains 75-79 in the ^{232}Th(p,Fission) with incident protons of energies 35-85 MeV. The sum of the cross sections at mass chain 77 was taken as the total chain cross sections as a first estimate, for subsequent evaluation of the independent fractional chain yield at other mass chains. The Gaussian curves were constructed and Z_A-Z_p values were displaced with Z_A values given by (Co53). The Z_p value at mass chain 77 is therefore converted from the experimental data and used in this work.

All available Z_p data measured by Yaffe and co-workers

are summarized in Table 10; these data will be compared to the calculation in a later section.

C. Fit to the Experimental Z_p Data in the (n_{th},F) Reactions

Based on different postulates, an attempt has been made in this work to calculate the most probable charge listed in Table 09. As shown in Eqs. (17) to (19), the A_L' and A_H' have to be evaluated as input for the Z_p calculation. In the last chapter the numbers of post-fission neutrons have been calculated for primary fragments from each different fissioning nuclide. The same treatment but in the reverse direction is used here. With an assigned fission product A and fissioning nuclide (Z_F,A_F), the number of prompt neutrons ν evaporated from a primary fragment A' which eventually deexcites to the fission product A is evaluated. After the ν is determined, the primary fragments $A' = A + \nu$ and $A_F - A'$ are therefore used as input to calculate the Z_p.

For thermal neutron induced fission, multi-chance fission is prohibited owing to the low excitation energy. The neutron binding energies 7.15 MeV, 6.89 MeV, and 6.99 MeV, taken from the tabulated value in (My77), have been used in this work as the excitation energies associated with the fissioning nuclides ^{234}U, ^{236}U, ^{240}Pu in the ^{233}U, ^{235}U, $^{239}Pu(n_{th},F)$ reactions, respectively. The uncertainty in

Table 10

Experimental Z_p data of the $^{232}Th(p,Fission)$ reaction.

Incident proton energy (MeV)	At fission product mass chain						
	77	96	132	133	135	136	144
8 ± 2	---	---	51.44 ± 0.08	---	---	---	---
14 ± 2	---	---	51.85 ± 0.85	---	---	---	---
20 ± 2	---	---	---	---	---	53.44 ± 0.25	---
25 ± 2	---	---	52.25 ± 0.15	---	---	---	---
30 ± 2	---	38.71 ± 0.25	---	52.60 ± 0.20	53.56 ± 0.20	---	---
35 ± 2	31.31 ± 0.16	---	---	---	---	---	---
40 ± 2	31.35 ± 0.16	38.79 ± 0.25	---	52.96 ± 0.20	53.82 ± 0.20	54.18 ± 0.25	---
45 ± 2	31.42 ± 0.21	---	52.65 ± 0.15	---	---	---	57.56 ± 0.21
50 ± 2	31.62 ± 0.16	38.95 ± 0.50	---	53.31 ± 0.20	54.01 ± 0.20	---	---
55 ± 2	31.49 ± 0.23	---	---	---	---	54.36 ± 0.50	---
60 ± 2	31.74 ± 0.18	39.02 ± 0.50	---	---	---	---	57.83 ± 0.18
65 ± 2	31.57 ± 0.15	---	52.74 ± 0.15	---	---	54.60 ± 0.50	---
70 ± 2	31.78 ± 0.18	39.07 ± 0.50	---	---	---	---	---
75 ± 2	31.81 ± 0.13	---	---	---	---	54.66 ± 0.50	---
85 ± 2	31.91 ± 0.15	39.18 ± 0.50	52.76 ± 0.08	---	---	54.71 ± 0.50	58.18 ± 0.85
Reference	(Di79)	(Mc71)	(Pa58A)	(Fo66)	(Fo66)	(Be69)	(Di78)

the calculated Z_p mainly involves the prompt neutron distribution discussed in the last chapter, which is about 0.2 charge unit in most cases and becomes 0.7 charge unit near the "saw-tooth" discrepancy.

The calculated Z_p(postulate), its uncertainty, and the difference from Z_p(experiment) are listed in Table 11. Also shown in the table are the sum of the squares of the differences for each postulate, reflecting the agreement of the calculation to the experiment. As indicated by this sum, Z_p(UCD) gives the worst fit in all cases; Z_p(MPE) yields the best fit to all experimental data although the fit by Z_p(ECD) is almost as satisfactory.

The large uncertainty of the calculated Z_p at mass region A = 128-131 is mainly because the division of the total excitation energy E^*_T in this work (refer to Eq. (14)) cannot lead to a saw-tooth post-fission neutron distribution in this specific mass region. Using a realistic post-fission neutron saw-tooth distribution for the Z_p calculation may improve the fit; however, regardless of the refinement, Z_p(UCD) still yields the worst fit among the postulates.

In all, Z_p(MPE) and Z_p(ECD) are able to reproduce the experimental data quite well, while Z_p(UCD) does not. This is in agreement with the observation by Wahl et al. (Wa62) except for their poor Z_p(MPE) fit as they calculated it. As mentioned in the first chapter, the calculation of Z_p(MPE) is very sensitive to the mass equation used; they evaluated

Table 11

Quantitative comparison between calculation and experiment of Z_p in the $^{233,235}U, ^{239}Pu(n_{th}, F)$ reactions.

Fission product mass chain	Z_p(postulate) and its difference to Z_p(experiment)					
	Z_p(MPE)	Δ^a	Z_p(UCD)	Δ	Z_p(ECD)	Δ
	$^{235}U(n_{th},F)$ reaction					
78	30.77 ± 0.24	−0.25	30.80 ± 0.24	−0.22	30.70 ± 0.24	−0.30
80	35.83 ± 0.13	+0.41	35.25 ± 0.13	−0.17	35.64 ± 0.13	+0.22
90	35.88 ± 0.21	+0.04	35.30 ± 0.21	−0.54	35.69 ± 0.21	−0.15
91	36.58 ± 0.11	+0.26	36.05 ± 0.11	−0.27	36.41 ± 0.11	+0.09
92	37.06 ± 0.19	+0.25	36.56 ± 0.19	−0.25	36.89 ± 0.19	+0.08
93	36.96 ± 0.31	−0.43	36.45 ± 0.31	−0.94	36.78 ± 0.31	−0.61
94	37.67 ± 0.03	−0.17	37.22 ± 0.03	−0.62	37.87 ± 0.03	+0.03
95	38.15 ± 0.45	−0.25	37.73 ± 0.45	−0.67	38.74 ± 0.45	+0.34
96	38.11 ± 0.33	−0.09	37.68 ± 0.33	−0.52	38.67 ± 0.33	+0.47
97	38.72 ± 0.11	+0.07	38.33 ± 0.11	−0.32	39.41 ± 0.11	+0.76
128	50.00 ± 0.69	−0.19	50.74 ± 0.69	+0.55	49.82 ± 0.69	−0.37
131	50.38 ± 0.31	−0.39	51.43 ± 0.31	+0.66	50.46 ± 0.31	−0.31
132	51.60 ± 0.39	+0.34	52.08 ± 0.39	+0.82	51.09 ± 0.39	−0.17
138	54.26 ± 0.52	+0.81	54.71 ± 0.52	+1.26	54.02 ± 0.52	+0.57
139	54.48 ± 0.32	+0.66	54.94 ± 0.32	+1.12	54.21 ± 0.32	+0.39
140	54.78 ± 0.26	+0.44	55.27 ± 0.26	+0.93	54.95 ± 0.26	+0.61
141	55.31 ± 0.40	+0.34	55.83 ± 0.40	+0.86	55.48 ± 0.40	+0.51
142	55.61 ± 0.29	+0.25	56.15 ± 0.29	+0.79	55.79 ± 0.29	+0.43
143	55.60 ± 0.11	−0.32	56.14 ± 0.11	+0.22	55.78 ± 0.11	−0.14
144	55.93 ± 0.19	−0.47	56.49 ± 0.19	+0.09	56.11 ± 0.19	−0.29
150	58.60 ± 0.17	−0.14	59.35 ± 0.17	+0.61	59.51 ± 0.17	+0.77
$\sum_i \Delta_{i_1}^2$ =		2.76		9.50		3.72

... cont'd

Table 11 - cont'd

Fission product mass chain	Z_p(postulate) and its difference to Z_p(experiment)					
	Z_p(MPE)	Δ^a	Z_p(UCD)	Δ	Z_p(ECD)	Δ
	——— $^{233}U(n_{th},F)$ reaction ———					
82	32.72 ± 0.03	+0.11	32.52 ± 0.03	−0.09	32.46 ± 0.03	−0.15
128	50.05 ± 0.68	−0.15	51.08 ± 0.68	+0.88	50.10 ± 0.68	−0.10
130	50.41 ± 0.16	−0.23	51.47 ± 0.16	+0.83	50.47 ± 0.16	−0.17
131	51.11 ± 0.46	+0.07	52.20 ± 0.46	+1.16	51.16 ± 0.46	+0.12
140	54.90 ± 0.10	+0.06	55.41 ± 0.10	+0.57	54.59 ± 0.10	−0.25
$\sum_i \Delta_{i_2}^2$ =		0.10		3.14		0.14
	——— $^{239}Pu(n_{th},F)$ reaction ———					
96	38.73 ± 0.09	+0.19	38.28 ± 0.09	−0.26	38.63 ± 0.09	+0.09
97	38.85 ± 0.18	−0.31	38.40 ± 0.18	−0.76	38.75 ± 0.18	−0.41
128	50.12 ± 0.73	−0.23	51.10 ± 0.73	+0.75	50.17 ± 0.73	−0.18
130	50.69 ± 0.51	−0.03	51.70 ± 0.51	+0.98	50.74 ± 0.51	+0.02
131	51.25 ± 0.57	+0.31	52.19 ± 0.57	+1.25	51.20 ± 0.57	+0.26
$\sum_i \Delta_{i_3}^2$ =		0.28		3.73		0.28
$\sum_{j=1}^{3}\sum_i \Delta_{ij}^2$ =		3.14 (MPE)		16.37 (UCD)		4.14 (ECD)

[a] $\Delta = Z_p$(postulate) − Z_p(experiment).

the Z_p(MPE) using the atomic mass formula derived from Cameron (Ca57). The main difference between this formula without shell correction and the Droplet Model mass equation used in this work has already been shown (refer to Figure 18(a)). We believe the refined Droplet Model mass equation provides a more reliable calculation of Z_p(MPE), in particular considering its sensitivity to the shell corrections.

The charge dispersion data in thermal neutron induced fission, characteristic of asymmetric fission, can therefore be reproduced by either the MPE hypothesis or ECD rule, but definitely not the UCD postulate.

D. Fit to the Experimental Z_p Data in the ^{232}Th(p,Fission) Reaction

The ideal way to evaluate the most probable charge is to couple the post-fission deexcitation process and charge distribution evaluation with the calculation of the Pre-equilibrium / Exciton Model. In order to cut down the computing time, the fission information calculated in the previous chapters has been binned on excitation energy E^*_F. This grouped information is used as the input to evaluate the primary fragments that lead to the observed fission product; the primary fragments are then used as the input to calculate Z_p for each individual fission product chain.

Again, one of the 166 bins of input information in the $^{232}Th(p,Fission)$ reaction with 85 MeV incident protons is taken as a brief example, namely, $(Z_F, A_F, E^*_F, \sigma_F)$ = (91, 232, 81.3 MeV, 20.28 mb). The calculation of Z_p is activated at fission product mass chain A = 144. By using a reversed treatment of the post-fission deexcitation process discussed in the last chapter, the number of prompt neutrons evaporated from a primary fragment which eventually leads to A = 144 is calculated as ν = 5.96 neutrons, thus making the average primary fragment $A' = A + \nu = 149.96$. Hence, the mass division of this specific case having one of the fission products as A = 144 is (A'_L, A'_H) = (82.04, 149.96) with $A_F = A'_L + A'_H$. Therefore, Z_p(UCD) becomes $A'_H \cdot Z_F/A_F = 58.82$; Z_p(ECD) is calculated as 58.94 using $Z_A(A'_L) = 35.71$ and $Z_A(A'_H) = 62.60$; and Z_p(MPE) equals 58.72 using $\bar{D}$ = 17.5 fm. All the calculated Z_p(postulate) for the observed fission products for each bin of individual fission information is stored.

To simplify the vast amount of comparison between the calculation and experimental data, the values of Z_p(postulate) for each fission product chain A are graded in terms of stars:

***** : if all of the fits have the absolute difference between the calculated and experimental Z_p less than the standard deviation of the former, σ_{cal}, or the uncertainty of the latter, σ_{exp}, whichever is smaller;

**** : if more than half of the fits are within the criterion

set in the ***** grade;

** : if more than half of the fits have the absolute difference between calculated and experimental Z_p greater than $[\sigma^2_{cal} + \sigma^2_{exp}]^{\frac{1}{2}}$;

* : if all of the fits are within the criterion set in the ** grade;

*** : if otherwise.

These star grades are used qualitatively to compare the calculation to experimental results.

D1. Fit by uniform Z_p(postulate)

The first step toward the highly complex analysis is using a uniform Z_p(postulate), obtained from weighing the stored Z_p(postulate) by its fission probability σ_F in each bin of input information, to fit the experimental data. This implies that the charge distribution always follows one specific postulate regardless of the identity of the fissioning nucleus or its excitation energy.

Results of the comparison between calculation and experiment are listed in Table 12 where each fit of the uniform Z_p(postulate) is classified by the star grades. As seen from the table, not a single set of uniform Z_p(postulate) satisfactorily fits all Z_p(experiment) data. Fits by the uniform Z_p(ECD) are totally unsuccessful, while uniform Z_p(UCD) fits quite well the experimental data in mass chains A = 96, 136, and 144 but not in the rest. The uniform

Table 12

Qualitative comparison of uniform Z_p to the experimental data in the $^{232}Th(p,Fission)$ reaction.

Fit at experimental product mass chain	Type of Z_p (postulate)		
	Z_p (MPE)	Z_p (UCD)	Z_p (ECD)
77	*	*	*
96	**	****	**
132	****	**	**
133	***	**	**
135	***	**	**
136	***	***	**
144	***	***	**

Z_p(MPE) provides very successful fits to experimental data in all heavy mass chains but very poor fits to those data in light mass chains. From these analyses one finds three conflicting situations: (1) uniform Z_p(UCD) fits are quite good for experimental data at mass chain A = 136 but are poor at immediately neighboring A = 135; (2) uniform Z_p(UCD) fits extraordinarily well for experimental data at A = 96; however, the fit to those in the complementary fission product chain $A \leq 132$ is very poor; and similarly (3) uniform Z_p(MPE) fits experimental data at mass chains A = 132 and 144 very well but cannot reproduce those in the complementary product chains $A \geq 96$ and $A \geq 77$, respectively.

Because of these conflicting predictions, the fit of the uniform Z_p(postulate) is totally unacceptable, implying that the uniformity of a specific charge distribution postulate regardless of the identity of fissioning nucleus or its excitation energy, in particular in high energy reactions involving multi-chance fission, is invalid.

Pappas was among the first to suggest that the charge distribution in fission is fragment mass dependent (Pa66). He pointed out that in some mass regions the contribution from asymmetric fission is greater than that from symmetric; hence the charge distribution follows the ECD rule, as it is in the thermal neutron induced asymmetric fission. He also suggested that in other mass regions where symmetric fission predominates, the charge distribution follows more closely

the UCD postulate. However, this mass-dependent charge distribution proposal is not valid in the present calculation either. For instance, if Pappas' proposal were always followed, one would expect that in the very asymmetric mass division leading to fission product mass chains A = 144 and 77 the charge distribution would follow the ECD rule; the present calculation, however, yields the worst fit of Z_p(ECD) to the experimental data at these mass chains.

D2. Fit by E^*_F-dependent Z_p

Despite the scarce and sometimes conflicting information on charge distribution at high excitation energies, Vandenbosch and Huizenga (Va73) concluded that the charge distribution at high excitation energies E^*_F resemble qualitatively the UCD postulate rather than the ECD rule observed at lower E^*_F. The second step toward the analysis is therefore using an E^*_F-dependent Z_p to fit the experimental data.

To define the dependence of excitation energy is somewhat difficult. However, the experimental mass distribution of the ^{232}Th(p,Fission) reaction (refer to Figure 21) provides a guideline. As shown in the figure, a gradual transition from an asymmetric, double-humped yield curve to a flat shape with increasing proton energy is observed; at 20 MeV bombarding energy, the third peak becomes noticeable. The highest excitation energy associated with fission at this bombarding energy is about 25.2 MeV. Hence, a critical

excitation energy E^*_F(crit.) is assigned at 25 MeV; fission events having excitation energy greater than the E^*_F(crit.) are assumed to contribute to the symmetric peak, and the calculated Z_p of these events are then grouped for the symmetric fission. This implies that one charge distribution postulate correlates to high E^*_F fission (or symmetric fission) while another postulate to the low E^*_F fission (or asymmetric fission).

Since each and every calculated Z_p in storage retains the identity of its E^*_F, it can be divided according to the E^*_F(crit.) value, 25 MeV, and weighted by its probability σ_F. Hence, six different types of E^*_F-dependent Z_p may be organized and calculated:

Type of combination	if $E^*_F \leq E^*_F$(crit.), the Z_p(postulate) goes	if $E^*_F > E^*_F$(crit.), the Z_p(postulate) goes
ECD(E_l)/MPE(E_h)	Z_p(ECD)	Z_p(MPE)
UCD(E_l)/MPE(E_h)	Z_p(UCD)	Z_p(MPE)
ECD(E_l)/UCD(E_h)	Z_p(ECD)	Z_p(UCD)
MPE(E_l)/UCD(E_h)	Z_p(MPE)	Z_p(UCD)
UCD(E_l)/ECD(E_h)	Z_p(UCD)	Z_p(ECD)
MPE(E_l)/ECD(E_h)	Z_p(MPE)	Z_p(ECD)

The E^*_F-dependent Z_p is then compared to the experimental data. Results of the fit on the basis of the star grades

are summarized in Table 13.

As reflected from the second column in the table, all six E^*_F-dependent Z_p combinations fail to reproduce the Z_p(experiment) data at fission product chain A = 77. This is because at this mass chain each and every calculated Z_p in storage underestimates the experimental data by an amount of -0.4 to -1.1 charge unit; the E^*_F-dependent Z_p, no matter what type of dependence is adopted, also underestimates the experimental data by a similar amount. The $Z_p(ECD(E_l) / MPE(E_h))$ and $Z_p(UCD(E_l) / MPE(E_h))$, both requiring correlation of the MPE hypothesis to high E^*_F fission (or symmetric fission), yield conflicting fits for the experimental data of neighboring mass chains 135-136 and 132-133, respectively. The $Z_p(UCD(E_l) / ECD(E_h))$ and $Z_p(MPE(E_l) / ECD(E_h))$, both requiring correlation of the ECD rule to high E^*_F fission (or symmetric fission), fail to reproduce most of the experimental data. The $Z_p(ECD(E_l) / UCD(E_h))$ also yields rather poor fits to the experimental data on one hand and conflicting fits to those data in neighboring mass chains 135-136. A comparison shows that the best fits are attained by the calculated $Z_p(MPE(E_l) / UCD(E_h))$, requiring correlations of the MPE hypothesis to the low E^*_F fission (or asymmetric fission) and the UCD postulate to the high E^*_F fission (or symmetric fission).

This dependence on excitation energy for the calculation of Z_p discussed above, however, yields an unrealistic

Table 13

Qualitative comparison of the E^*_F-dependent Z_p
to the experimental data
in the $^{232}Th(p,Fission)$ reaction.

Type of excitation energy-dependent Z_p	Fit to the experimental Z_p at fission product mass chain						
	77	96	132	133	135	136	144
$Z_p(ECD(E_l) / MPE(E_h))$	*	*	**	*	*	***	****
$Z_p(UCD(E_l) / MPE(E_h))$	*	**	*	***	***	****	****
$Z_p(ECD(E_l) / UCD(E_h))$	*	***	**	***	*	****	**
$Z_p(MPE(E_l) / UCD(E_h))$	*	***	**	****	***	****	****
$Z_p(UCD(E_l) / ECD(E_h))$	*	**	*	***	***	***	**
$Z_p(MPE(E_l) / ECD(E_h))$	*	*	**	**	*	*	**

distribution of asymmetric and symmetric fissions. If one sums all fission events having excitation energy greater than the E^*_F(crit.) value, assumed to lead to symmetric fission, one will find the weighted symmetric fission yield is about 75% at incident proton energies above 40 MeV. Hence, one would expect the observed ratio of the symmetric/asymmetric fission yield to be 3:1 and the mass yield curve to become very symmetric. However, the experimental mass distribution in this energy region (again refer to Figure 21) is relatively flat rather than symmetric, having a ratio of about 1:1. Furthermore, the situation is worsened by the fact that the E^*_F(crit.) value, equivalent to the highest excitation energy in the 20 MeV incident protons, represents the highest limit of the division of asymmetric/symmetric fissions. If, rather, a lower value of E^*_F(crit.) is chosen, more events are attributed to the symmetric fission which in turn yields even higher ratios of symmetric/asymmetric fission yields, in worse agreement with the experimental fact.

Owing to the unrealistic correlation of the asymmetric/symmetric fissions to the observed mass distribution, the E^*_F-dependent Z_p calculated in this work must be treated with reservation, despite the fact that a reasonably good agreement to the experimental data is attained by Z_p(MPE(E_l)/UCD(E_h)).

D3. Fit by combined Z_p dependent upon (Z_F,A_F)

Perry and Fairhall (Pe71) were among the first to point out the asymmetric/symmetric fissions may correlate to the identity of the fissioning nucleus rather than the more commonly used excitation energy. The third step toward the analysis in this work is therefore seeking a combination of Z_p on the basis of the identity of the fissioning nucleus.

It is noteworthy that at the final stage of the preparation of this work, Eaker et al. (Ea79) also suggested that the observed onset of the symmetric peak in the ^{232}Th-(p,Fission) reaction at 14 MeV is attributable to the newly available fissioning nucleus from third-chance fission. This was certainly an encouragement to the approach which had been undertaken.

To define a combined Z_p which is not purely arbitrary, some guidelines may be obtained from experimental observations. First, the mass yield curve of the ^{232}Th(p,Fission) reaction with 20 MeV protons (refer to Figure 21) again provides the experimental split. As calculated in the previous chapter, the (p,3nF) is about to be available at this energy (refer to Table 07); hence, the newly emerged peak may be attributed to the symmetric fission of ^{230}Pa in the ^{232}Th(p,3nF) reaction. Similarly, the third peak in the middle of the mass yield curve of ^{226}Ra(p,Fission) at 13 MeV (Pe71) may be attributed to the (p,nF) reaction having the fissioning nuclide ^{226}Ac. Based on these two fissioning

nuclides, a line is proposed for each fissioning element to divide the calculated Z_p into two different categories:

$$(Z^2/A)_{A/S} = 36 + \frac{1}{2} \cdot (Z_F - 91) \qquad (21)$$

where $(Z^2/A)_{A/S}$ is defined as that asymmetric/symmetric split; the fissioning nuclide with charge Z_F and mass A_F may go to symmetric fission if Z^2_F/A_F is greater than the respective $(Z^2/A)_{A/S}$ value; otherwise it may go to asymmetric fission.

Since each and every calculated Z_p in storage retains the identity of (Z_F, A_F), it may be divided by Eq. (21) and weighted by its probability σ_F. Hence, six different types of combined Z_p may be organized and calculated:

Type of combination	if $Z^2_F/A_F \leq (Z^2/A)_{A/S}$ the Z_p(postulate) goes	if $Z^2_F/A_F > (Z^2/A)_{A/S}$ the Z_p(postulate) goes
ECD/MPE	Z_p(ECD)	Z_p(MPE)
UCD/MPE	Z_p(UCD)	Z_p(MPE)
ECD/UCD	Z_p(ECD)	Z_p(UCD)
MPE/UCD	Z_p(MPE)	Z_p(UCD)
UCD/ECD	Z_p(UCD)	Z_p(ECD)
MPE/ECD	Z_p(MPE)	Z_p(ECD)

The combined Z_p is then compared to the experimental Z_p data. Results of the fit on the basis of the star grades are summarized in Table 14.

Again, as reflected from the table, fits by any combined Z_p to the experimental data of fission product mass chain A = 77 is poor; the reason is the same as discussed earlier. In addition, any combined Z_p involving either the ECD or the MPE postulate correlating to the symmetric fission, such as Z_p(UCD/ECD), Z_p(MPE/ECD), Z_p(UCD/MPE), and Z_p(ECD/MPE), cannot reproduce all the experimental data and in most cases fits the Z_p(experiment) data quite poorly. Only the Z_p(MPE/UCD), or to a lesser extent the Z_p(ECD/UCD), yields a good fit to the experimental data. This requires a combination of Z_p(MPE), or to a lesser extent the Z_p(ECD), for those fissions having their Z^2_F/A_F less than the respective $(Z^2/A)_{A/S}$ value and Z_p(UCD) otherwise. The division of the asymmetric/symmetric fission according to the identity of the fissioning nucleus, unlike the unrealistic excitation energy split discussed in the last section, is quite consistent with the observed mass distribution; this will be discussed in the next chapter.

For a quantitative comparison among all kinds of calculated Z_p, the sums of the squares of differences between Z_p(experiment) and Z_p(calculation), except those in fission product chain A = 77, are listed in Table 15. As discussed earlier, the fit by the uniform Z_p, in particular the Z_p(ECD),

Table 14

Qualitative comparison of the combined Z_p
to the experimental data
in the $^{232}Th(p,Fission)$ reaction.

Type of the combined Z_p	Fit to the experimental Z_p at fission product mass chain						
	77	96	132	133	135	136	144
Z_p(ECD/MPE)	*	*	**	*	*	**	**
Z_p(UCD/MPE)	*	***	*	****	***	****	****
Z_p(ECD/UCD)	*	***	***	***	**	***	**
Z_p(MPE/UCD)	*	***	**	****	****	****	*****
Z_p(UCD/ECD)	*	***	**	**	***	***	***
Z_p(MPE/ECD)	*	*	***	**	**	***	*****

Table 15

Quantitative comparison of all calculated Z_p
to the experimental data
in the ^{232}Th(p,Fission) reaction.

Type of Z_p calculation	Sum of the squares of the differences
Z_p(MPE)	5.209
Z_p(UCD)	4.779
Z_p(ECD)	13.586
Z_p(ECD(E_l) / MPE(E_h))	7.600
Z_p(UCD(E_l) / MPE(E_h))	4.358
Z_p(ECD(E_l) / UCD(E_h))	3.724
Z_p(MPE(E_l) / UCD(E_h))	2.274
Z_p(UCD(E_l) / ECD(E_h))	5.378
Z_p(MPE(E_l) / ECD(E_h))	9.186
Z_p(ECD/MPE)	9.696
Z_p(UCD/MPE)	3.697
Z_p(ECD/UCD)	3.086
Z_p(MPE/UCD)	1.689
Z_p(UCD/ECD)	3.155
Z_p(MPE/ECD)	6.588

is unacceptable; this is indeed reflected from the table where Z_p(ECD) has the greatest sum of differences (the least agreement to the experimental data) and Z_p(MPE) and Z_p(UCD) also have relatively large sums. From among the E^*_F-dependent Z_p, despite their unrealistic implication, Z_p(MPE(E_l) / UCD(E_h)) maintains the best agreement (with the least sum) to the experimental data, as discussed in the last section. From among the combined Z_p, the Z_p(MPE/UCD) provides the best agreement to the experimental data; indeed it is the best of all the 15 calculations. The second best fit, neglecting the unrealistic Z_p(MPE(E_l) / UCD(E_h)), is maintained by the Z_p(ECD/UCD).

The best fit is now narrowed down to the Z_p(MPE/UCD), a combination of Z_p(MPE) and Z_p(UCD) on the basis of the asymmetric/symmetric split.

D4. <u>The combined Z_p(MPE/UCD)</u>

The combined Z_p(MPE/UCD) and Z_p(experiment) are plotted against incident proton energy and illustrated in Figure 24. Lines are drawn to connect all calculations to show the fit to experimental data. As the proton energy increases, the Z_p(experiment) for each fission product chain increases but levels off at high proton energies; this experimental trend is very well reproduced by the calculation. The quantitative result of this fit in detail, including the difference of the Z_p(MPE/UCD) to Z_p(experiment), together with

Figure 24

Calculated and experimental Z_p
in the $^{232}Th(p,Fission)$ reaction

● : Z_p (experiment)

○ : Z_p (MPE/UCD)

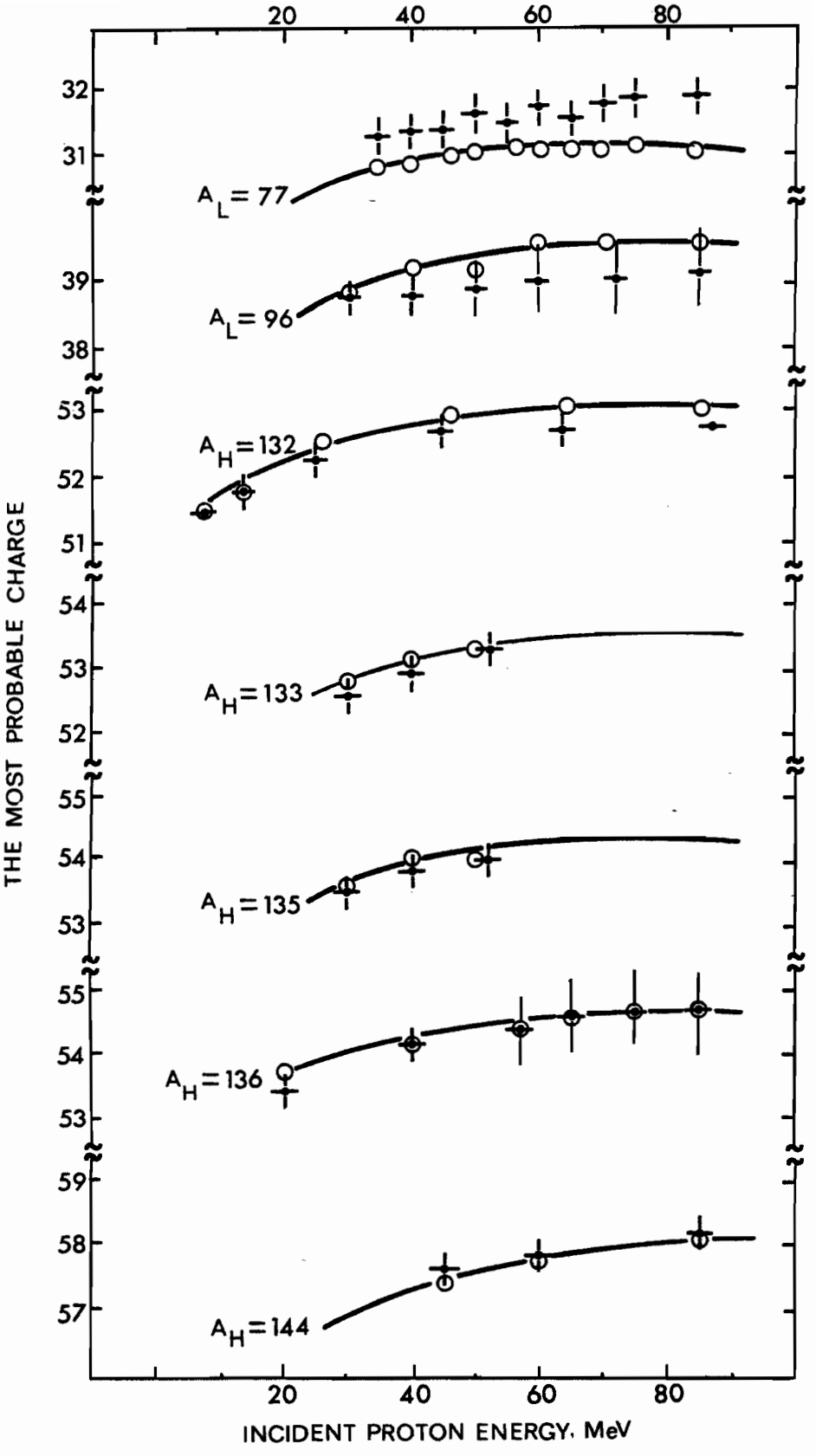
20
40
60
80
32
31
$A_L = 77$
39
$A_L = 96$
38
53
$A_H = 132$
52
51
54
53
$A_H = 133$
52
55
54
$A_H = 135$
53
55
54
$A_H = 136$
53
59
58
57
$A_H = 144$
20
40
60
80
THE MOST PROBABLE CHARGE
INCIDENT PROTON ENERGY, MeV

the calculated uncertainty, are listed in Table 16.

The fit to Z_p(experiment) for fission product chain A = 77, as discussed above, is poor. Calculation of Z_p(MPE/UCD) underestimates the experimental data ranging from -0.36 to -0.82 charge unit. However, the fit to those at A = 144 is strikingly good. If the treatment of post-fission de-excitation and Z_p calculation were wrong at around A = 77, an overestimate by that similar amount would be observed in the fit of the complementary fission product chain A $\geq$ 144.

Experimental Z_p data for fission product chain A = 96 are slightly overestimated in the present calculation by an amount of about +0.4 charge unit. However, the experimental result was constructed by (Mc71) on the basis of a questionable assumption, that is, the fission product mass yield curve is flat in the mass region A = 90-101, as discussed in the previous section. Croall and Cuninghame (Cr69) measured the fragmental mass yield curves and found that in this mass region, the mass yield curve is not flat and indeed varies with incident proton energies (refer to Figure 21). If one accounts for this observed fact, the N/Z_p value estimated in (Mc71) should be shifted toward the low side, hence yielding higher Z_p(experiment) than the presented data. Qualitatively, this correction yields better agreement to the calculated Z_p(MPE/UCD).

The low energy data of Z_p(experiment) for fission

Table 16

Quantitative comparison between
the combined Z_p(MPE/UCD) and Z_p(experiment)
of the ^{232}Th(p,Fission) reaction.

Incident proton energy (MeV)	Fit to the experimental Z_p data by the combined Z_p(MPE/UCD) at fission product mass chain						
	77	96	132	133	135	136	144
8 ± 2	---	---	0.06 ± 0.08	---	---	---	---
14 ± 2	---	---	-0.05 ± 0.20	---	---	---	---
20 ± 2	---	---	---	---	---	0.35 ± 0.25	---
25 ± 2	---	---	0.33 ± 0.19	---	---	---	---
30 ± 2	---	0.04 ± 0.28	---	0.31 ± 0.22	0.20 ± 0.21	---	---
35 ± 2	-0.49 ± 0.17	---	---	---	---	---	---
40 ± 2	-0.46 ± 0.17	0.43 ± 0.27	---	0.12 ± 0.22	0.13 ± 0.22	0.01 ± 0.26	---
45 ± 2	-0.47 ± 0.22	---	0.32 ± 0.17	---	---	---	-0.11 ± 0.22
50 ± 2	-0.59 ± 0.17	0.32 ± 0.51	---	-0.05 ± 0.22	0.00 ± 0.21	---	---
55 ± 2	-0.36 ± 0.24	---	---	---	---	0.09 ± 0.50	---
60 ± 2	-0.73 ± 0.19	0.58 ± 0.51	---	---	---	---	-0.08 ± 0.20
65 ± 2	-0.58 ± 0.16	---	0.41 ± 0.17	---	---	-0.05 ± 0.50	---
70 ± 2	-0.66 ± 0.19	0.49 ± 0.50	---	---	---	---	---
75 ± 2	-0.68 ± 0.14	---	---	---	---	-0.01 ± 0.50	---
85 ± 2	-0.82 ± 0.16	0.43 ± 0.50	0.30 ± 0.11	---	---	-0.03 ± 0.50	-0.12 ± 0.17

product chain A = 132 are fit excellently by the calculation; at higher energy, Z_p(experiment) is slightly overestimated by an amount of about +0.3 charge unit. This is mainly because of the possibility of an overestimate of the evaporation of post-fission neutrons near the doubly closed-shell fragment $^{132}_{50}Sn_{82}$, which is unaccounted for in the present post-fission calculation.

The remaining experimental data for fission product mass chains A = 133, 135, and 136 are fit extraordinarily well by the combined Z_p(MPE/UCD). This excellent fit is of particular importance for the self-consistency of the prediction, since a successful charge distribution approach must reproduce neighboring experimental data in different mass chains and different incident proton energies without a single exception.

The satisfactory fit by the combined Z_p(MPE/UCD) gives firm support for the asymmetric/symmetric split proposed in Eq. (21). The correlation of the $(Z^2/A)_{A/S}$ value to asymmetric and symmetric fissions remains to be discussed in the next chapter.

E. Summary of the Fit

In this chapter the most probable charge Z_p has been calculated and compared to the experimental Z_p data in both $^{233,235}U, ^{239}Pu(n_{th},F)$ reactions and $^{232}Th(p,Fission)$ reactions.

The fit to the single-chance fission data of (n_{th},F) by Z_p(MPE) is excellent; the Z_p(ECD) results where the calculation is based on primary fragments, rather than the traditional fission products, also reproduces experimental data quite well. This prediction contradicts the traditional claims; that is, the calculation with the ECD rule (based upon fission products) gives better prediction than that of the MPE hypothesis. However, the previous calculation, as discussed earlier, is an unrealistic approach. The calculated Z_p(UCD), as expected, cannot reproduce the experimental data at all in thermal neutron induced fission.

A new method of dividing the asymmetric/symmetric fissions by the identity of the fissioning nucleus, rather than the excitation energy, is proposed. Based on this proposal, the fit to the experimental data in the multi-chance fission reaction of ^{232}Th(p,Fission) by a combined Z_p(MPE/UCD) is found to be very successful. This fit requires the MPE hypothesis to be correlated with asymmetric fission and the UCD postulate to symmetric fission. The fit by a combined Z_p(ECD/UCD) is also found to be acceptable. These successful fits, using the MPE or ECD hypotheses for asymmetric fission are consistent with the prediction of the data in thermal neutron induced fission.

The detailed information of fission in the ^{232}Th(p, Fission) reaction, derived from earlier chapters, enable us to divide the asymmetric/symmetric fissions on the basis

of the empirical $(Z^2/A)_{A/S}$ value proposed in this work. This simple division also finds support in thermal neutron induced fission. The $(Z^2/A)_{A/S}$ values for U and Pu evaluated by Eq. (21) are 36.50 and 37.50, respectively. The fissioning nuclides $^{234,236}U$ in $^{233,235}U(n_{th},F)$ reactions have their Z^2_F/A_F values, 36.17 and 35.86, both smaller than the critical value for uranium, 36.50. The fissioning nuclide ^{240}Pu in $^{239}Pu(n_{th},F)$ reaction has its Z^2_F/A_F value 36.82, again smaller than the critical value for plutonium, 37.50. According to the present assumption of asymmetric/symmetric split, a fissioning nucleus goes to asymmetric fission if its Z^2_F/A_F is less than the respective $(Z^2/A)_{A/S}$ value; therefore we expect all of the three mass yield curves of thermal neutron induced fissions to be characteristic of double-peaked asymmetric fission, which are indeed the well-established experimental facts.

The correlation of the MPE hypothesis and UCD postulate to the asymmetric and symmetric fissions is supported by the fit of calculated Z_p to experimental data in the reactions discussed above. However, this correlation cannot be considered justified by only the limited reaction data unless the asymmetric/symmetric split is also satisfied for other fissioning nuclei and at different excitation energies. The general correlation of charge distribution postulates to asymmetric/symmetric fissions will be therefore discussed in detail in the next chapter.

VII

CORRELATION OF THE ASYMMETRIC/SYMMETRIC FISSIONS TO THE IDENTITY OF THE FISSIONING NUCLEUS

The mass distribution in the fission of bismuth and heavier elements with energies to the order of 200 MeV may be examined in terms of the two-mode fission hypothesis first suggested by Turkevich and Niday (Tu51). According to this hypothesis, any mass distribution measured in fission is due to the superposition of two components, one characteristic of an asymmetric part having a double-peaked curve with a valley in between and the other a symmetric component having a single-peaked curve with the peak location usually in the valley of the former. This hypothesis, however, allows even a single-chance fission such as spontaneous fission to break into asymmetric and symmetric parts, thus making the correlation between charge distribution and asymmetric/symmetric fissions extremely complicated.

In this work, the "asymmetric" and "symmetric" fissions are defined slightly differently in order to minimize the complexity mentioned above. The main difference to Turkevich's hypothesis is this: in the present studies the mass distribution of a single-chance fission reaction is treated with a single mass distribution. It is assigned either asymmetric or symmetric; no further decomposition of this elemental mass yield curve is allowed. For instance, the observed mass distribution of the spontaneous fission of ^{256}Fm, a single-chance fission measured by Flynn et al. (Fl72), has a double-peaked character and a valley in between. According to Turkevich's hypothesis, this mass yield curve

may be decomposed into asymmetric and symmetric parts, having the symmetric yield around 1.6%; in the present studies, however, this single-chance fission is treated only as a purely asymmetric fission, no symmetric component is allowed.

The present treatment of asymmetric and symmetric fissions can explain most of the observed mass distributions in fission, including those triple-peaked mass yield curves induced by energetic charged particles involving multi-chance fission processes. However, it cannot explain the triple-peaked mass distribution observed in some single-chance fission reactions such as $^{232}Th(n_f,F)$ reported by (Iy63) and $^{227}Ac(n_f,F)$ reported by (Iy65), since they require a break-up of the elemental asymmetric mass distribution. Recently, Zaghloul (Za79) suggested that the third peak observed in the above reactions may be due to contamination from some symmetric fission reaction induced by high energy neutrons in the nuclear reactor. The symmetric fissions leading to the contamination will be discussed later.

A. Decomposition of Mass Yield Curves

The mass distributions of multi-chance fission reactions of interest are decomposed in this work. There are several standards used for the decomposition of the fission product mass yield curve:

(1) If a valley is clearly observed around $A_F/2$ in the mass

distribution, it is assumed to arise from a superposition of asymmetric fissions having different A_F; no symmetric fission is introduced in this case.

(2) For a single-peaked mass yield curve without shoulders, the decomposition is assumed to arise from a superposition of symmetric fissions having different A_F; no asymmetric fission is allowed.

(3) The median mass number at half-maximum height of the heavy wing in the asymmetric fission curve is locked on $A_H = 139$, regardless of the identity of the fissioning nucleus; this is supported by the experimental observation compiled by Flynn et al. (Fl72).

(4) The peak of the light wing in the asymmetric fission curve therefore adjusts itself to $A_L = A_F - A_H - \nu_{post}$.

(5) The full width at half maximum (FWHM) for both wings in asymmetric fission curve is 15 mass units; this is supported by the experimental observation in many (n,F) reactions given by Flynn and Glendenin (Fl70).

(6) The peak/valley ratio in the asymmetric fission curve is allowed to decrease with increasing excitation energy; this is also supported by the experimental observation in (Fl70).

(7) The FWHM of the symmetric fission curve is allowed to be adjustable in the decomposition, ranging around 30 ± 15 mass units, corresponding to 50% uncertainty at most.

(8) The peak of the symmetric fission curve is located at

$A = (A_F - \nu_{post})/2.$

Based on these standards, the mass yield curves of ^{232}Th(p,Fission) reactions (refer to Figure 21) are first decomposed. The results are illustrated in Figure 25; labelled values are the incident proton energy and percentage of symmetric fission yield. With 13 MeV incident protons, according to the present definition, the mass yield curve is purely asymmetric; no decomposition for symmetric fission is necessary; with 20 MeV incident protons, the peak of the symmetric fission curve is emerging. As the incident proton energy increases, the symmetric peak becomes more important and eventually higher than the asymmetric peaks. Hence, the symmetric fissions are believed emerging just below 20 MeV of incident proton energy, then rapidly increasing, and leveling off at about 40-50% with protons above 50 MeV.

The decomposed percentage of symmetric fission is quite consistent with the $(Z^2/A)_{A/S}$ split in the last chapter. If one weights those calculated fission reactions which have their fissioning Z^2_F/A_F greater than the respective $(Z^2/A)_{A/S}$ value (as proposed to correlate to symmetric fission), one finds the weighted results match the decomposed percentage of symmetric fission quite well. Both the symmetric fission yield decomposed from experiment and weighted from the calculation are illustrated in Figure 26(a). This provides further support of the correlation of $(Z^2/A)_{A/S}$

Figure 25

Decomposition of the mass yield curves of the $^{232}Th(p,Fission)$ reaction into asymmetric and symmetric fissions

solid curves: experimental mass distribution, after (Cr69)

dashed curves: decomposed result in this work

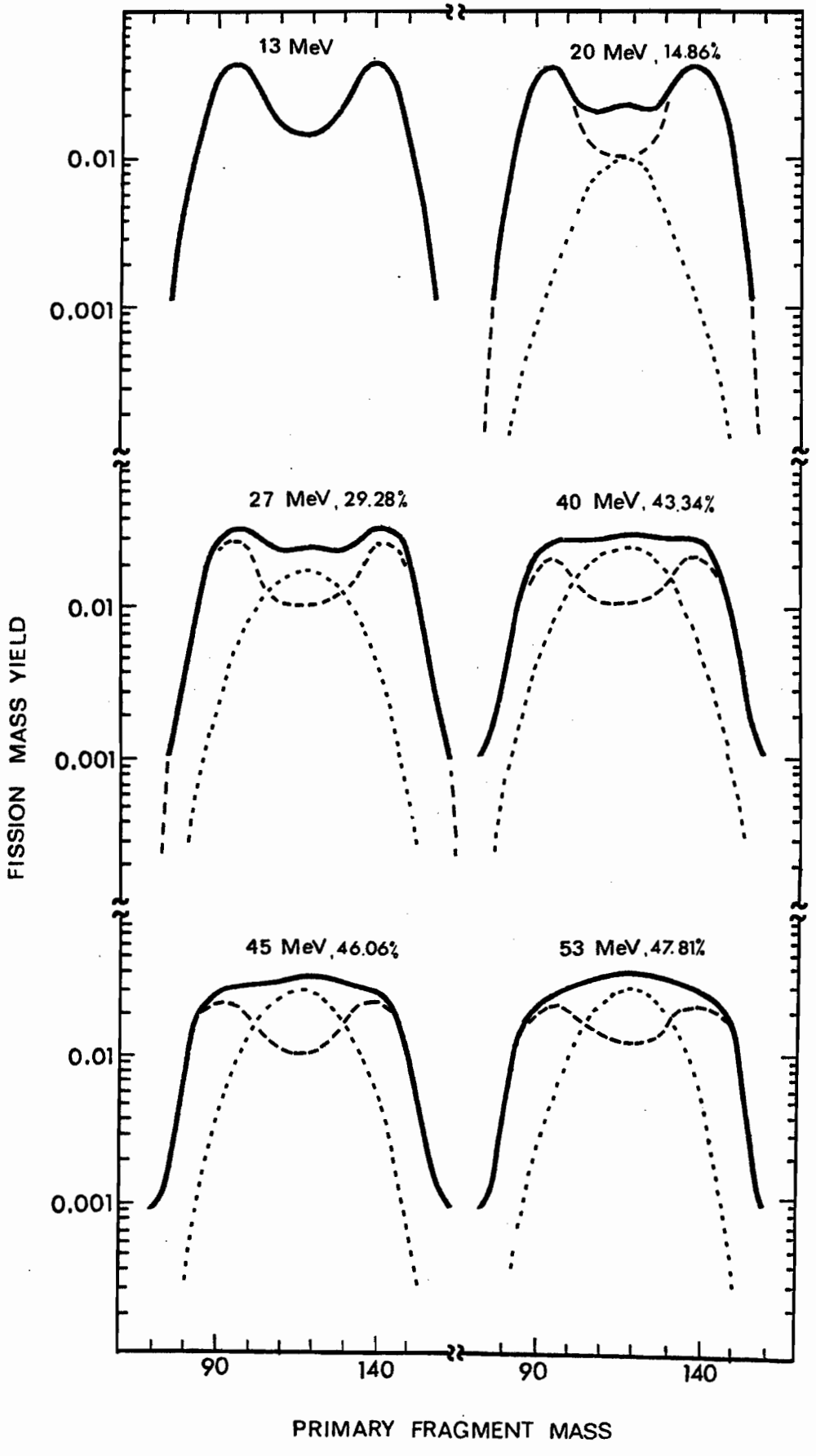
13 MeV
20 MeV, 14.86%
27 MeV, 29.28%
40 MeV, 43.34%
45 MeV, 46.06%
53 MeV, 47.81%
0.01
0.001
FISSION MASS YIELD
90
140
PRIMARY FRAGMENT MASS

Figure 26

Symmetric fission in experimental

mass distribution of the (p,Fission) reactions

(a) ^{232}Th(p,Fission) reactions

● : from Figure 25

o : from present calculation

(b) U(p,Fission) reaction

curves and points: after (Pa66A)

comments: this work

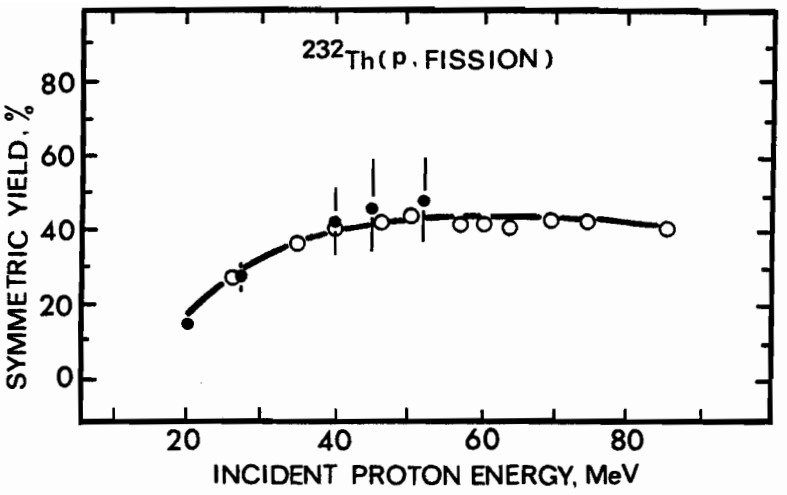

FIGURE-26(a)

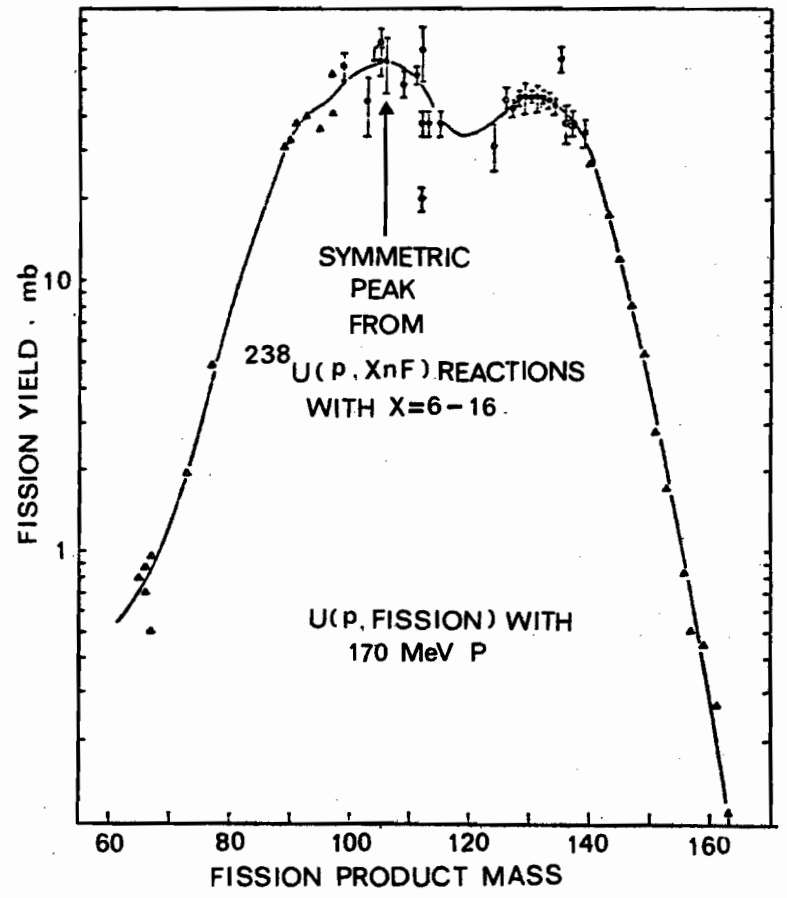

FIGURE-26(b)

split to the asymmetric/symmetric fissions.

On the other hand, the consistency of the $(Z^2/A)_{A/S}$ value for asymmetric/symmetric split can be extended to even higher energy reactions. Pappas and Hagebø (Pa66A) have completed the fission product mass yield curve of U(p,Fission) with 170 MeV protons. Their mass distribution, as reproduced in Figure 26(b), includes an eccentric peak centered around A $\sim$ 108 in addition to the two asymmetric peaks. According to the asymmetric/symmetric split introduced in the last chapter, fission reactions of ^{238}U-(p,XnF) with X = 6 - 16, corresponding to the fissioning nuclides $^{233\text{-}223}$Np with Z^2_F/A_F ranging from 37.12 to 38.18, are all symmetric since the Z^2_F/A_F of these fissioning nuclides are greater than the critical value of $(Z^2/A)_{A/S}$ for neptunium, 37.00. The average number of post-fission neutrons for these reactions is estimated in the same way as discussed in the previous chapter, varying from $\bar{\nu}_{post} \simeq$ 15 for the (p,6nF) reaction having a highly excited (to 140 MeV) ^{233}Np to $\bar{\nu}_{post} \simeq 5$ for the (p,16nF) reaction from a relatively cold fissioning nuclide ^{223}Np. The peak of these symmetric fissions are therefore all centered around $A = (A_F - \bar{\nu}_{post})/2 \simeq 109$, which indeed matches the experimental observation in Figure 26(b).

B. The Asymmetric/Symmetric Split

In this section, all available experimental mass distributions in fission are collected for the study of asymmetric/symmetric fissions. They range from very low energy fissions such as spontaneous and thermal neutron induced fissions to multi-chance fission reactions induced by energetic projectiles with excitation energy up to 60 MeV, involving fissioning nuclides up to $^{262}105$. The collected fission reactions are listed in Table 17.

All the collected mass yield curves of multi-chance fission are decomposed according to the standards set in the last section. If it is possible to evaluate the excitation energy at which the symmetric peak in the mass distribution just becomes noticeable in a predominantly asymmetric curve, that fissioning nucleus which just becomes available is assigned as the critical one for the newly emerged symmetric fission. For each fissioning element, there is one critical value of Z^2/A among the isotopes where the transition from asymmetric to symmetric fission occurs. For instance, in the last chapter, the protactinium isotopes having mass number $A \geq 231$ (low Z^2_F/A_F value) go to asymmetric fission; on the other hand, those having $A < 231$ (high Z^2_F/A_F value) go to symmetric fission; the asymmetric/symmetric transition for protactinium isotopes is therefore around 231/230.

Table 17

Data used for asymmetric/symmetric split in this work.

Target	Projectile	Reference
$^{262}_{105}$	SF	(Fe79)
^{252}No	SF	(Be77)
^{259}Md	SF	(Hu79)
^{259}Fm	SF	(Ho76)
^{258}Fm	SF	(Ho76)
^{257}Fm	SF	(Ba71)
^{257}Fm	n_{th}	(Jo71)
^{256}Fm	SF	(F172)
^{255}Fm	n_{th}	(Ra74)
^{254}Fm	SF	(Ha73)
^{254}Es	to 24 MeV (^{3}He,pF)	(Br79)
^{254}Es	to 15 MeV (^{3}He,dF)	(Br79)
^{254}Es	to 15 MeV (t,pF)	(Br79)
^{254}Es	to 15 MeV (d,pF)	(Br79)
^{253}Es	SF	(F176)
^{254}Cf	SF	(Br63)
^{252}Cf	SF	(Br63)

Target	Projectile	Reference
^{238}U	to 45 MeV ^{4}He	(Va58A)
^{238}U	to 55 MeV p	(Ba71A)
^{238}U	14 MeV n	(F170)
^{235}U	14 MeV n	(F170)
^{233}U	reactor n	(F170)
^{235}U	to 45 MeV ^{4}He	(Va58A)
^{233}U	to 45 MeV ^{4}He	(Va58A)
^{233}U	to 24 MeV d	(Fo59)
^{231}Pa	reactor n	(F170)
^{232}Th	14 MeV n	(F170)
^{232}Th	to 46 MeV ^{4}He	(Fo59)
^{232}Th	to 14 MeV d	(A157)
^{232}Th	to 53 MeV p	(Cr69)
^{230}Th	to 30 MeV ^{4}He	(Br64)
^{229}Th	n_{th}	(F170)
^{227}Th	n_{th}	(F170)
^{226}Ra	to 15 MeV n	(Zh73)

... cont'd

Table 17 - cont'd

Target	Projectile	Reference
^{250}Cf	SF	(Ho73A)
^{250}Cf	to 16 MeV (t,pF)	(Wi79)
^{249}Cf	n_{th}	(Fl70)
^{250}Cm	SF	(Ho73A)
^{248}Cm	SF	(Un72)
^{246}Cm	SF	(Pl73)
^{245}Cm	n_{th}	(Un72)
^{242}Cm	SF	(St54)
^{242}Am	n_{th}	(We69)
^{241}Am	n_{th}	(We69)
^{241}Am	14.8 MeV n	(Pr79)
^{241}Pu	n_{th}	(Fl70)
^{240}Pu	SF	(La62)
^{239}Pu	n_{th}	(Fl70)
^{239}Pu	to 24 MeV d	(Gi56)
^{237}Np	reactor n	(Fl70)
^{238}U	SF	(Yo60)
^{226}Ra	to 27 MeV ^{4}He	(Br63A)
^{226}Ra	to 24 MeV ^{3}He	(Br63A)
^{226}Ra	to 23 MeV t	(We76)
^{226}Ra	to 14 MeV d	(Br63A)
^{226}Ra	to 11 MeV p	(Je58)
^{209}Bi	to 42 MeV ^{4}He	(Un64)
^{209}Bi	to 25 MeV ^{3}He	(Br63A)
^{209}Bi	to 22 MeV d	(Fa56)
^{209}Bi	to 58 MeV p	(Su61)
Pb	to 42 MeV ^{4}He	(Ne63)
^{206}Pb	to 25 MeV ^{3}He	(Br63A)
Pb	to 54 MeV p	(Va61)
Tl	to 25 MeV ^{3}He	(Br63A)
^{197}Au	to 42 MeV ^{4}He	(Ne63)
^{197}Au	to 25 MeV ^{3}He	(Br63A)
Pt	to 65 MeV ^{4}He	(Ne69)

The fissioning nuclides assigned to asymmetric and symmetric fissions are displaced according to their Z^2_F/A_F identities in Figure 27. One may immediately find a striking result from this plot: all fissioning nuclides having their Z^2_F/A_F greater than the respective $(Z^2/A)_{A/S}$ value go to symmetric fission, while fissioning nuclides having their Z^2_F/A_F less than that value go to asymmetric fission. The detailed split of asymmetric/symmetric fissions is discussed below:

(1) Fissioning nuclides lighter than radium.

Mass yield curves for charged particle induced fission on Pt, Au, Tl, Pb, and Bi targets (references are listed in Table 17) are observed as purely symmetric; this is in good agreement with the present prediction since all fissioning nuclides involved in the said reactions go to symmetric fission because their Z^2_F/A_F values are much greater than the respective $(Z^2/A)_{A/S}$ value.

(2) Radium.

The mass yield curve used for asymmetric/symmetric split is the ^{226}Ra(n,Fission) with neutron energies to 15 MeV, measured by Zhagrov et al. (Zh73). The symmetric peak in the mass distribution is attributed to the (n,3nF) reaction having the fissioning nuclide ^{224}Ra with $Z^2_F/A_F \simeq 34.57$. According to the present prediction, the fissioning radium with mass number $A \leqslant 224$ goes to symmetric fission, which

Figure 27

The asymmetric and symmetric fissions

of the fissioning nuclides, $80 \leqslant Z_F \leqslant 105$

experimental data

Asymmetric fission	Symmetric fission	Fission reaction
○	●	Spontaneous fission
◇	◆	Neutron induced fission
▽	▼	Charged particle induced fission

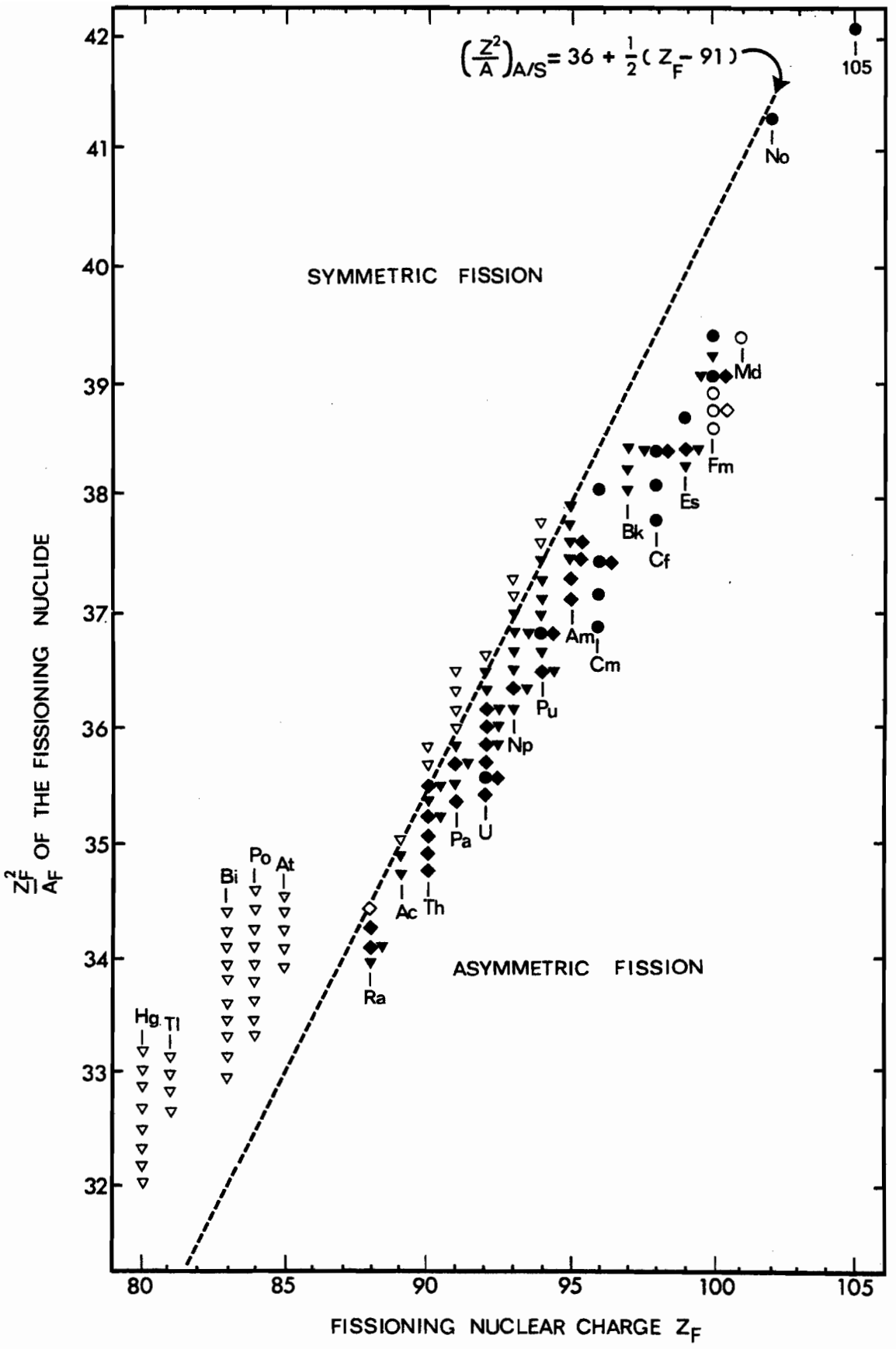
$\left(\frac{Z^2}{A}\right)_{A/S} = 36 + \frac{1}{2}(Z_F - 91)$
105
No
Md
Fm
Es
Bk
Cf
Am
Cm
Pu
Np
Pa
U
Ac
Th
Ra
Bi
Po
At
Hg
Tl
SYMMETRIC FISSION
ASYMMETRIC FISSION
$\frac{Z_F^2}{A_F}$ OF THE FISSIONING NUCLIDE
FISSIONING NUCLEAR CHARGE Z_F
42
41
40
39
38
37
36
35
34
33
32
80
85
90
95
100
105

is indeed the experimental observation.

(3) Actinium.

The triple-peaked mass distribution in the $^{226}Ra(p,$ Fission) reaction with 11 MeV protons, measured by (Je58) and (d,Fission) reaction with 11.7 MeV deuterons, measured by Britt, Wegner, and Gursky (Br63A), can be decomposed into asymmetric and symmetric components. The fissioning nuclide ^{226}Ac, corresponding to the (p,nF) reaction in the former and (d,2nF) in the latter case, is considered to produce the symmetric fission which causes the middle peak in the mass yield curve. According to the $(Z^2/A)_{A/S}$ split, fissioning actinium nuclides having mass number $A \leqslant 226$ go to symmetric fission; again, this is in good agreement with experimental observation.

As mentioned earlier, the third peak in the mass distribution of $^{227}Ac(n_f,F)$ reaction is mainly coming from some symmetric fissions induced by high energy neutrons; it is suggested here that these contaminating reactions be $^{227}Ac(n_f,2nF)$ leading to the fissioning nuclide ^{226}Ac on one hand, and $^{227}Th(n_f,nF)$ leading to the fissioning nuclide ^{227}Th on the other. The ^{227}Th is in secular equilibrium with the target ^{227}Ac and also goes to symmetric fission, as will be discussed later.

(4) Thorium.

The asymmetric mass yield curves of $^{227,229,232}Th(n,F)$

reactions, compiled by Flynn and Glendenin (Fl70), indicate that symmetric fission has been ruled out in these thorium nuclides having mass numbers A $\geq$ 228. This information enables us to narrow down the contribution of the symmetric peak in the triple-peaked mass yield curves in ^{226}Ra(^{3}He, Fission) with 20.9 MeV ^{3}He, measured by (Br63A) as mainly coming from the (^{3}He,2nF) reaction in which the fissioning ^{227}Th has $Z^2_F/A_F \simeq 35.68$. This is consistent with the present prediction since the critical $(Z^2/A)_{A/S}$ value for thorium is 35.50.

The third peak observed in the ^{232}Th(n_f,F) reaction may therefore be attributed to the possible interfering reaction ^{228}Th(n_f,2nF) having the fissioning nuclide ^{227}Th, where ^{228}Th is in secular equilibrium with the natural thorium target.

(5) Protactinium.

As mentioned in the last chapter, fissioning protactinium isotopes having mass number A < 231 are assigned to symmetric fission. This is further supported by experimental observation of the ^{230}Th(p,Fission) reaction with 8 MeV protons (Br63A). The triple-peaked mass yield curve may be decomposed into asymmetric fission from the (p,F) reaction and symmetric fission from the (p,nF) reaction, having the fissioning nuclide ^{230}Pa.

(6) Uranium.

The asymmetric mass yield curve of the ^{230}Th(α,Fission) reaction with 29.5 MeV alphas, measured by Britt and Whetstone (Br64), indicates that symmetric fission has been ruled out in those reactions of (α,XnF) with X = 0-2, corresponding to the fissioning nuclides $^{234-232}$U. This observation may be used to deduce that the third peak observed in the mass distribution of ^{232}Th(α,Fission) reaction with 45 MeV alphas, measured by Foreman et al. (Fo59) arises from the fissioning nuclide ^{231}U with $Z^2_F/A_F \simeq 36.64$; this is produced by the (α,5nF) reaction, and it has been found to go to symmetric fission. This is consistent with the present prediction since the $(Z^2/A)_{A/S}$ value for uranium is 36.50.

(7) Neptunium.

The third peak observed in the mass distribution of the ^{233}U(d,Fission) reaction with 21.5 MeV deuterons (Fo59) may be attributed to the symmetric fission of the newly emerged (d,2nF) reaction having the fissioning nuclide ^{233}Np with $Z^2_F/A_F \simeq 37.12$. Again, this is in good agreement with the present prediction since the $(Z^2/A)_{A/S}$ value for neptunium is 37.00

(8) Plutonium.

The emerging symmetric peak in the mass distribution of the ^{233}U(α,Fission) reaction with 30.7 MeV alphas (Fo59)

is attributed to the symmetric fission of the energetically available reaction of $(\alpha,2nF)$, having the fissioning nuclide ^{235}Pu with $Z^2_F/A_F \simeq 37.60$. The present prediction is once again consistent with experimental observation since the $(Z^2/A)_{A/S}$ value for plutonium is 37.50.

(9) Fissioning nuclides in the transplutonium region.

Mass distributions of those fission reactions involving transplutonium nuclides, ranging from ^{238}Am to $^{262}105$, are predicted asymmetric since the corresponding Z^2_F/A_F in each case is less than the respective $(Z^2/A)_{A/S}$ value. Indeed, we observe the asymmetric mass distribution in all cases except the mass yield curves in the spontaneous fissions of ^{259}Md, $^{258,259}Fm$, and $^{257}Fm(n_{th},F)$ reactions. The mass distributions in these exceptions are characterized by a sharp central peak with two side shoulders; in addition, the total kinetic energy released in these fissions cannot be predicted by the rather well described function of Coulomb forces, as shown in Eq. (13). For these strange mass distributions, Hoffman (Ho79) suggested that "the fission properties of the heavy Fm isotopes may be unique and can be qualitatively explained on the basis that symmetric fission of the heavy Fm isotopes results in two fragments with configurations close to the doubly magic $^{132}_{50}Sn$ nucleus".

In all, the asymmetric/symmetric split on the basis

of the proposed $(Z^2/A)_{A/S}$ values is consistent with the wide range of experimental data discussed above. However, the fits are limited to those data collected in Table 17. Mass distributions of (γ,Fission), charged particle induced fissions with excitation energy above 60 MeV, and heavy ion induced fissions are not considered here; this is because the exact excitation energies transferred from projectile to the fissioning nuclei and their identities are not well known, unless a distinct asymmetric/symmetric mass distribution such as the one reproduced in Figure 26(b) is presented. Furthermore, the $(Z^2/A)_{A/S}$ value, as shown in Eq. (21), is purely empirical and should be treated as only a first approximation; a further refinement of the equation may lead to a small shift of the asymmetric/symmetric split. Still, it is sufficient to provide a convenient way to decompose qualitatively the asymmetric/symmetric fissions in many fission reactions.

C. Charge Distribution and Asymmetric/Symmetric Fissions

For years, many investigators have suggested that the predominantly determining factor for asymmetric and symmetric fissions is the excitation energy, that is, high excitation energy leads to symmetric fission while low excitation energy leads to asymmetric. We have been suggesting

that the identity of the fissioning nucleus is the main determining factor for the asymmetric/symmetric fissions. Thus, the symmetric part of high energy fission is mainly coming from the fission of some specific fissioning nuclides which are produced by evaporation of several neutrons prior to fission.

More important is the fact that we have found a strikingly good fit to the Z_p(experiment) data by proposing that the charge distribution in those fissions having Z^2_F/A_F less than the respective $(Z^2/A)_{A/S}$ value goes by the MPE hypothesis (or to a lesser extent the ECD rule) and otherwise by the UCD postulate. Now that we believe the correlation of this $(Z^2/A)_{A/S}$ split to the asymmetric/symmetric fissions to be firmly supported, we may say that the charge distribution is following the MPE hypothesis (or the ECD rule) in the case of asymmetric fission and the UCD postulate for symmetric fission. This indicates that the process from saddle to scission is rather slow in asymmetric fission while it is fast in symmetric fission.

In asymmetric fission, the ECD rule finds slightly less support from the fits to experimental data than those by the MPE hypothesis; this should not generate significant concern since the ECD rule is purely empirical and the traditional ECD is calculated from an unrealistic approach on the basis of the fission products.

VIII

SUMMARY AND CONTRIBUTION TO KNOWLEDGE

The cross sections of $^{231,228,227,226}Th$ and $^{225,224,223}Ra$ produced in the $^{232}Th(p,X)$ reactions by protons of energies to 90 MeV have been measured radiochemically. Excitation functions of (p,pXn) with X = 1, 4-6 and (p,3pXn) with X = 5-7 were evaluated. The measured excitation functions, together with those (p,Xn) with X = 1, 3, 5-7, (p,2pXn) with X = 3-7, and the total fission cross sections of ^{232}Th(p, Fission) reactions compiled from the literature were compared to the calculation on the basis of the Pre-equilibrium / Exciton Model with a newly developed fission option.

The theoretical fit to the experimental excitation functions and total fission cross sections has been found strikingly good; neither normalization nor any adjustment from case to case is required. The excellent fits are retained simultaneously in simple reactions such as (p,n) and highly complex ones like (p,3p7n) on one hand and high cross sections in the (p,Fission) reaction (about 1 000 mb) and low cross sections in (p,3p7n) reactions (about 0.02 mb) on the other hand. The agreement between the calculation and experiment yields solid support to the treatment of fission associated with the well-established Pre-equilibrium / Exciton Model.

The calculation has been expanded to evaluate the details of fission information, such as the identity of the fissioning nucleus, its excitation energy, and the specific fission probability. The calculated results, though difficult

to be verified experimentally, are as reliable as the spallation calculation since fission and spallation are interlocking each other in each and every step of the calculation.

Based on the detailed information of fission, the numbers of post-fission neutrons in ^{232}Th(p,Fission) reactions have been calculated assuming that the excitation energy is shared by primary fragments according to their mass ratio. The calculated post-fission neutron yield is also found in agreement with the experimental evaluation.

Attempts have been made to evaluate the most probable charge by different charge distribution postulates on the basis of the pre- and post-fission treatments set up in this work. The experimental Z_p data in the ^{232}Th(p,Fission) reaction have been fit excellently by a combined Z_p(MPE/UCD) calculation. The combination is designated by an empirical $(Z^2/A)_{A/S}$ value proposed in this work. Z_p(UCD) has been evaluated and assigned for those fission events having their Z^2_F/A_F greater than the respective $(Z^2/A)_{A/S}$ value, otherwise Z_p(MPE) is assigned. The second best fit is obtained with the Z_p(ECD/UCD) calculation. The ECD rule calculation, based on fission fragments rather than fission products, also yields good agreement with the asymmetric fission data. It implies that the distinction between the MPE and ECD postulates is small, though the agreement with the experimental data by the former is better than that by the latter.

The excellent fits to Z_p(experiment) leads to a more

detailed investigation of the universality of the simple $(Z^2/A)_{A/S}$ critical value. Mass distributions in fission, collected from a wide range of experiments, have been decomposed into asymmetric and symmetric parts and correlated to the identity of the fissioning nucleus rather than the excitation energy. Surprisingly, all fissioning nuclides going to symmetric fission have their Z^2_F/A_F lying above the critical $(Z^2/A)_{A/S}$ value, while those going to asymmetric fission lie below that value. This is applicable to all the fissioning nuclides collected, ranging from ^{193}Hg to ^{262}105 with the only exception being the heavy Fm isotopes.

The quantitative correlation between charge distribution postulates and asymmetric/symmetric fissions is then summarized as the MPE hypothesis (or the ECD rule) being associated with asymmetric fission while the UCD postulate is associated with symmetric fission.

APPENDIX

THE SI UNITS

The International System of Units (SI) is used in most cases in this work. However, for historical reasons or reasons of clear reader preference, other traditional units are also used. The SI equivalent of these units are given below:

To convert from the unit used in this work	To the SI equivalent	Multiply by
inch (length)	metre	$2.540\ 000 \times 10^{-2}$
fm (length)	metre	$1.000\ 000 \times 10^{-15}$
mb (area)	$metre^2$	$1.000\ 000 \times 10^{-31}$
amu (mass)	kilogram	$1.660\ 566 \times 10^{-27}$
degree Celsius (temp.)	degree Kelvin	add 273.15
MeV (energy)	joule	$1.602\ 19 \times 10^{-13}$

REFERENCES

Al57 J.M. Alexander and C.D. Coryell, Phys. Rev. 108, 1274 (1957).

Ba71 J.P. Balagna, G.P. Ford, D.C. Hoffman, and J.D. Knight, Phys. Rev. Lett. 26, 145 (1971).

Ba71A S. Baba, H. Umezawa, and H. Baba, Nucl. Phys. A175, 177 (1971).

Be69 Y.P. Benjamin, D.A. Marsden, N.T. Porile, and L. Yaffe, Can. J. Chem. 47, 301 (1969).

Be77 C.E. Bemis, Jr., R.C. Ferguson, F. Plasil, R.J. Silva, F. Pleasonton, and R.L. Hahn, Phys. Rev. C 15, 705 (1977).

Bi70 C.J. Bishop, R. Vandenbosch, R. Aley, R.W. Shaw, Jr., and I. Halpern, Nucl. Phys. A150, 129 (1970).

Bl75 M. Blann, Ann. Rev. Nucl. Sci. 25, 123 (1975).

Bo39 N. Bohr and J.A. Wheeler, Phys. Rev. 56, 426 (1939).

Br62 C. Brun and N. Simonoff, J. Phys. Radium 23, 12 (1962).

Br63 R. Brandt, S.G. Thompson, R.C. Gatti, and L. Philips, Phys. Rev. 131, 2617 (1963).

Br63A H.C. Britt, H.E. Wegner, and J. Gursky, Phys. Rev. 129, 2239 (1963).

Br64 H.C. Britt and S.L. Whetstone, Jr., Phys. Rev. 133, B603 (1964).

Br79 H.C. Britt, D.C. Hoffman, J.B. Wilhelmy, E. Cheifetz, R.J. Dupzyk, and R.W. Lougheed, in Int. Symp. on Phys. and Chem. of Fission, Report IAEA-SM/241-F41, (Julich, F. R. Germany, 1979), p. 215.

Bu80 Kerry I. Burns, Ph.D. Thesis, McGill University, 1980.

Ca57 A.G.W. Cameron, presented at Proc. Symp. Phys. Fission, Chalk River, Canada, 1957, Report CRP-690 (unpublished).

Ch63 G.R. Choppin, J.R. Meriwether, and J.D. Fox, Phys. Rev. 131, 2149 (1963).

Ch71 G.R. Choppin and A.J. Tofe, J. Inorg. Nucl. Chem. 33, 1535 (1971).

Ch71A Y.Y. Chu, E.M. Franz, G. Friedlander, and P.J. Karol, Phys. Rev. C 4, 2202 (1971).

Co53 C.D. Coryell, Ann. Rev. Nucl. Sci. 2, 305 (1953).

Co63 S. Cohen and W.J. Swiatecki, Ann. of Phys. 22, 406 (1963).

Cr69 I.F. Croall and J.G. Cuninghame, Nucl. Phys. A125, 402 (1969).

De78 H. Delagrange, A. Fleury, and J.M. Alexander, Phys. Rev. C 17, 1706 (1978).

Di78 M. Diksic (private communication, 1978).

Di79 M. Diksic, J.-L. Galinier, H. Marshall, and L. Yaffe, J. Inorg. Nucl. Chem. 41, 795 (1979).

Do58 I. Dostrovsky, Z. Frankel, and P. Rabinowitz, in Proc. 2nd U.N. Conf. Peaceful Uses of At. Energy, (Geneva, Austria, 1958), Paper P/1515.

Do59 I. Dostrovsky, Z. Frankel, and G. Friedlander, Phys. Rev. 116, 683 (1959).

Ea76 R.W. Eaker and G.R. Choppin, J. Inorg. Nucl. Chem. 38, 31 (1976).

Ea79 R. Eaker, H.S. Plendl, A.F. Zeller, A. Clem, L. Muga, and J.M. Nicovich, Phys. Rev. C 20, 1055 (1979).

El76 Y.A. Ellis, Nucl. Data Sheets 17, No. 3 (1976).

Fa56 A.W. Fairhall, Phys. Rev. 102, 1335 (1956).

Fe79 R.L. Ferguson, C.E. Bemis, Jr., F. Plasil, R.J. Silva, G.D. O'Kelley, R.L. Hahn, D.C. Hensley, M.L. Kiefer, M.G. Mustafa, E.K. Hulet, and R.W. Lougheed, in Int. Symp. on Phys. and Chem. of Fission, Report IAEA-SM/241-F37, (Julich, F.R. Germany, 1979), p. 208.

Fe79A A. Ferrero, E. Gadioli, E. Gadioli-Erba, I. Iori, N. Molho, and L. Zetta, presented in Proceedings of the XVII International Meeting on Nuclear Physics, Bormio, Italy, 1979 (unpublished).

Fl70 K.F. Flynn and L.E. Glendenin, Report No. ANL-7749, 1970.

Fl72 K.F. Flynn, E.P. Horwitz, C.A. Bloomquist, R.F. Barnes, R.K. Sjoblom, P.R. Fields, and L.E. Glendenin, Phys. Rev. C 5, 1425 (1972).

Fl76 K.F. Flynn, J.E. Gindler, L.E. Glendenin, and R.K. Sjoblom, J. Inorg. Nucl. Chem. 38, 661 (1976).

Fo59 B.M. Foreman, Jr., W.M. Gibson, R.A. Glass, and G.T. Seaborg, Phys. Rev. 116, 382 (1959).

Fo66 J.H. Forster, N.T. Porile, and L. Yaffe, Can. J. Chem. 44, 2951 (1966).

Fo72 M. Fowler (private communication, 1972).

Fo74 M. Fowler and A.C. Wahl, J. Inorg. Nucl. Chem. 36, 1201 (1974).

Fr52 J.S. Fraser, Phys. Rev. 88, 536 (1952).

Fr68 S.H. Freid, J.L. Anderson, and G.R. Choppin, J. Inorg. Nucl. Chem. 30, 3155 (1968).

Ga62 H. Gauvin, M. Lefort, and X. Tarrago, Nucl. Phys. 39, 447 (1962).

Ga63 H. Gauvin, J. Phys. Radium 24, 836 (1963).

Ga69 G.T. Garvey, W.J. Gerace, R.L. Jaffe, I. Talmi, and I. Kelson, Rev. Mod. Phys. Suppl. 41, S1 (1969).

Ga73 E. Gadioli and L. Milazzo-Colli, Lecture Notes in Physics, 1st ed. (Springer, Berlin, 1973), Vol. 22, p. 84.

Ga77 E. Gadioli, E. Gadioli-Erba, and J.J. Hogan, Phys. Rev. C 16, 1404 (1977).

Ga77A E. Gadioli, E. Gadioli-Erba, and J.J. Hogan, Nuovo Cimento 40, 383 (1977).

Ga78 E. Gadioli, E. Gadioli-Erba, and A. Moroni, Z. Phys. A288, 39 (1978).

Ga78A E. Gadioli, E. Gadioli-Erba, and A. Ferrero, presented at Proc. Workshop Reaction Models for Continuous Spectra of Light Particles, Bad Honnef, F. R. Germany, 1978 (unpublished).

Ga79 E. Gadioli and E. Gadioli-Erba (private communication, 1979).

Gi56 W.M. Gibson, Report UCRL-3493, 1956.

Gl49 L.E. Glendenin, C.D. Coryell, and R.R. Edwards, Phys. Rev. 75, 337 (1949).

Gl51 L.E. Glendenin, C.D. Coryell, and R.R. Edwards, in Radiochemical Studies: The Fission Products, edited by C.D. Coryell and N. Sugarman (N.Y. McGraw-Hill Book Co., Inc., 1951), Paper 52, p. 489.

Gl55 L.E. Glendenin, K.F. Flynn, R.F. Buchanan, and E.P. Steinberg, Anal. Chem. 27, 59 (1955).

Go48 R.H. Goeckermann and I. Perlman, Phys. Rev. 73, 1127 (1948).

Go49 R.H. Geockermann and I. Perlman, Phys. Rev. 76, 628 (1949).

Ha39 O. Hahn and F. Strassmann, Naturwissenschaften 27, 11 (1939).

Ha72 R.L. Hahn, K.S. Toth, and M.F. Roche, Nucl. Phys. A185, 252 (1972).

Ha73 R.M. Harbour, K.W. MacMurdo, D.E. Troutner, and M.V. Hoehn, Phys. Rev. C 8, 1488 (1973).

Ho73 K. Holub and L. Yaffe, J. Inorg. Nucl. Chem. 35, 3991 (1973).

Ho73A D.C. Hoffman, G.P. Ford, and J. Balagna, Phys. Rev. C 7, 276 (1973).

Ho76 D.C. Hoffman, J. Weber, J.B. Wilhelmy, E.K. Hulet, R.W. Lougheed, J.H. Landrum, and J.F. Wild, in Transplutonium 1975, Proceedings of the 4th International Transplutonium Element Symposium, (Amsterdam, North Holland, 1976), p. 363.

Ho77 J.J. Hogan and E. Gadioli, in Proceedings of Int. Conf. on Nuclear Reaction Mechanisms, (Varenna, Italy, 1977), p. 198.

Ho77A J.J. Hogan, K.I. Burns, E. Gadioli, and E. Gadioli-Erba, in Proceedings of the 4th European Physical Society Nuclear Physics Conference, (Florence, Italy, 1977), p. 57.

Ho79 D.C. Hoffman, in Int. Symp. on Phys. and Chem. of Fission, Report IAEA-SM/241-F14, (Julich, F. R. Germany, 1979), p. 169.

Hu79 E.K. Hulet, J.F. Wild, R.W. Lougheed, P.A. Baisden, J.H. Landrum, R.J. Dougan, M. Mustafa, A. Ghiorso, and J.M. Nitschke, in Int. Symp. on Phys. and Chem. of Fission, Report IAEA-SM/241-F15, (Julich, F. R. Germany, 1979), p. 170.

Iy63 R.H. Iyer, C.K. Mathews, N. Ravindran, K. Rengan, D.V. Singh, M.V. Ramaniah, and H.D. Sharma, J. Inorg. Nucl. Chem. 25, 465 (1963).

Iy65 R.H. Iyer, H.C. Jain, M.N. Namboodivi, M. Rajagopalan, M.V. Rajkishore, M.V. Ramaniah, C.L. Rao, N. Ravindran, and H.D. Sharma, in Proc. of the Symp. on Phys. and Chem. of Fission, (Salzburg, Austria, 1965), 1, p. 439.

Ja56 J.D. Jackson, Can. J. Phys. 34, 767 (1956).

Je58 R.C. Jensen and A.W. Fairhall, Phys. Rev. 109, 942 (1958).

Jo71 W. John, E.K. Hulet, R.W. Lougheed, and J.J. Weslolwski, Phys. Rev. Lett. 27, 45 (1971).

Ka61 T.M. Kavanagh and R.E. Bell, Can. J. Phys. 39, 1172 (1961).

Ka76 M.V. Kantelo and J.J. Hogan, Phys. Rev. C 13, 1095 (1976).

Ke57 G.R. Keeping, T.F. Wimett, and R. Ziegler, Phys. Rev. 107, 1044 (1957).

Kr53 K.A. Kraus and G.E. Moore, J. Amer. Chem. Soc. 75, 1460 (1953).

La61 D.W. Lang, Nucl. Phys. 26, 434 (1961).

La62 J.L. Laidler and F. Brown, J. Inorg. Nucl. Chem. 24, 1485 (1962).

Le57 H.B. Levy, Phys. Rev. 106, 1265 (1957).

Le61 M. Lefort, N. Simonoff, and X. Tarrago, Nucl. Phys. 25, 216 (1961).

Le62 M. Lefort, N. Simonoff, and X. Tarrago, J. Phys. Radium 23, 123 (1962).

Le67 Y. Lebeyec and M. Lefort, Nucl. Phys. A99, 131 (1967).

Li60 M. Lindner and A. Turkevich, Phys. Rev. 119, 1632 (1960).

Lo67 W.D. Loveland, A.W. Fairhall, and I. Halpern, Phys. Rev. 163, 1315 (1967).

Ma65 H. Maier-Leibnitz, P. Armbruster, and H.J. Specht, in Proc. of the Symp. on Phys. and Chem. of Fission, (Salzburg, Austria, 1965), 2, p. 113.

Ma73 C. Maples, Nuclear Data Sheets 10, No. 6 (1973).

Ma77 C. Maples, Nuclear Data Sheets 22, No. 2 (1977).

Mc54 G.H. McCormick and B.L. Cohen, Phys. Rev. 96, 722 (1954).

Mc71 T. McGee, C.L. Rao, and L. Yaffe, Nucl. Phys. A173, 595 (1971).

Me39 L. Meitner and O. Frisch, Nature (London), 143, 239 (1939).

Me49 W.W. Meinke, Report USAEC D-2738, 1949.

Me56 W.W. Meinke, G.C. Wick, and G.T. Seaborg, J. Inorg. Nucl. Chem. 3, 69 (1956).

Me58 N. Metropolis, R. Birins, M. Storm, A. Turkevich, J.M. Miller, and G. Friedlander, Phys. Rev. 110, 204 (1958).

Mi62 J.C.D. Milton, Report UCRL-9883, 1962.

Mo75 R.B. Moore (private communication, 1975).

My66 W.D. Myers and W.J. Swiatecki, Nucl. Phys. 81, 1 (1966).

My77 W.D. Myers, Droplet Model of Atomic Nuclei, 1st ed. (IFI/Plenum, N.Y., 1977).

Ne49 A.S. Newton, E.K. Hyde, and W.W. Meinke, Report USAEC D-2738, 1949.

Ne62 P.E. Nemirovski and Yu. V. Adamchuk, Nucl. Phys. 39, 551 (1962).

Ne63 E.F. Neuzil and A.W. Fairhall, Phys. Rev. 129, 2705 (1963).

Ne69 E.F. Neuzil and K. Apt, J. Inorg. Nucl. Chem. 31, 1571 (1969); 1575 (1969).

Ne71 D.A. Newton, Computer code EXPONENT (McGill University, Canada, 1971).

Ne73 D.A. Newton, S. Sarkar, L. Yaffe, and R.B. Moore, J. Inorg. Nucl. Chem. 35, 361 (1973).

Pa58 B.D. Pate, Can. J. Chem. 36, 1707 (1958).

Pa58A B.D. Pate, J.S. Foster, and L. Yaffe, Can. J. Chem. 36, 1691 (1958).

Pa66 A.C. Pappas, Z. Naturf. 21, 995 (1966).

Pa66A A.C. Pappas and E. Hagebø, J. Inorg. Nucl. Chem. 28, 1769 (1966).

Pe71 D.G. Perry and A.W. Fairhall, Phys. Rev. C 4, 977 (1971).

Pl73 F. Pleasonton, R.L. Ferguson, F. Plasil, and C.E. Pemis, Jr., Phys. Rev. C 8, 1018 (1973).

Pr47 R.D. Present, Phys. Rev. 72, 7 (1947).

Pr58 R.J. Prestwood, Report LA-1721, 1958.

Pr79 A.L. Prindle, D.H. Sisson, D.R. Nethaway, M.V. Kantelo, and R.A. Sigg, Phys. Rev. C 20, 1824 (1979).

Ra74 R.C. Ragaini, E.K. Hulet, R.W. Lougheed, and J. Wild, Phys. Rev. C 9, 399 (1974).

Rul9 E. Rutherford, Phil. Mang. 37, 581 (1919).

Sc77 M.R. Schmorak, Nucl. Data Sheets 20, No. 2 (1977).

St54 E.P. Steinberg and L.E. Glendenin, Phys. Rev. 95, 431 (1954).

St56 H.M. Steiner and J.A. Jungerman, Phys. Rev. 101, 860 (1956).

St66 P.C. Stevenson, in Processing of Counting Data, Report NAS-NS-3109, (Springfield, Va., USA, 1966).

Su61 T.T. Sugihara, J. Roesmer, and J.M. Meadows, Phys. Rev. 121, 1179 (1961).

Su74 H.C. Suk, J.E. Crawford, and R.B. Moore, Nucl. Phys. A218, 418 (1974).

Te52 H.A. Tewes and R.A. James, Phys. Rev. 88, 860 (1952).

Te55 H.A. Tewes, Phys. Rev. 98, 25 (1955).

Th66 T.D. Thomas and S.L. Whetstone, Phys. Rev. 144, 1060 (1966).

To69 A.J. Tofe, Ph.D. Thesis, Florida State University, 1969.

To77 K.S. Toth, Nucl. Data Sheets 20, No. 2 (1977).

Tu51 A. Turkevich and J.B. Niday, Phys. Rev. 84, 52 (1951).

Tu78 J.K. Tuli, Nucl. Data Sheets 25, No. 4 (1978).

Un64 J.P. Unik and J.R. Huizenga, Phys. Rev. 134, 1390 (1964).

Un69 J.P. Unik, J.G. Cuninghame, and I.F. Croall, in 2nd IAEA Symp. on Phys. and Chem. of Fission, (Vienna, Austria, 1969), p. 717.

Un72 J.P. Unik, L.E. Glendenin, J.E. Gindler, K.L. Wolf, and A.J. Gorski, ANL Chemistry Division Annual Report, 1971 July - 1972 June.

Va58 R. Vandenbosch and J. Huizenga, in Proc. 2nd U.N. Conf. Peaceful Uses At. Energy, (Geneva, Austria, 1958), 15, Paper P/688.

Va58A R. Vandenbosch, T.D. Thomas, S.E. Vandenbosch, R.A. Glass, and G.T. Seaborg, Phys. Rev. 111, 1358 (1958).

Va61 U.L. Vallinder and A.C. Pappas, J. Inorg. Nucl. Chem. 22, 161 (1961).

Va73 R. Vandenbosch and J.R. Huizenga, Nuclear Fission, 1st ed., (Academic Press, N.Y., 1973).

Vi66 V.E. Viola, Jr., Nucl. Data A1, 391 (1966).

Wa48 K. Way and E.P. Wigner, Phys. Rev. 73, 1318 (1948).

Wa58 W.G. Warren, Report LA-1721, 1958.

Wa62 A.C. Wahl, R.L. Ferguson, D.R. Nethaway, D.E. Troutner, and K. Wolfsberg, Phys. Rev. 126, 1112 (1962).

Wa69 A.C. Wahl, A.E. Norris, R.A. Rouse, and J.C. Williams, in 2nd IAEA Symp. on Phys. and Chem. of Fission, (Vienna, Austria, 1969), p. 813.

Wa71 A.H. Wapstra and N.B. Gove, Nucl. Data A9, 268 (1971).

We69 W. Weinlaender, in 2nd IAEA Symp. on Phys. and Chem. of Fission, (Vienna, Austria, 1969), p. 951.

We76 J. Weber, H.C. Britt, A. Gavron, E. Konecny, and J.B. Wilhelmy, Phys. Rev. C 13, 2413 (1976).

Wi66 C.F. Williamson, J.P. Boujot, and J. Picard, Saclay Report No. CEA-R3042, 1966.

Wi79 J.B. Wilhelmy, H.C. Britt, J. Weber, and A. Gavron, in Int. Symp. on Phys. and Chem. of Fission, Report IAEA-SM/241-B14, (Julich, F. R. Germany, 1979), p. 62.

Ya68 L. Yaffe, Nuclear Chemistry, 1st ed., (Academic Press, N.Y., 1968), p. 113.

Yo60 B.G. Young and H.G. Thode, Can. J. Phys. 38, 1 (1960).

Za79 R. Zaghloul, in Int. Symp. on Phys. and Chem. of Fission, Report IAEA-SM/241-F18, (Julich, F. R. Germany, 1979), p. 175.

Zh73 E.A. Zhagrov, I.M. Kuks, Yu.A. Nemilov, Yu.A. Selitskii, and V.B. Funstein, Nucl. Phys. A213, 436 (1973).